7-1-2015

Land Use /Land Cover Driven Surface Energy Balance and Convective Rainfall Change in South Florida

Hari P. Kandel
Florida International University, hkand001@fiu.edu

FLORIDA INTERNATIONAL UNIVERSITY

Miami, Florida

LAND USE/ LAND COVER DRIVEN SURFACE ENERGY BALANCE AND CONVECTIVE RAINFALL CHANGE IN SOUTH FLORIDA

A dissertation submitted in partial fulfillment of

the requirements for the degree of

DOCTOR OF PHILOSOPHY

in

GEOSCIENCES

by

Hari Prasad Kandel

2015

To: Dean Michael R. Heithaus
College of Arts and Sciences

This dissertation, written by Hari Prasad Kandel, and entitled Land Use/Land Cover Driven Surface Energy Balance and Convective Rainfall Change in South Florida, having been approved in respect to style and intellectual content, is referred to you for judgment.

We have read this dissertation and recommend that it be approved.

Ping Zhu

Georgio Tachiev

Michael C. Sukop

Dean Whitman

Assefa M. Melesse, Major Professor

Date of Defense: July 1, 2015

The dissertation of Hari Prasad Kandel is approved.

Dean Michael R. Heithaus
College of Arts and Sciences

Dean Lakshmi N. Reddi
University Graduate School

Florida International University, 2015

DEDICATION

To my late father, Chet Prasad Kandel, a true adorer and source of the encouragement for my hard work who missed my graduation just by a couple of months.

ACKNOWLEDGMENTS

Foremost, I would like to express my sincere gratitude to my graduate advisor Dr. Assefa Melesse for his continuous guidance, motivation and enthusiasm since the very first day of my acceptance into the program. Both his mentorship in academic life and care in personal life have been extremely valuable during this study.

Equally, my appreciation goes to the rest of my dissertation committee: Dr. Ping Zhu, Dr. Dean Whitman, Dr. Michael Sukop and Dr. Georgio Tachiev for their teaching, time and cooperation. Dr. Zhu, as a novice learner in boundary layer atmosphere, I have learned a lot from your class and from the reviews of convective rainfall part of the dissertation. With your very thorough and critical reviews, Dr. Whitman, you helped refine my way of backing and clarifying the presentations. Basics of numerical models and system balance approach that I learned from Dr. Sukop's class were of immense help in designing the energy balance part of this research. I owe Dr. Tachiev a debt of gratitude for his kind availability and insightful comments throughout this work.

I am grateful to the Graduate School, College of Arts and Sciences, and Department of Earth and Environment of FIU, and Florida section of American Water Resources Association for the travel fund to make the conference presentations that led me towards the wider avenues of sharing and hearing the science beyond the school. A big credit goes to the Department of Earth and Environment for the teaching assistantship throughout my study. I thank all the faculties, staff and my colleagues of FIU Department of Earth and Environment.

Behind the scenes are my wife Laxima, and parents along with all family members, whose sustained support in my graduate study is greatly acknowledged.

ABSTRACT OF THE DISSERTATION

LAND USE/ LAND COVER DRIVEN SURFACE ENERGY BALANCE AND CONVECTIVE RAINFALL CHANGE IN SOUTH FLORIDA

by

Hari Prasad Kandel

Florida International University, 2015

Miami, Florida

Professor Assefa M. Melesse, Major Professor

Modification of land use/land cover in South Florida has posed a major challenge in the region's eco-hydrology by shifting the surface-atmosphere water and energy balance. Although drainage and development in South Florida took place extensively between the mid- and late- 20th century, converting half of the original Everglades into agricultural and urban areas, urban expansion still accounts for a dominant mode of surface cover change in South Florida. Changes in surface cover directly affect the radiative, thermophysical and aerodynamic parameters which determine the absorption and partitioning of radiation into different components at the Earth surface. The alteration is responsible for changing the thermal structure of the surface and surface layer atmosphere, eventually modifying surface-induced convection.

This dissertation is aimed at analyzing the extent and pattern of land cover change in South Florida and delineating the associated development of urban heat island (UHI), energy flux alteration, and convective rainfall modification using observed data, remotely sensed estimates, and modeled results.

Urban land covers in South Florida are found to have increased by 10% from 1974 to 2011. Higher Landsat-derived land surface temperatures (LST) are observed in urban areas ($\overline{LST}_{u-r}$ =2.8°C) with satisfactory validation statistics for eastern stations (Nash-Sutcliffe coefficient =0.70 and R^2 =0.79). Time series trends, significantly negative for diurnal temperature range (DTR= -1°C, p=0.005) and positive for lifting condensation level (LCL > 20m) reveal temporal and conspicuous urban-rural differences in nocturnal temperature (ΔTu-r = 4°C) shows spatial signatures of UHI. Spatially higher (urban: 3, forest: 0.14) and temporally increasing (urban: 1.67 to 3) Bowen's ratios, and sensible heat fluxes exceeding net radiation in medium and high-intensity developed areas in 2010 reflect the effect of urbanization on surface energy balance. Radar reflectivity-derived surface-induced convective rainfall reveals significantly positive mean differences (thunderstorm cell density: 6/1000 km^2 and rain rate: 0.24 mm/hr/summer, p <0.005) between urban and entire South Florida indicating convective enhancement by urban covers.

The research fulfils its two-fold purposes: advancing the understanding of post-development hydrometeorology in South Florida and investigating the spatial and temporal impacts of land cover change on the microclimate of a subtropical city.

TABLE OF CONTENTS

LIST OF TABLES

TABLE PAGE

LIST OF FIGURES

FIGURE PAGE

ABBREVIATIONS AND ACRONYMS

AMO	Atlantic Multi-decadal Oscillation
AVHRR	Advanced Very High Resolution Radiometer
CAPE	Convective Available Potential Energy
CCAP	Coastal Change Analysis Program
CDR	Climate Data Records
CLC	Cooperative Land Cover
DTR	Diurnal Temperature Range
EAA	Everglades Agricultural Area
ENSO	El Niño Southern Oscillation
ESF	Entire South Florida
ET	Evapotranspiration
EUSF	Eastern Urbanized South Florida
FAWN	Florida Automatic Weather Network
FCLTER	Florida Coastal Everglades Long Term Ecological Research
FDEP	Florida Department of Environmental Protection
FLUCCS	Florida Land Use Cover Classification System
FNAI	Florida Natural Area Inventory
GHCN	Global Historical Climatology Network
HDSS	Hydromet Decision Support System

LAI	Leaf Area Index
LCL	Lifting Condensation Level
LEDAPS	Landsat Ecosystem Disturbance Adaptive Processing System
LFC	Level of Free Convection
LSE	Land Surface Emissivity
LST	Land Surface Temperature
LULC	Land Use / Land Cover
MSA	Metropolitan Statistical Area
METROMEX	Metropolitan Meteorological Experiment
MIA	Miami International Airport
NAPP	National Aerial Photography Program
NCDC	National Climatic Data Center
NDVI	Normalized Difference Vegetation Index
NEXRAD	Next Generation Radar
NLCD	National Land Cover Database
NOAA	National Oceanic and Atmospheric Administration
RD	Relative Difference
RMSE	Root Mean Square Error
SFWMD	South Florida Water Management District
TM	Thematic Mapper
UHI	Urban Heat Island

USEPA	United States Environmental Protection Agency
USGS	United States Geological Survey
UTC	Coordinated Universal Time
WCA	Water Conservation Area
WSR-88D	Weather Surveillance Radar – 1988 Doppler

Chapter 1

Introduction

1.1 Background

Rapid urbanization has continued globally over the last 200 years and is an inevitable process for the future in an increasingly industrialized society. The world's population living in urban areas has increased from 2% in 1800, 14% in 1900, 30% in 1950 (Wu, 2010) to 54% in 2014 which is projected to rise to 66% by 2050 (UN, 2014). Increase of urban population demands the conversion of natural lands to developed lands which results in several environmental perturbations. The influence of urbanization on long-term temperature records has been detected for cities with populations less than 10,000 (Karl *et al*., 1988). Heterogeneous surface covers with their varied thermal characteristics in urban areas have major implications on energy and water budgets of the surface, and stability and structure of the boundary layer atmosphere. The presence of an insulating layer of vegetation reduces solar heat storage in wet and forested areas (Oke, 1978), whereas effective storage occurs in the stone, concrete, asphalt and deeper compacted soil layers in the urban areas. Such storage together with the heat expelled from the city creates a strongly positive heat balance in urban areas (Landsberg, 1970) called an urban heat island (UHI). Rainfall over and/or downwind of urban areas is found to be enhanced in intensity if the UHI gradient is strong enough to create a pressure field setting a concentric breeze into motion (Landsberg, 1970; Dixon and Mote, 2003; Shepherd and Burian, 2003). South Florida, undergoing recent urbanization at an expense of natural vegetated wild lands, and being surrounded by sources of sea and lake breezes, makes a

unique site for this study that aims to analyze alteration of surface-induced water and energy exchanges triggered by human intervention.

Changes in land use/ land cover introduce changes in physical, radio-thermal, and aerodynamic properties that determine the radiation and thermal characteristics of the surface. Albedo, emissivity, thermal conductivity, specific heat, density, and roughness length are important factors. The literature suggests that thermal conductivity and specific heat are lower, and aerodynamic roughness lengths are higher, in urban areas compared to water and wetlands (Arya, 2001; Oke, 1978). Aerodynamic roughness of the urban buildings is reported to reduce the wind speed by 25% which increases the convective efficiency (Landsberg, 1970). Surface cover materials, hydrology, and vegetation transpiration characteristics also affect partitioning of net radiation into latent and sensible heat fluxes (McGuffie *et al.*, 1995). Typical average values of Bowen's ratio, the ratio between sensible and latent heat fluxes, is 0.1 for tropical oceans, 0.1 to 0.3 for tropical wet forests, 0.4 to 0.8 for grasslands, 0.75 to 2 for urban areas with lawns and trees, and greater than 2 reaching maximum value of 6 for dry urban areas (Oke, 1978). The availability of water and nature of exchange surfaces primarily control these fluxes. The ground heat flux component is also expected to increase in urbanized areas.

The land covers in South Florida have undergone great changes in the mid- to late-20th century. The transformations that began in early 1900s were stimulated by a rapid growth of population and need for a flood control system. During the construction of the Central and South Florida project to build drainage and water management structures between 1948 and 1975, there has been extensive transformation of wetlands converting almost half of the original Everglades to agricultural and urban uses (McVoy *et al.*, 2011).

Predominantly pine forest areas and part of the wetlands of the natural landscape have been converted to the current land use patterns including mixed agriculture, cities, roads, residential areas, and urban complexes (Marshall *et al.*, 2004). The sequences of these conversions imposed by diversion of natural flow through canals, and confinement of free surface water into the water conservation areas have had huge impacts on the hydrologic regime and ecological health of the region. The surface hydrologic budget of the managed system is dominated by stored and channelized flows as opposed to widespread evapotranspiration and downward infiltration of the pre-drainage Everglades. Disappearance of wetlands, soil subsidence, severe droughts resulting into fire posing extreme stress on wild life, and salt water intrusion in the underlying aquifers are some major problems already being observed. Motivated by these challenges, this dissertation work focuses on the hydrologic part of the impact.

As opposed to the general tendency of rural to urban reduction of albedo, a peculiarity that urban albedo is higher compared to surrounding water, wet, and vegetated surface is observed in South Florida (Kandel *et al.*, 2015). Also, apparent thermal inertia, a representative term for thermal conductivity, specific heat, and density of the materials, is estimated to be nearly the same or higher in urban areas compared to water bodies and wetlands (Kandel *et al.*, 2015). These specifics highlight the role of thermal inertia, aerodynamic roughness, and emissivity in urban heating in South Florida,

More than 50% of the land area in South Florida is occupied by water bodies and wetlands. South Florida loses 70–90% of its rainfall through evapotranspiration annually (Duever *et. al.*, 1994). Suffering from fragmentation, drying, vegetation loss, wetland shrinkage, anthropogenic encroachment and consequent environmental degradation,

South Florida now hosts the world's largest wetland restoration project, the project Comprehensive Everglades Restoration Plan (CERP) (Sklar *et al.*, 2001). Even with the restoration efforts in place, urban expansion and shrinkage of natural lands, principally the rangelands are still ongoing processes in South Florida. Just between 1975 and 1986, about 2000 km^2 of natural areas were converted to anthropogenic purposes in the region, accounting 13% of the natural lands of 1975 (Walker *et al.*, 1997).

It is possible that the replacement of wet and forested lands by agricultural and urban covers in South Florida results in an increase of Bowen's ratio in those converted areas thereby increasing the land surface temperature. Such high temperature areas may act as convergence centers for breezes in motion and modify the distribution and intensity of surface-induced convection. The thermally-induced circulation rises at the center and subsides over the surroundings with a motion that is radially inward toward the city center at lower levels and outward from the city center at upper levels (Arya, 2001). Since thunderstorms related to convection are one of the two phenomena primarily responsible for the wet season rainfall in South Florida (Pielke, 1974), variation in surface-driven convective rainfall, most likely in the outer fringe of cities, could impact the overall wet season rainfall. An assessment of post-drainage land cover change and associated modifications of the states and fluxes of water and energy between surface and atmosphere in South Florida is, therefore, believed to provide insight into the human-modified microclimate. The results may also benefit water management agencies in evaluating the progress of restoration.

1.2 Problem Statement

A complete understanding of the unique behavior of different land covers towards water and energy fluxes would require observations of surface-level temperatures, energy fluxes, and purely convective precipitation at high spatial resolution and over long temporal periods. Although relatively widespread distributions of temperature and precipitation stations exist in the study area, there are no observations of energy flux made in the urban, agricultural, and transitional lands, which precludes both land cover-wise and temporal comparison. There are only a few eddy covariance towers to measure energy flux installed and maintained in South Florida by United States Geological Survey (USGS), Florida Coastal Everglades Long Term Ecological Research (FCE LTER), and Ameriflux. The towers are restricted within the geographic boundary of the natural Everglades and have captured the data only for a limited number of years. To overcome the shortcoming of data scarcity, there are two commonly used approaches: numerical modeling and remote sensing estimates.

Influence of landscape change from pre-1900 to 1993 land cover conditions on sensible weather in Florida was modeled and modifications were found in latent and sensible heat fluxes as well as in thermally-induced sea breeze circulations (Marshall et al., 2004; Pielke *et al.*, 1999). Appropriate parameterization of land use land cover in land surface numerical models is a big challenge because, first, representing small scale features in the model domain is almost impossible, and second, error propagation in the models increase end-results' uncertainty. The computing and time resources required by three-dimensional numerical models for a large area like South Florida further complicate the modeling choice. In the present study, we combined meteorological station records, and

Landsat surface reflectance and brightness temperature products to estimate land surface temperatures, surface albedos, surface emissivities, and components of energy fluxes. Likewise, radar reflectivities above 40 dBZ for synoptically-benign summer afternoons are used to estimate locally-induced convective storms. This combined approach helped make the analysis straightforward by fulfilling the data requirements, complementing the observed records, and providing the results in higher spatial resolutions for reasonably long periods.

1.3 Previous Studies and Rationale for the Present Work

Several previous studies that carried out similar work were reviewed, methodological gaps and unaddressed issues were identified, and new approaches are proposed for this study.

The literature shows credible evidence of a link between urban land cover and surface temperature increase (Kalnay and Cai, 2003), cloud enhancement (Inoue and Kimura, 2004), and precipitation anomalies (Collier, 2006; Hand and Shepherd, 2009; Kaufmann *et al.*, 2007; Shepherd, 2005). Impacts of urban development on local weather- especially UHI- have been demonstrated by several previous studies in major cities across the globe (e.g., Bornstein, 1968; Oke, 1973; Draxler, 1986; Balling and Cerveny, 1987; Lo *et al.*, 1997; Bornstein and Lin, 2000; Morris *et al.*, 2001; Collier 2006). Influences of urbanization on temperature within United States are imprinted well on minimum (compared to maximum or mean) temperature records (Karl *et al.*, 1988). Following the suggestions made by (Runnals and Oke, 2000) that UHI are greatest in summer because

of enhanced rural cooling rate during these months, this study uses daily minimum temperatures from May to October.

Land surface temperature (LST) estimated from Landsat was found to have accuracy within 1°C (Li *et al.*, 2004).

Previously in South Florida, water and energy balance studies have focused primarily on estimation of evapotranspiration (ET). Direct measurements of ET using lysimeters, Bowen's ratio approach, and computational software with a water balance approach based on input from weather station records (Abtew, *et. al.*, 2003) are some examples of the past research. Two distinct areas of increased sensible heat flux were shown by an atmospheric model in South Florida that compared pre- and post-drainage land-use data. These areas shown by Marshall et al. (2004) corresponded to the areas that were drained and converted to agricultural use, and the areas of urban development. From a remote sensing study, Melesse et al. (2007) found a significant increase of fractional vegetation cover and latent heat flux along the restoration axis of the Kissimmee River Basin. Their study shows the potential of remote sensing methods to comprehend the drainage and restoration impacts on heat exchange.

Urban rural differences of precipitation were initially recognized mainly in two ways: temporal analysis by comparing pre-urban and urban precipitation in an area, and spatial analysis by comparing precipitation amounts in gauges within and beyond the city. Changnon (1962) analyzed 10-year mean annual isohyetal maps based on a network of gauges within and beyond the city limit in Urbana-Champaign, Illinois and depicted increased precipitation at the eastern boundary of the urban area. A research on a widely-known feature, La Porte Anomaly, noted the great increase in annual rainfall at the small

town of La Porte, about 60 km to the east of the Chicago industrial areas. The rainfall increase coincided with increased steel production. A five-year project, the Metropolitan Meteorological Experiment (METROMEX), a major field observation program centered on St Louis, Missouri, studied the effects of the urban-industrial complex on the urban environment and showed that the St. Louis metropolitan area fuels summer–time thunderstorms (Huff and Vogel, 1978). Shepherd et al. (2002) found that Atlanta produced a 19.5% increase in precipitation downwind of its metropolitan area when compared with upwind control area during the warm seasons of 1998-2000. In a study of urban-induced rainfall anomalies in a coastal city, Shepherd and Burian (2003) detected a rainfall anomaly in the warm season, but not in annual distribution and explained it as the result of interaction between UHI -induced mesoscale convergence-circulation pattern and the sea breeze circulation. The factors enhancing the convection were suggested to be UHI intensity, increased urban roughness, and urban boundary layer instability (Vukovich and Dunn, 1978; Hjemfelt, 1982).

A summer-time (May-August) radar image analysis during both day and night hours from 2000 to 2009 in the Indianapolis urban area concluded that positive buoyancy within the urban environment causes more changes in storm composition during the day than during the night (Niyogi *et al.*, 2011). Ashley *et al.* (2012) used high resolution radar-based climatology for warm season convection in Southeastern U.S. cities and demonstrated significant details of urban effects on thunderstorm frequency and intensity. Aforesaid radar studies are the motivation for the present work to extend the analysis to an eighteen year-long (1995-2012) period in South Florida.

Studies that verify the development of UHIs for a humid subtropical city at land surface, surface-air interface, and surface layer atmosphere were lacking. Therefore, a combination of daily minimum near-surface air temperatures, Landsat-derived surface temperatures, and a Radiosonde-based analysis are used in this study so that the existence of an UHI in the South Florida region can be examined. Furthermore, an effort has been made for the first time to provide physical representation of small-scale land features by combining the parameters obtained from observed and remotely-sensed data sources. Combined data help to elucidate the details of spatial and temporal variation of energy flux components in South Florida. Also, analysis of base radar reflectivity and derived intensity of convective rainfall from the seasons and times of the day that are more conducive to UHI-induced circulation over a long period of time for a sub-tropical city is an innovative approach used in this study.

1.4 Hypothesis

It is hypothesized that with the increased urban cover in South Florida, Landsat-derived estimates would closely approximate increases in sensible heat flux and increases in land surface temperatures. Similarly, radar-based estimates would reveal an enhancement of convective rainfall in urbanized South Florida.

1.5 Objectives

Specific objectives of this study are to:

1) analyze land use land cover change in South Florida representing different stages of post-drainage conditions
2) analyze UHI in south Florida on land surface and surface layer atmosphere levels for the same temporal coverage as used for land use land cover change analysis

3) estimate surface energy balance and evaluate its temporal and spatial variation

4) examine the effect of any UHI on convective rainfall in South Florida

1.6 Structure of the Dissertation

The dissertation is organized into five chapters. Chapter one is the introduction of the study that incorporates the background, problem statement, study significance, hypothesis, objectives of the study, and the organization of the manuscript. The chapter generally outlines the conceptual framework of the entire study and attempts to address how the current study advances the existing knowledge of land use impacts on sensible weather. Chapters two to four address the findings of objectives two to four, respectively, and chapter five contains conclusions and recommendations.

Chapter two to four are each organized into introduction, study area and dataset, methods, results and discussion, and conclusion and recommendations sections. The introduction overviews the research questions and statement of problem, refers to previous findings, and sketches a route along which the current study takes the research further. The study area and data set section describes the South Florida from the perspective of corresponding objectives including the source and type of the data. The methodology sections basically outline the details of how the data are processed and fed into the algorithm, what algorithms are used, how the results are prepared and what statistical techniques are used to interpret the results. The results and discussion sections present the findings of the study in textual, graphical, and tabular forms and discuss how the current results are relevant in terms of specified objectives. A connection with the previous

findings and any improvements from there are also included. The last section makes remarks on the major findings and suggests a direction for future studies.

The final chapter is the conclusions and recommendations which links the conclusions from individual chapters in order to address the broader quest of how land cover change in South Florida affects its microclimate. Whether the methods adopted performed well, and if not, the limitations that restricted the performance of the model are identified. The same chapter sheds light on what the future directions of research should be guided by the conclusions and limitations of the current study.

1.7 References

Abtew, W., J. Obeysekera, M. Ortiz, D. Lyons, A. Reardon (2003) Evapotranspiration estimation of South Florida, *Technical Paper EMA # 407, Proceeding of the World Water and Environmental Resources Congress 2003*, Symposium on Integrated Surface and Groundwater Modeling, ASCE Conference at Philadelphia, PA, June 22-26, 2003

Ashley, W.S., M.L. Bentley, J.A. Stallins (2012) Urban induced thunderstorm modification in the Southeast United States. *Climatic Change,* **113**: 481-498. DOI: 10.1007/s10584-011-0324-1.

Arya, S.P. (2001) *Introduction to Micrometeorology*, i*nternational geophysical series,*36, edited by R. Dmowaska, J. R. Holton, and H. T. Rossby, Academic Press, New York.

Balling, R.C., Jr., and R.S. Cerveny (1987) Long-term associations between wind speeds and the urban heat island of Phoenix, Arizona, J. Climate Appl. Meteor., **26**, 712-716

Bornstein, R. D. (1968) Observations of the urban heat island effect in New York City. *Journal of Applied Meteorology*, **7** (4), 575-582.

Bornstein, R. and Q. Lin (2000) Urban heat islands and summertime convective thunderstorms in Atlanta: Three case studies. *Atmos. Environ.,* **34,** 507–516.

Changnon, S.A. (1962) A climatological evaluation of precipitation patterns over an urban area. In *Air Over cities*, *Technical Report* A 62-5, Washington DC: US Public Health Service, 37-67.

Collier, C. G. (2006) The impact of urban areas on weather, *Quarterly Journal of the Royal Meteorological Society,***132** 1-25.

Dixon, P.G. and T.L. Mote (2003) Patterns and causes of Atlanta's urban heat island initiated precipitation, *Journal of Applied Meteorology,* ***42***, 1273-1283.

Draxler, R.R. (1986) Simulated and observed influence of the nocturnal urban heat island on the local wind field, *J. Climate Appl. Meteor.*, **25**, 1125-1133.

Duever M.J., J.F. Meeder, L.C. Meeder, J.M. McCollom (1994) The climate of South Florida and its role in shaping the Everglades ecosystem, in *Everglades: The Ecosystem and Its Restoration*, edited by Steven Davis and John Ogden, CRC Press, Boka Raton FL, 860 pp.

Hjemfelt, M. R. (1982) Numerical simulation of the effects of St. Louis on mesoscale boundary layer airflow and vertical motion: Simulations of urban vs. non-urban effects. *J. Appl.Meteor.,* **21,** 1239–1257.

Huff F.A., and J.L. Vogel (1978) Urban, topographic and diurnal effects on rainfall in the St. Louis region, *J. Appl. Meteor.*,**17**, 565-577.

Hand, L. and J. M. Shepherd (2009) An investigation of warm season spatial rainfall variability in Oklahoma City: possible linkages to urbanization and prevailing wind, *Journal of Applied Meteorological Climatology*,**48,** 251-269.

Inoue, T., F. Kimura (2004) Urban effects on low-level clouds around the Tokyo metropolitan area on clear summer days, *Geophysical Research Letters,* **31**(5), doi:0.1029/2003GL018908.

Kalnay, E., M. Cai (2003) Impact of urbanization and land-use change on climate, Nature, **423(6939),** 528-531.

Karl, T.R., H. F. Diaz, and G. Kukla (1988) Urbanization: Its detection and effect in the United States climate record, *J. Climate*, **1**, 1099-1123.

Kaufmann R K, Seto KC, Schneider A, Liu Z, Zhou L,WangW, (2007) Climate response to rapid urban growth: evidence of a human-induced precipitation deficit, *Journal of Climate,* **20,**
2299- 2309.

Landsberg, H.E. (1970) Man-made climatic changes, *Science,* ***170*** (3964), 1265-127455.

Marshall, C.H., R.A. Pielke, L.T. Steyaert, and D.A. Willard (2004) The impact of anthropogenic land cover change on the Florida Peninsula sea breezes and warm season sensible weather, *Monthly Weather Review*, **132**, 28-52.

McGuffie, K., A. Henderson-Sellers, H. Zhang, T. B. Durbidge, A. J. Pitman (1995) Global climate sensitivity to tropical deforestation, *Global and Planetary Change,* **10**, 97-128.

McVoy, C.W., W.P. Said, J. Obeysekera, J.A. VanArman, and T.W. Dreschel (2011) Phases of Everglades drainage, 1880s to early 1950s, in *Landscapes and Hydrology of Pre-drainage Everglades*, University Press of Florida, Gainesville Fla.

Melesse, A.M., V. Nangia, X, Wang, and M. McClain (2007) Wetland restoration response analysis using MODIS and groundwater data, *Sensors,* 7(9)1916-1933.

Niyogi, D., P. Pyle, M. Lei, S.P. Arya, C.M. Kishtawal, M. Shephard, F. Chen, and B.Wolfe (2011) Urban modifications of thunderstorms: An observational storm climatology and model case study for the Indianapolis Urban Region, *Journal of Applied Meteorology and Climatology,* **50**, 1129-1144.

Karl, T.R., H. F. Diaz, and G. Kukla (1988) Urbanization: Its detection and effect in the United States climate record, *J. Climate*, **1**, 1099-1123.

Li, F.; T. J. Jackson, W. P. Kustas, T. J. Schmugge, A. N. French, M. H. Cosh, R. Bindlish (2004) Deriving land surface temperature from Landsat 5 and 7 during SMEX02/SMACEX. *Remote sensing of environment***, 92** (4), 521-534.

Lo, C.P., D.A. Quatrochi, and J.C. Luvall (1997) Application of high resolution thermal infrared remote sensing and GIS to assess the urban heat island effect, *Int. J. Remote Sens.*, **18**, 287-304

Morris, C.J.G., I. Simmonds, N. Plummer (2001) Quantification of the influences of wind and cloud on the nocturnal urban heat island of a large city, *Journal of Applied Meteorology,* **40**: 169–182.

Oke T.R. (1973) City size and the urban heat island, *Atmos. Environ.*, **7**, 769-779.

Oke, T.R. (1978) *Boundary Layer Climates*, 372 pp, Methuen and Co Ltd, New York.

Pielke, R.A. (1974) A three-dimensional numerical model of the sea breezes over south Florida, *Monthly Weather Review,* **102**, 115–139.

Runnalls, K.; T. Oke (2000) T. Dynamics and controls of the near-surface heat island of Vancouver, British Columbia. *Physical Geography,* **21** (4), 283-304.

Shepherd, J. M. (2005) A review of current investigations of urban-induced rainfall and recommendations for the future, *Earth Interactions,* **9,** 1-27.

Shepherd, J.M. and S.J. Burian (2003) Detection of urban induced rainfall anomalies in a major coastal city, *Earth Interactions,* **7** (4), 1-17

Shepherd, J.M., H. Pierce, and A.J. Negri (2002) Rainfall modification by major urban areas: Observations from spaceborne rain radar on the TRMM satellite, *Journal of Applied Meteorology,* **41,** 689–701.

Sklar, F.H., H.C. Fitz, Y. Wu, R. Van Zee, and C. McVoy (2001) South Florida: The reality of change and the prospects for sustainability: the design of ecological landscape models for Everglades restoration, *Ecological Economics*, **37**(3):379-401.

United Nations, Department of Economic and Social Affairs, Population Division (2014) *World Urbanization Prospects: The 2014 Revision, Highlights*, Available at: http://esa.un.org/unpd/wup/Highlights/WUP2014-Highlights.pdf. Accessed May 20, 2015.

Vukovich, F. M., and J. W. Dunn (1978) A theoretical study of the St. Louis heat island: Some parameter variations, *J. Appl. Meteor.,* **17,** 1585–1594.

Walker, R. T., Solecki, W. D. and C. Harwell (1997) Land use dynamics and ecological transition the case of South Florida, *Urban Ecosystems*, **1**, 37-47.

Wu, J. (2010) Urban Sustainability: an inevitable goal of landscape research, *Landscape Ecol.*, **25**, 1-4

Chapter 2

Delineation of Urban Heat Island in South Florida Using Land-Based Stations, Radiosonde Profiles, and Landsat Imagery

Kandel, H., A.M. Melesse, and D. Whitman (2015) Delineation of the Urban Heat Island in South Florida Using Land-Based Stations, Radiosonde Profiles, and Landsat Imagery, (submitted)

Abstract

Decades-long effects of drainage and development in south Florida that began in early to mid-20th century have resulted in the loss of natural forested lands and rangelands, and expansion of agricultural and urban areas. These land cover changes have brought a change in the thermalscape of the surrounding areas. The surface and near surface layers become drier and warmer in anthropogenic land covers compared to the natural ones, introducing an effect called the Urban Heat Island (UHI). The present study aims to delineate the spatial and temporal existence of the UHI on the land surface and near surface atmosphere during the summer using land use/land cover data, surface based weather station records, radiosonde profiles, and Landsat–5 TM images mainly after 1970's in south Florida. Urban cover is increased by ≈10% from 1974 to 2011. Stations in and around urban and agricultural covers are found with higher daily minimum temperatures ($\Delta T_{u\text{-}r}$ = 4°C) showing gradual increase through time. Decreasing near surface diurnal temperature range (DTR), and heightening lifting condensation level (LCL) (-~1°C DTR, p=0.005 and > 20 m increase in LCL) are detected from Miami radiosonde. Higher Landsat-derived land surface temperatures (LST) for urban stations ($\overline{LST}_{u-r}$ =2.8°C) and satisfactory validation results from the eastern urban stations (NSC =0.70, R^2=0.79) further substantiate the findings on UHI explored by the observed data.

Keywords: UHI; Radiosonde; Landsat; LST, Atmospheric Surface Layer; Lifting Condensation Level; Land Use/ Land Cover; south Florida

2.1. Introduction

Since the second half of the 20th century, there have been dramatic changes in the land use of south Florida. Drainage of Everglades has altered south Florida from a subtropical wetland to a landscape dominated by anthropogenic activities. Suffering from fragmentation, drying, vegetation loss, wetland shrinkage, anthropogenic land expansion and consequent environmental degradation, south Florida now hosts the world's largest wetland restoration project (Sklar et al., 2001). Beginning extensively in the mid-20th century, anthropogenic alteration of land cover is still an ongoing phenomenon in south Florida. Removal of vegetation cover, change in land use options, and introduction of urban fabrics greatly influence the urban micro-climates (Stabler et al., 2005). The post-drainage urbanization and crop land expansion in south Florida have made the region an ideal study site for examining the human influence on micro-climate. Human-modified areas, particularly, the urban built-up and agricultural covers tend to accumulate large heat content because of their low albedo and reduced emissivity. Stored heat is released later through conduction and convection, warming the surrounding environment Collier, 2006). Resulting higher temperatures in the urban environment compared to their rural counterpart is an immediate effect called the urban heat island (UHI). The dryness caused by UHI on the surface heightens the lifting condensation level (LCL) in the boundary layer characterized by the height at which an ascending air parcel from the surface first becomes saturated. The persistence of this dryness during the evening depends on how much heat was stored during the day, because after sunset net radiative loss of energy

from the surface forms a temperature inversion (Arya, 2001). Therefore, the LCL in early to late evening hours can be used as an approximation of the day-time strength of an UHI.

After the initial recognition of the UHI by Howard (Howard, 1818), the effect has been documented in several studies from various cities around the world (e.g., Balling and Cerveny, 1987; Bornstein, 1968; Bornstein and Lin, 2000; Chow and Svoma, 2011; Collier, 2006; Dixon and Mote, 2003; Draxler, 1986; Lo et al., 1997; Morris et al., 2001; Oke, 1973; Stewart and Oke, 2012). Lower specific heat and higher thermal conductivities of impervious land surfaces and anthropogenic materials than that of rural areas, reduced evapotranspiration from dry areas, and additional heat discharge from human activities are considered to be the main factors contributing to the development of the UHI (Kato and Yamaguchi, 2007). Stone, concrete, asphalt and deeper compacted soil layers of the city decrease heat capacities, but increase heat conductivities compared to water and vegetation. Peak of diurnal surface temperature wave on a sunny day attenuates at a depth of 20 – 40 cm from the surface under a light vegetation cover, whereas the equivalent peak in compacted pavement penetrates to 80-100 cm (Landsberg, 1981). Rapid runoff of precipitation and reduction in evaporation that characterizes an urban area is also equivalent to heat gain. Local heat produced from fossil fuel burning; air-conditioning units; and metabolic activities of human and animals also contribute to additional heat production (Oke, 2002).

Apart from the thermo-physical inputs, (Landsberg, 1970) mentions that reduced wind speed by increased aerodynamic roughness together with reduced albedo caused by insolation trapping by tall buildings in cities also intensifies the UHI. Addition of a

building in a landscape modifies the radiative, thermal, and aerodynamic environment of the surrounding and redistributes its moisture status. Radiative effects occur in the form of local increases and/ or decreases of short wave and long wave radiations. Areas in shadow receive less solar radiation, sunlit walls reflect the sunlight thus increasing solar receipt locally, and surfaces near the building reduce net long-wave cooling by decreasing upwelling long-wave radiance from reduced sky view factor and by increasing down-welling long-wave radiance from warmer buildings (Oke, 2002). In contrast, in vegetated rural areas, there is loss of incoming radiation in the routes of reflection, and evapotranspiration thereby leaving less radiation for surface heating.

The existence of an urban heat island affects the city residents in number of ways. It contributes to the cooling load; and increases thermal discomfort, and air pollution. The UHI have also proven to be an inducing factor for convective rainfall in the cities, thus changing the local hydrology (Changnon, 1968; Landsberg, 1970; Huff and Changnon, 1972; Shepherd and Burian, 2003).

Considerable research over many years have quantified micrometeorological impact of land cover using surface-based weather station measurements (Karl et al., 1988; Tarleton and Katz, 1995) remote sensing based estimates (Gallo et al., 1993; Balling and Brazel, 1988; Kim, 1992; Roth et al., 1989) and modeling approaches (Baik, 1992; Baik et al., 2001). While the simple difference in air temperature from urban and rural stations may express the existence of an UHI, the magnitude of the difference and its spatio-temporal pattern is needed to discern the intensity, distribution and evolution of the impact. Weather stations are point measurements which do not reflect the wide range of surface properties, and also their records may be location biased particularly for airport stations.

Modeling of the influence of landscape change from pre-1900 to 1993 land cover conditions on sensible weather in Florida found modifications of latent and sensible heat fluxes and thermally induced sea breeze circulation (Marshall et al., 2004; Pielke et al., 1999). Appropriate parameterization of land use/ land cover in land surface models is a big challenge. Characterization of small scale complexities in urban surfaces such as pitched roofs, variable building height, and urban vegetation is not possible in numerical models because of inadequate grid resolution, which the spatial models can depict well with advanced descriptions (Voogt and Oke, 2003). Also, an incomplete understanding of whether models capture the contrast between natural and anthropogenic land cover in sufficient detail is another hindrance of coupled land surface -atmospheric regional models (Pielke, et al., 2011). The model accuracy always has to be compromised with its simplicity.

In the present study, we delineate anthropogenic heat island in south Florida utilizing three different sources of data: meteorological station records, radiosonde observations, and Landsat 4-5 Thematic Mapper imageries. The approach captures the space-time variability of land surface properties, surface and near-surface air temperatures, and resulting modifications on atmospheric surface layer. The findings of (Oke, 1979) that the influence of micro-scale features related to land use and building density prevail in the internal pattern of the heat island of cities also motivates the present study. Following the suggestions made in recent works (Hawkins et al., 2004), the study also investigates the variability of rural temperature fluctuations so that estimates of the magnitude of the UHI signatures could be complemented. High spatial density of weather station distribution in south Florida, and availability of nearly 30 years of satellite observations

are two key factors that support the approach used in the current study. The specific objectives are to (1) analyze Landsat era land use/ land cover patterns in south Florida and quantify its change through time, (2) analyze the pattern and evolution of surface, and near surface air temperature and atmospheric surface layer structure in south Florida, and (3) compare urbanization and its signature on temperature, thus delineate the development of UHI. The study is distinctive in the sense that previous works on UHI have paid less attention to coastal cities attributing coastal breezes to neutralize the UHI intensity. Use of high resolution spatial data can delineate micro-scale development of the UHI within land areas which are not affected much by the coastal breezes.

2.2 Study Area and Dataset

2.2.1 Study Area

South Florida (Figure 2.1) encompasses a total land area of 3,6000 km^2 bordered by Lake Okeechobee in the mid-North, the Gulf of Mexico in the West, Florida Bays and Keys in the South, and Atlantic Ocean in the East. Characterized by heterogeneous mosaics of surface cover types, south Florida comprises a prominent wetland basin, the Everglades; tall pine, cypress and dwarf forests; agricultural crop and rangeland; natural and artificial lakes, and impoundments; estuaries and coastal landforms; and urban developed areas. The eastern part encloses the most populated cities of south Florida, Miami, Fort Lauderdale and West Palm Beach. Total estimated population of three eastern urbanized counties Palm Beach, Broward and Miami-Dade in 2013 was 5.7 million (US Census Bureau), a 70% increase from 1980.

Hydrology is a major determinant of community and landscape structure in south Florida connecting natural and man-made systems (Obeysekera et al., 1999). South Florida is

characterized by subtropical climate with less variation in summer to winter temperature (mean maximum daily temperatures range: 22°C to about 30°C) in comparison with the high seasonality and spatiality of rainfall (average annual rainfall of 152 to 165 cm in Atlantic coastal ridge and 88 to 114 cm in the Florida Keys).

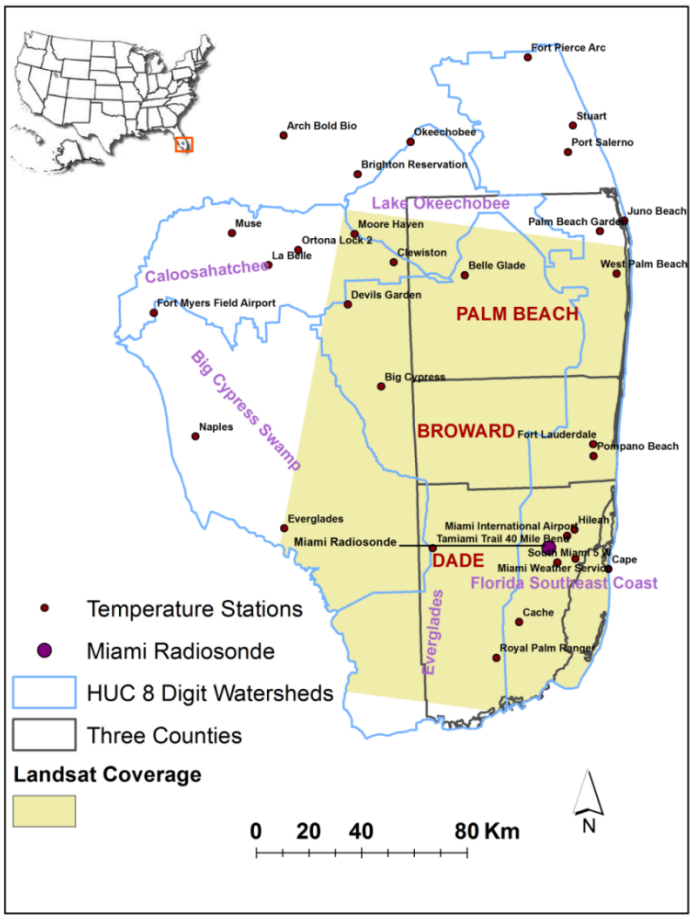

Figure 2.1 Map of study area basins showing locations of data stations, focused counties, and Landsat image coverage in South Florida.

2.2.2 Dataset

An analysis of the UHI becomes complete when it incorporates the land use pattern in space, its evolution through time, and associated changes in surface and boundary layer temperature. The data for the surface and near surface air temperature distribution for

each land use categories, and boundary layer temperature profile through time were acquired as discussed below.

2.2.2.1 Land Use/Land Cover

Three land use/ land cover datasets from south Florida for the years 1974, 1992, and 2011 are employed in this analysis. Land use of 1974 represents the historical land use/ land cover data of 1970s. The United States Geological Survey (USGS) originally collected these data using base maps and images from the 1970s and later modified and edited by USGS and US Environmental Protection Agency (USEPA) to produce the enhanced version (Price et al., 2006). The USGS used 1:250,000 scale topographic maps as base maps and NASA high altitude aerial photographs and National High-Altitude Photography program's air photos usually at scales smaller than 1:60,000 as land use source data (Links, 1999). The land use land cover classification standards follow the USGS Land Use/ Land Cover (LU/LC) classification format. The USGS format uses the Anderson level I classification system (Links, 1999), which classifies south Florida land cover into the following LUCODE 1 classes: Urban/built up, Agriculture, Rangeland, Forest, Water, Wetland, and Barren. The system has a hierarchical system of classification such that LUCODE 2s are the subclasses of LUCODE 1.

National Land Cover Dataset (NLCD) of 1992 and 2011 are the two other datasets used for the comparative analysis. The NLCD is considered as an update to the intermediate scale land use and land cover dataset developed in 1970s (Vogelmann et al., 2001)]. Both of these data have a 30 m spatial resolution and are derived primarily from the Landsat-5 TM. The classification system of NLCD follows a consistent hierarchical approach

defining 18 classes of land cover across south Florida which later merged into seven major classes to enable comparison with 1974 land use.

2.2.2.2 Near-Surface Air-Temperature

Historical temperature records for different length of time periods are available in several South Florida meteorological stations. Only a few of the stations have data since early 1900, many of them have post-drainage era data and a very few have short temporal range covering time only after 1990. These data have been used in studies of climate anomalies, and long-term temperature trend in several previous studies (Duever et al., 1994, Mitchell, 1912). However, there is a dearth of studies that used this temperature record for the detection of urbanization. Seasonal variation of the magnitude of nocturnal UHI is reported to be greatest in the summer because of the fact that rural cooling rates are more than twice as great in summer compared to winter (Runnalls and Oke, 2000). The present study uses the six-month daily minimum temperatures covering extended summer period (May to October) for four stations for the purpose of time series analysis and for 29 stations for the purpose of spatial interpolation over South Florida obtained from Global Historical Climatology Network (GHCN).

2.2.2.3 Radiosonde Measurements

A radiosonde measures the vertical profile of pressure, temperature, humidity, wind speed and direction and can be used to validate the satellite data as well as the prediction model. The present study acquired data from NOAA's Integrated Global Radiosonde Archive for the Miami station (72202) located at 25.75° North latitude, 80.38° West longitude, 5 m elevation. A radiosonde captures the vertical profiles twice a day at or around 0000 and 1200 UTC. The present study uses base level potential temperature of

July sounding at or around 800 and 2000 local time, and base level temperature and relative humidity of 2000 local time of June, July, and August sounding. The evening sounding is considered useful because the local time in Miami during that hour closely corresponds with the reported time of sharp heat island intensity, i.e., three to five hour after sunset (Oke, 1982).

2.2.2.4 Landsat Imagery

Several studies have utilized satellite derived temperature for urban climate analyses. The prospect of urban area identification using satellite derived data was first demonstrated by (Rao, 1972). Retrieval of surface temperature in moderate resolution has become possible after the addition of thermal bands in Landsat (Vinukollu et al., 2011). Band 6 of Landsat is the thermal infrared channel (10.4 –12.5 μm) that measures the upwelling longwave radiance from the surface and atmosphere. Land surface temperature is the portion of that radiance after atmospheric and emissivity corrections are applied.

The thermal band of the Landsat has eight bit radiometric resolution, 120 m spatial resolution, a 10.4 to 12.5 μm spectral bandwidth, and a 16 day overpass cycle. Previous work has estimated the accuracy of estimated LST to be within 1°C (Li et al., 2004). Established accuracy from previous temperature estimations, spectrally close to the Earth's maximum irradiating wavelength zone (λ_{max}= 9.7 μm), ability to use half-a-month temporal change, and moderate spatial resolution enabling the analysis for smaller land cover units make Landsat an adequate remote sensor the present study. In addition, Landsat 5 TM is advantageous because of its nearly three decades of data since 1984. USGS Climate Data Records' (CDRs) surface reflectance products are the dataset used in the analysis. These data are long-term, consistently processed datasets consisting of two

important land surface parameters: land surface reflectance for band 1-5 and 7, and brightness temperature for band 6. The CDR surface reflectance products are atmospherically corrected Landsat data using an algorithm called Landsat Ecosystem Disturbance Processing System (LEDAPS) (Schmidt et al., 2013). The acquired Landsat images (Row 15 and Path 42) cover most of the parts of the three eastern counties: Miami Dade, Broward, and Palm Beach (Figure 2.1). Two eastern watersheds in South Florida: Everglades towards the west and Florida Southeast Coast towards the east are used to extract LSTs for the comparison between different land cover categories. The selected dates of Landsat CDR imageries along with percentage cloud free pixels obtained from cloud mask processing are presented in Table 2-1.

2.3. Methods

This section outlines the processes implemented for data processing, algorithm use, output preparation and results validation.

2. 3.1 Summer Minimum Temperature Analyses

The near surface atmospheric temperature is the primary indicator that reveals the effect of the UHI on sensible weather. Influences of urbanization on temperature within United States are imprinted well on minimum (compared to maximum or mean) temperature records (Karl et al., 1988). The study used daily minimum temperature obtained from Global Historical Climatology Network stations located in south Florida for the month May to October to calculate the average of minimum temperatures for each of these months from 1968 to 2012. Average temperatures from each station for each summer

Table 2-1 Selected Landsat CDR imageries with percentage cloud free pixels obtained from cloud masking.

Date	Percent Cloud-Free	Date	Percent Cloud-Free	Date	Percent Cloud-Free
05/07/1984	68.53	10/15/1990	87.77	06/20/2000	69.93
07/10/1984	66.94	06/28/1991	67.71	07/06/2000	78.74
09/02/1986	72.83	05/16/1993	82.81	05/6/2001	67.05
04/30/1987	97.47	07/03/1993	74.74	08/10/2001	70.71
10/07/1987	94.61	08/04/1993	73.73	08/26/2001	77.72
05/18/1988	82.01	05/06/1995	97.02	05/30/2004	90.89
06/03/1988	96.71	05/22/1995	76.65	05/04/2006	99.57
08/22/1988	74.79	08/12/1996	75.6	05/20/2006	81.52
09/23/1988	82.5	09/13/1996	84.23	09/25/2006	90.96
10/09/1988	70.27	05/14/1998	93.43	10/11/2006	89.86
10/25/1988	83.53	06/15/1998	84.8	07/10/2007	70.55
05/21/1989	85.71	05/17/1999	61.74	10/03/2009	90.16
06/06/1989	54.94	09/22/1999	73.4	10/19/2009	77.55
07/08/1989	65.34	10/24/1999	97.2	06/16/2010	69.75
07/27/1990	60.61	05/19/2000	60.19		

were later averaged for each decades centering in 1974, 1982, 1992, 2002, and 2012. The resulting averages were interpolated using the ordinary Kriging geostatistical method in geostatistical analysis wizard of ArcGIS. Eventually, temperature prediction maps were produced. There were total 19 stations available to interpolate for 1974, 1982, 1992, and 2012 with additional four stations for 2002. A semivariogram model was used with default model parameters. The values of nugget ranged from minimum of 0.12 for 2002 to maximum of 1.10 for 1992. Similarly, lag size was lowest (0.06) for 2002 and highest (0.21) for 1974. A very small variation in these model calculated parameters between years allowed to confidently compare the interpolated temperatures with acceptable accuracy.

Also, summer averages of daily minimum temperatures from the four stations representing mainly of highly urbanized (Miami International Airport), wet and forested (Big Cypress), city surrounded by natural cover (Naples), and agricultural cover (La Belle) (Appendix 1) were plotted. Along with these station plots, trend of May-October average global temperatures between 1974 and 2012 was also shown. Percentage of each major land cover class within the radii of ten kilometer surrounding area was considered when categorizing the stations for dominant land cover type.

2.3.2 Surface Layer Atmosphere

Base level (in the range of three to seven meters) potential temperature from morning and evening (UTC 0000 and 1200 hours) soundings for each July was averaged over 1974-2010. Only July was chosen because that is the central month of the study season. The difference between evening and morning soundings provides a quasi-diurnal temperature range. The lowest level observed temperature and relative humidity from radiosonde were employed to compute the dew point temperature, and in turn, the lifting condensation level. Because the variation in altitude of LCL means the variation of cloud-base heights in the surface layer, which in turn is affected by the underlying surface cover (Rabin et al., 1990), altitude of LCL variation for the evening hour over the study period was calculated as a surrogate of surface layer height using (1) and averaged for each summer.

$$LCL = 125\ (t - t_d) \tag{1}$$

where t and t_d are the surface level ambient and dew point temperatures, respectively. Since there are no humidity data available between the years 1988 to 1992, LCL height could not be computed for those years. The average lowest level temperature and relative

humidity from all summer evenings (June to August) were used to calculate LCL height for the corresponding summer.

2.3.3 Derivation of Land Surface Temperature from Landsat

The surface reflectance CDR data were accessed from the USGS Earth Explorer website: http://earthexplorer.usgs.gov/. The step-wise procedure applied for LST estimation was as follows:

i) Application of cloud masking algorithm in the level 1 products

ii) Derivation of land surface emissivity

iii) Estimation of land surface temperature

2.3.3.1 Application of cloud masking algorithm

Surrounded by major water bodies in all four sides, the sky over the land of south Florida is widely known for its notorious cloud cover. The cloud and cloud shadows are the significant sources of noise causing imperfect atmospheric corrections, and introducing biases in land surface temperatures (Irish, 2000). Landsat images of south Florida particularly during summer need to be cloud masked before LST estimation.

The present study has employed an algorithm called "Fmask (function of mask)" (Zhu and Woodcock, 2012). The algorithm Fmask computes the cloud mask, and cloud shadows. Spectral images of all seven bands and metadata (MTL) file are the input data and a classified image with five classes: clear land, clear water, cloud shadow, snow and cloud are the output from this automated algorithm. Fmask also reports the overall percentage of clear pixels in the image. It has been found to be more accurate compared to other automated methods with overall accuracy of 96.41% (Zhu and Woodcock, 2012).

2.3.3.2 Emissivity Estimation

Out of several methods available, this study used the normalized difference vegetation index (NDVI) threshold method proposed by (Sobrino and Raissouni, 2000; Sobrino et al., 2008) to compute land surface emissivity (LSE). The method takes two NDVI values: 0.2 and 0.5 as lower and upper thresholds in order to distinguish between vegetation free, mixed and fully vegetated pixels. The algorithm used to derive the composite emissivity is

$$LSE = \begin{cases} a + b\rho_{red}, & NDVI < 0.2 \\ \varepsilon_v P_v + \varepsilon_s (1 - P_v) + C, & 0.2 \le NDVI \le 0.5 \\ \varepsilon_v + C, & NDVI > 0.5 \end{cases} \quad (2)$$

where, a and b are spectral statistical fit coefficients (a= 0.980, and b = -0.042) as used in Advanaced Very High Resoultion Radiometer (AVHRR) channel 4 (Sobrino and Raissouini, 2000), and ρ_{red} is the reflectivity of the red band (equivalent to channel 1 of AVHRR). The emissivities $\varepsilon_{s,}$ and ε_v for non-vegetated and fully vegetated pixels were used from the literature as 0.97 and 0.985, respectively. The term C accounts for the cavity effect which depends on the surface characteristics and takes into account the internal reflections (i.e., C = 0) for homogenous flat surfaces. In this case, C was obtained as average of the value used by Sobrino and Raissouini (2000) from Channel 4 and Channel 5 of AVHRR, and found equal to 0.016-0.012Pv. The variable P_V is the proportion of vegetation and was computed as in equation (2) for the pixels with NDVI intervals between 0.2 to 0.5, setting 0 and 1 for below and above threshold pixels according to Carlson and Ripley (Carlson and Ripley, 1997) (Appendix 2).

$$Pv = \left(\frac{NDVI - NDVIs}{NDVIv - NDVIs}\right)^2 \quad (3)$$

$NDVI_s$ and $NDVI_v$ are NDVI values for non-vegetated and fully vegetated areas, respectively. According to this method, the final equations of emissivity are:

$LSE = 0.980 - 0.042 \times \rho_{red}$ for non-vegetated areas (4)

$LSE = 0.986 + 0.003P_v$ for mixed pixel areas (5)

$LSE = 0.985 + 0.005$ for vegetated areas (6)

The composite emissivity for the layer was calculated combining individual emissivity obtained from (4), (5) and (6) using conditional function of raster calculator in ArcGIS.

2.3.3.3 LST Estimation and Validation

The brightness temperature obtained from Climate Data Record was corrected for the scale, and conversion to land surface temperature using land surface emissivity was carried out employing the method suggested by Weng (Weng and Schubring, 2004). For the purpose of excluding cloud, and cloud shadow pixels from the analysis, only clear land and clear water pixels (classes 0 and 1 of Fmask output) were assigned with their real values of reflectivity and brightness temperature setting nodata otherwise. Figure 2.2 shows the model in ArcGIS that was used to calculate LST using band 3, 4, and 6 of CDR surface reflectance product, and output grid of Fmask. The temperature thus obtained were in degrees centigrade.

The temperatures derived from landsat were validated against the observed temperatures. Two sources for observed records, the morning sounding of Miami radiosonde, and daily observed temperature of global historical climatology network from south Florida stations were used. Although the time difference and elevation difference between

modeled and observed data preclude a robust validation test, it would be reasonable to assume that the results become fairly representative in the absence of ground reference data. Commonly used statistical parameters Model bias, Nash-Sutcliffe coefficient, and coefficient of determination were used to check the performance of the model. A relationship between land use land cover and LSTs and their change through time were analyzed. The comparable dates in terms of cloud cover and days of the year were selected for the LST analysis so that influence of the variations of cloud cover and amount of incoming radiation between the dates can be minimized. A statistical comparison between observed temperature and extracted LSTs at sixteen different weather stations in south Florida on August 26, 2001 was carried out. Both the constraints of finding fairly clear image date and an availability of good number of station records were considered to pick this particular date.

2.4. Results and Discussion

This section explains and rationalizes the results of the spatiotemporal pattern of land use/ land cover, summer-minimum temperature, Landsat-derived LSTs; and temporal evolution of LCL in south Florida.

2.4.1 Land Use/ Land Cover

The polygonal area of land use vectors of the respective years were used for the quantitative comparison of land use/ land cover. Comparison was also made visually by using their rasterized maps (Figure 2.3).

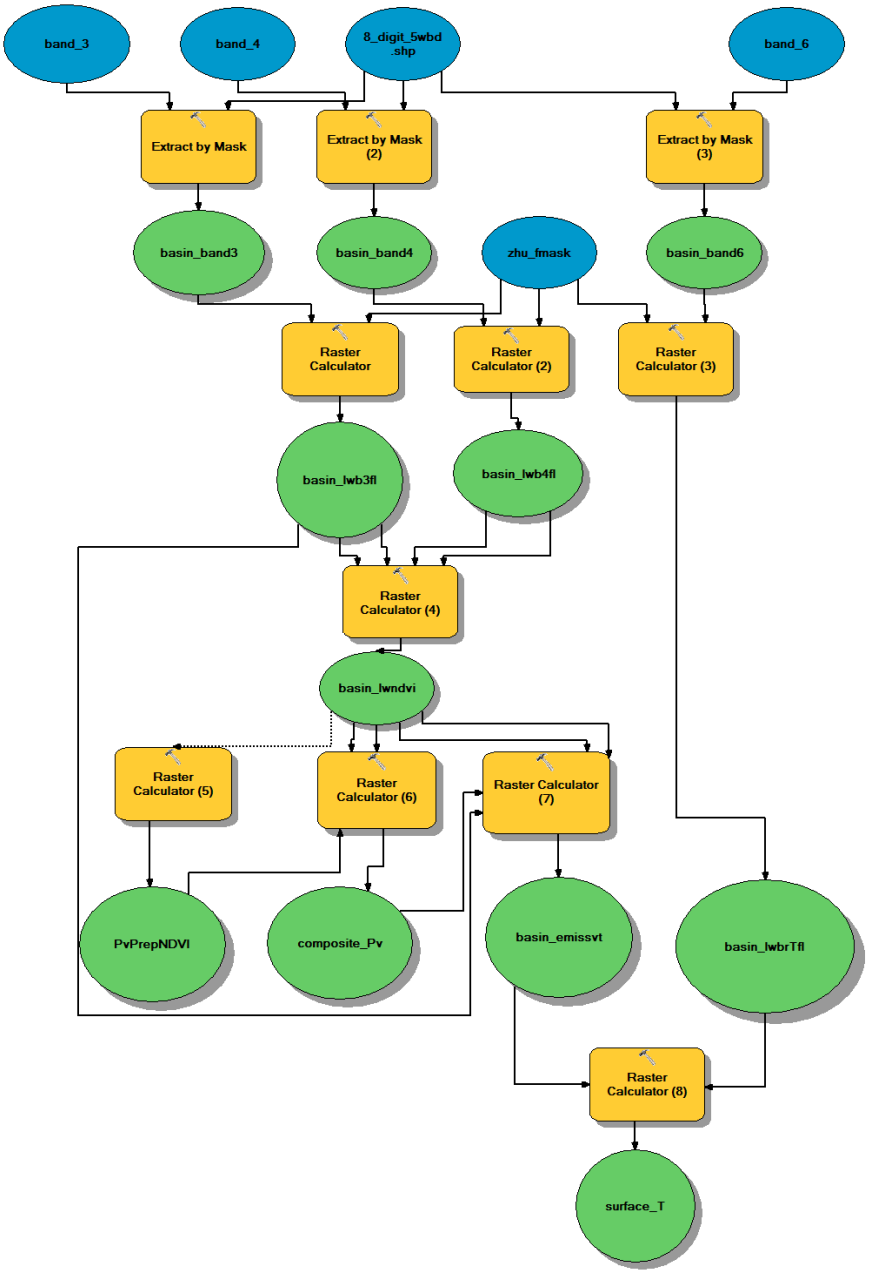

Figure 2.2 Graphic representation of LST model built in ArcGIS showing input data (blue ovals), processing tools (orange rectangles), and intermediate and final outputs (green ovals). The tools labelled as raster calculators 1, 2 and 3 conditionally evaluate the fmask grid and the basin reflectivity for band 3, 4 and 6, respectively. Ratser calculator 4 applies the NDVI algorithm. Raster calculator 5 calculates P_V as in eq. (3), and 6 evaluates the composite P_V. Raster calculators 7 and 8 calculate land surface emissivity and land surface temperatures, respectively.

Table 2-2 Comparisons of South Florida land use land cover by percentage coverage of major categories in 1974, 1992, and 2011.

LU/LC Class	1974 (%)	1992 (%)	2011 (%)
Developed	5.12	11.65	15.59
Agriculture	21.14	18.77	18.76
Barren	3.24	0.67	0.22
Forest	5.41	3.75	1.51
Range	14.65	8.34	2.29
Wet	34.97	45.46	52.64
Open Water	15.46	11.35	9.00

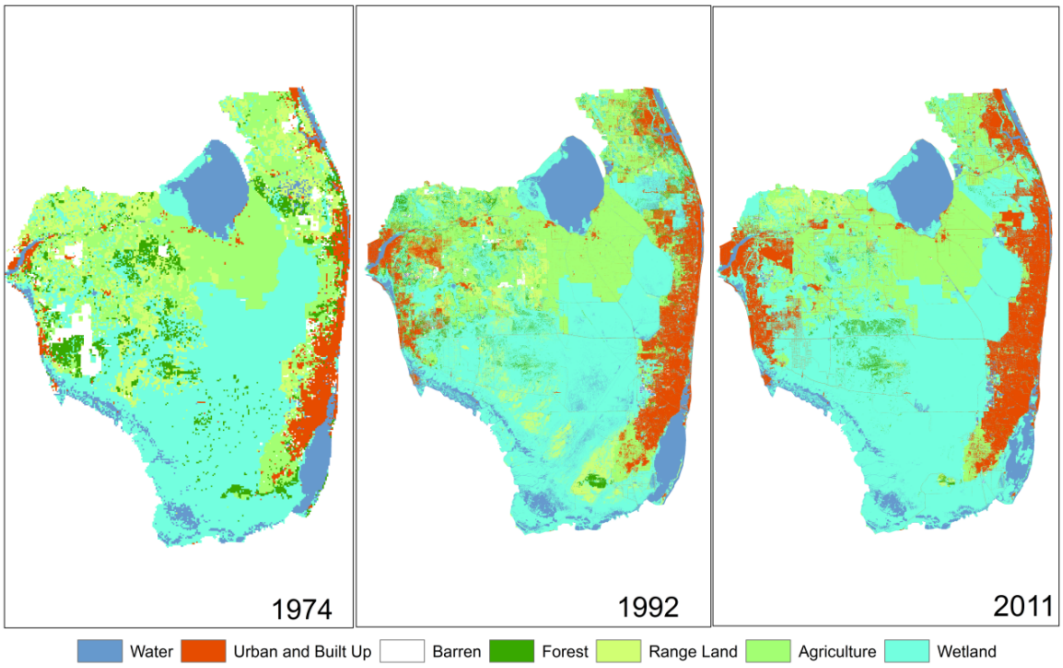

Figure 2.3 Land use land covers comparison in South Florida in 1974, 1992 and 2011.

Major land use/ land cover changes are found as the increase of urban and built-up (> +10%), and wetlands; and the decrease in rangeland and water cover (Table 2-2). Albeit in small extent, forest, barren, and agricultural covers have also been shrunk during this period. The majority of urban intensification is concentrated spatially in the eastern

coastal ridge. Urban expansion is found mainly in three forms: high density residential (> 5 dwelling units/ acre); transportation, communication, and utilities; and institutional. Some of the urban open lands, transitional lands, strip mines and quarries categorized as barren lands are found to be decreased. Figure 2.3 shows that the barren lands in the western part and agricultural lands in the eastern part are replaced by urban and built-up cover in 2011. The loss of agricultural land in the east, however, has been compensated by the transformation of rangeland in the western part of south Florida and eastern areas of Lake Okeechobee. The shrinkage in rangelands, whose principal cover is grass and forbs alongside seasonally inundated dense strand of shrubs, possibly has significant impact on surface thermal response. Expansion of wetlands and shrinkage of water cover in 2011 may have seemed so partly because of the declining water levels in lakes and estuaries in 2011 as that was relatively a dry water year. Modified classification algorithms: a slight modification in NLCD classification system (1992 and 2011) from Anderson Level I classification (1974), and slight change in the definition of woody wetland in 2011 (vegetation cover of > 20%) from that of 1992 (vegetation cover of > 25%) may have contributed for the apparent increase of wetland and decrease of open water particularly from Biscayne National Park.

2.4.2 Near-surface Air Temperature

Figure 2.4 compares the extent and the rate of change of long-term daily minimum temperature averaged for summer months plotted from different weather stations in south Florida representing various land cover (Appendix 1). Miami International Airport, in which the surrounding urban land cover within the radius of 10 km increased from 75% in 1974 to 88% in 2011, exhibits the highest minimum temperature. Naples, with a switch

of the dominant surrounding land cover from wet, water and forest (52% in 1974 to 42% in 2011) to urban, open, and disturbed (41% in 1974 to 57% in 2011), shows second highest minimum temperature. Likewise, La Belle which has a total 14% decrease in surrounding natural and agricultural covers and has about 12% increase in urban, open and disturbed lands between these two years exhibits the third highest minimum temperature. Small portion of urban land (1.6%) in its surrounding justifies the lowest minimum temperature at Big Cypress.

As shown by the linear trend, there is a slight increase of minimum temperatures (0.1 °C/decade, $p = 0.001$) at Miami International Airport, moderate increase (0.3 °C/decade, $p < 0.001$) at Naples, highest rate of increase (0.6 °C/decade, $p = 0.01$) at La Belle, and an insignificant trend ($p = 0.8$) at Big Cypress station. Naples and La Belle stations show higher than global average trend (0.1/decade, $p < 0.05$). La Belle, whose peripheral land cover showed a profound decrease of natural cover and increase (~12%) of urban cover from 1974 to 2011, contains more than 4% scrub/shrub. Urban increase and substantial share of natural cover by scrub/shrub perhaps contribute for the highest rate of temperature increase at La Belle as scrub/shrub departs from other vegetated lands in its thermal behavior.

The interpolated maps for the years 1974, 1982, 1992, 2002 and 2012 (Figure 2.5) show the variation in spatial and temporal distribution of the daily minimum temperatures. The prediction errors of interpolation are analyzed in terms of RMSE which are plotted on each map. Relatively lower values of RMSE suggest that the temperature prediction surface is an adequately accurate interpolation. Temperature patterns exhibit spatially lower values towards the west and gradual increase towards east and south east reaching

maximum in the Florida south east coast watershed, which is predominantly an urbanized sub-basin. Very obvious association between the near surface air temperature (Figure 2.5) and the land cover (Figure 2.3) is evident. Presence of higher temperature classes, (23-24) °C and (24-25) °C, in 2002 and 2012 that were almost absents in 1974 manifests the temporal increase. The temperature difference between eastern urbanized areas and western and northwestern natural areas ranges from 1°C to 3°C. Both, the trend of annual average temperatures and interpolation of 10-year average temperatures, reveal thermal impact of anthropogenic alteration of land cover.

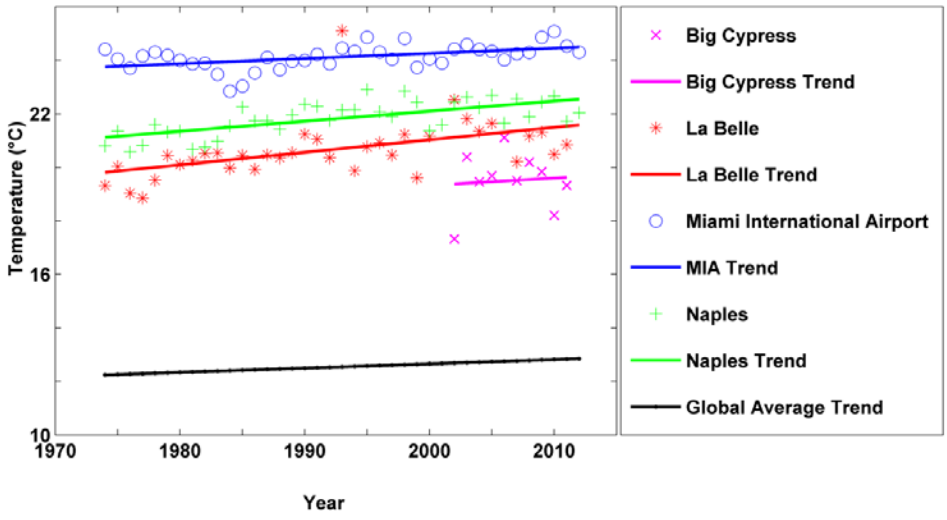

Figure 2.4 Mean annual summer-time daily minimum temperatures from stations in South Florida compared with global trend of summer minimum temperatures.

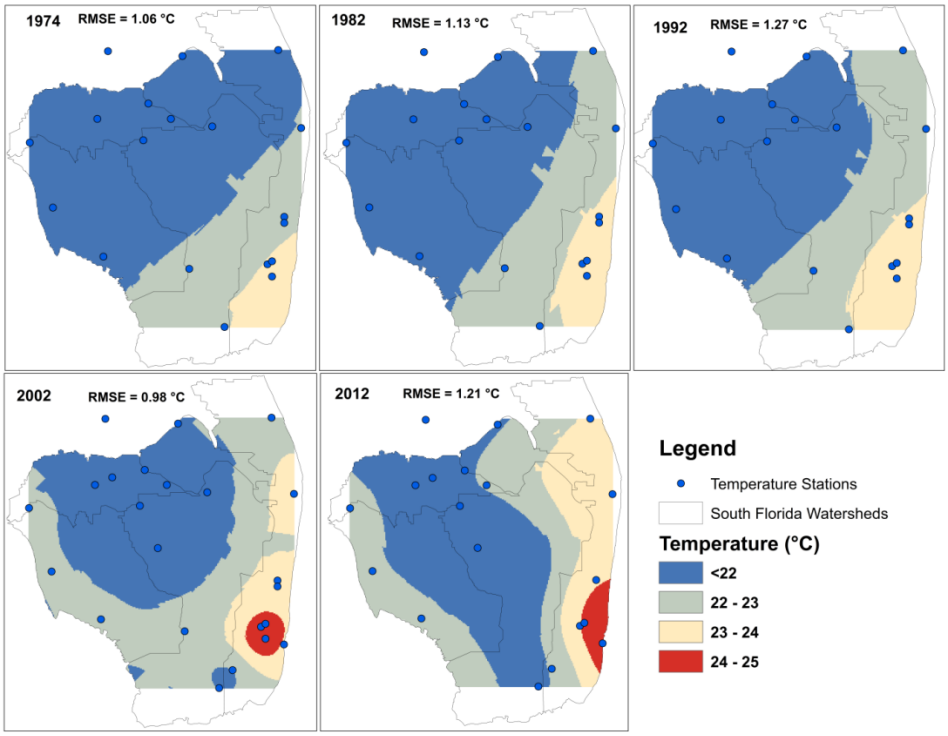

Figure 2.5 Comparison of summer-time daily minimum air temperatures in South Florida for the years: 1974, 1982, 1992, 2002, and 2012. Each year represents the central year for decadal average except for 2012 which is the average from 2007 to 2012.

2.4.3 Atmospheric Surface Layer

Variation of the computed height of LCL is a function of near-surface local variations of temperature and moisture. The height of the lifting condensation level is analogous to the depth of the atmospheric surface layer in the present study. A deep surface layer is considered unstable and the principal source of instability is the surface heat generating turbulence above it. In general, the altitude of the evening LCL is increasing (total increase of 21.1 m). Even though the LCL height averaged by summer fluctuates year-to-year, a continuous drop reaching minimum LCL level during the years 1984-1987 may be an influence of the large scale climatic events, such as El Nino, which brings wet weather. From 1982 to 1990, there were four El Nino years with the most intense in 1987 (Pielke et al., 1999). The general trend of LCL height is increasing all the time if we

exclude those records between 1984 and 1987. The rate of increase is pronounced with b_1 = 6.64 m/year (p = 0.05) over 1993 to 2012 (Figure 2.6). The positive slope of the trend line confirms with the previous findings that the warming and drying surface raises LCL height (Schreiber et al., 1996).

In addition, when lowest level temperature, which closely resembles ground surface temperature, in the evening, increases at the rate greater than that in the morning, it results in decreased diurnal temperature range. The trend of the July diurnal temperature range observed at the same Radiosonde station (Figure 2.6) is decreasing at the rate of 0.2°C per decade with p = 0.05 which may be linked directly with the development of UHI. The extreme low DTR in 1988 may be associated with the intense La Niña event during that year, which could cause rapid surface warming (Pielke et al., 1999).

The total increase in the depth of summer average LCL (> +20 m) and a decrease in the diurnal temperature range (< -1°C, p = 0.005) of July resulted from about four decades radiosonde records are consistent with Lidar based studies that showed the development of surface UHI influences its boundary layer height (Davies et al., 2004; Middleton et al., 2005). Although extensive observations are required throughout the day and season to predict the structure of planetary boundary layer over different types of land cover (Dabberdt et al., 2004), it is reasonable to assume that these results are fairly representative for urbanized south Florida. Furthermore, the result obtained here is very essential and symptomatic information to be incorporated in a UHI study of this kind.

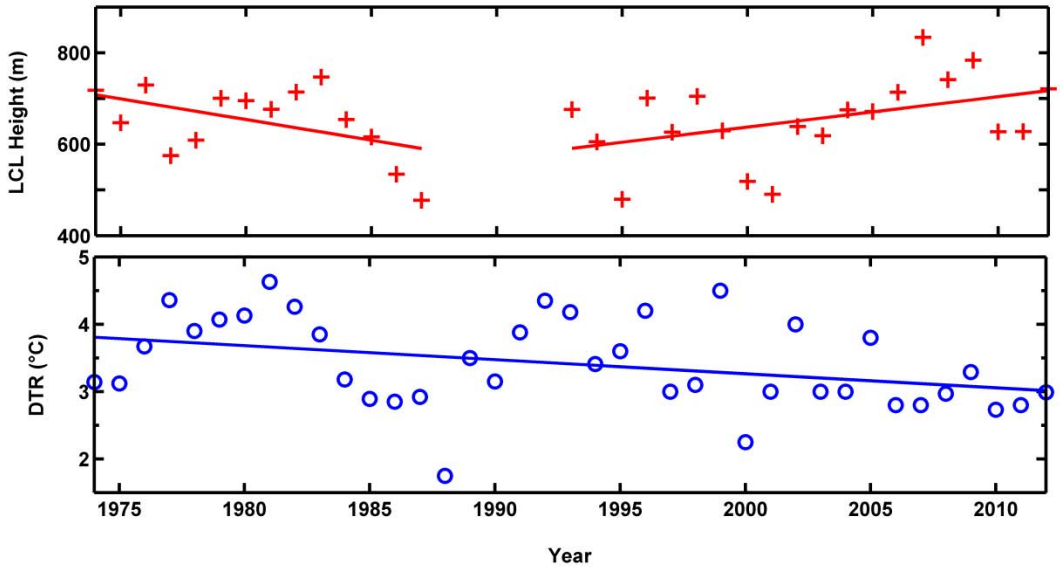

Figure 2.6 Radiosonde derived surface layer properties: (a) height of lifting condensation level, (b) base level diurnal temperature range. The thick solid lines are the linear fit line and the cross and circles are the data points.

2.4.4 Landsat Derived LST

Early summer LSTs are found to be distinctly higher (average 27.68 °C) than that of July (25.34 °C) and August (24.57 °C). The variation is believed to be associated with the monthly variation in solar radiation and percentage of cloud cover. A solar radiation observation in summer of 1991-2010 at Miami-Kendall-Tamiami station reveals that June, July and August are in decreasing order of irradiance: (June average: 11274 W-h/m^2, August Average: 10596 W-h/m^2, July in between). Also, three images with > 80% cloud free pixels analyzed in Figure 2.7 are associated with highest LSTs. Likewise; four images that have < 70% cloud free pixels in Figure 2.7 are associated with lower LSTs. For example, the three highest LSTs are 03 June, 1988 (LST = 30.21 °C, cloud free = 96.7%), 15 June, 1998 (LST = 30.88 °C, cloud free = 84.80%), and 30 May, 2004 (LST = 29.04 °C, cloud free = 90.89%). And, the two lowest LSTs are: 08 July, 1989 (LST =

24.69 °C, cloud free: 65.39%) and 20 June, 2000 (LST = 25.11 °C, cloud free: 69.93%). An increase of 0.28 °C LST /percent of cloud free pixels (p = 0.07) is obtained from a regression analysis using ten images with 70 to 90% cloud free pixels. These results confirm that the clearer the images we have, the higher the LSTs are estimated and vice versa.

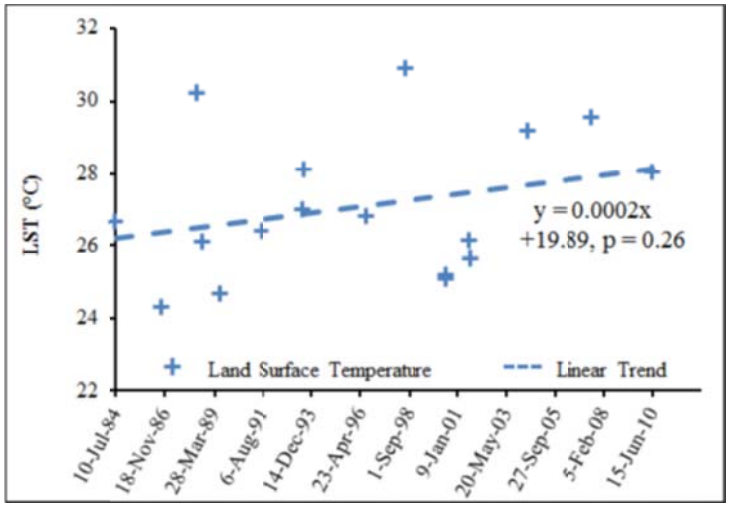

Figure 2.7 Change in summer LSTs extracted from > 65% cloud free images for urban areas from two eastern watersheds in South Florida (1984-2010). Urban polygons from land cover data of 2011 were used to calculate zonal average temperatures from each image.

The change in summer LSTs with time from 1984 to 2010 (Figure 2.7) has also been affected by the variation in cloud cover. The exclusion of two > 80% cloud free and analysis of rest of the almost uniform cloud free images from the dates used in Figure 2.7 resulted in an increase of nearly 2 °C ($p < 0.05$) over the period which is in close agreement with observed temperature increase (Figure 2.5). Derivation of reliable LSTs from uniform and maximum cloud-free images shows that although cloud masking has certainly improved the estimations and also helped to classify LSTs grouping them into

clean and cloudy products, variation in cloud cover still seems to introduce uncertainty in the estimations (Appendix 3).

2.4.5 Validation of LST

A statistical comparison between observed temperature and extracted LSTs at sixteen different weather stations in south Florida on August 26, 2001 (Figure 2.8) resulted in two contrasting validation outcomes. Six stations located mostly in urban periphery in the eastern south Florida (red cross marks in Figure 2.8) produced a Nash-Sutcliffe coefficient of 0.70 and model bias of -0.54 accompanied by a coefficient of determination (R^2) of 0.79. For instance, West Palm Beach, Pompano Beach, Miami NW SFO, Hialeah, Ft Lauderdale, and Cape all have the LST and oberved temperature difference within 1°C. This statistic reveals a good agreement between observed and estimated temperatures in urban areas. In contrast, Raccoon Point, Ochopee, Moore Heaven Lock, Devil's Garden, Loxahattee, and Tamiami Trail 40 Mile Bend have the LST and observed temperature difference of ≥3°C. Belle Glade, Clewiston and Everglades, which are small cities surrounded by vegetated and wet covers have the discrepancy within 1-3°C. The larger discrepencies in those areas are in the form of underestimation by Landsat. The underestimation particularly in wetland, forested land, and rangelands may have been introduced from increasing wetness and cloud cover in the field of view of Landsat (Appendix 3). The increased wetness in those areas may alter the emissivity. Lower than real brightness temperature may have been recorded because of increased canopy cover of the trees and plants further lowering the LST estimations. In general, the average LST difference between urban stations and natural and vegetated stations is 2.8°C.

Time series LSTs do not accord well with observed temperatures as found in a comparison of LSTs with temperatures from Palm Beach Airport and base level radiosonde. Nevertheless, the better performances are obtained for the comparison between multiple stations from the same day particularly for the eastern area. Since the inconsistency between LST and observed temperatures are found mostly in the form of underestimation by Landsat from the areas and dates containing mostly cloudy pixels, selecting cloud free images or finding equivalent distribution of cloud cover among images should be a criterion of paramount importance in this type of study.

2.4.6 Land Cover-LST Association

An analysis of land use land cover and subsequent LST analysis for the area bounded by the Landsat image resulted in an urban covergae (average LST) of 6.01% (24.9 °C) in 1974, 10.38% (25.44 °C) in 1992, and 13.95% (26.45 °C) in 2011. Also a total increase of urban cover from six to thirteen percent in the landsat coverage part of the watershed complies with a total increase in average urban temperatures of about 1.9 °C (from 1984 to 2010, Figure 2.7). The increase in LST is significant ($p < 0.05$) for the images with relatively uniform cloud cover. An increase in average LST for the Landsat coverage part is suggestive of the changes in characteristic fabrics, such as from less intense to more intense within the urban category and from green, and wet to bare and dry for other covers over the period.

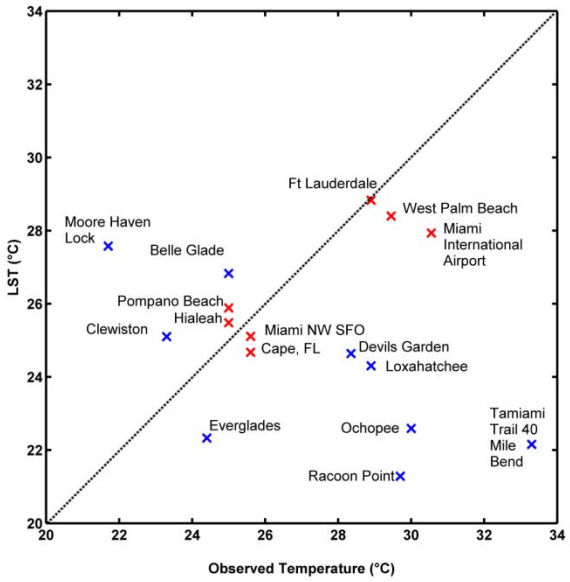

Figure 2.8 Annotated scatterplot showing observed air temperature versus LST from stations in South Florida on August 26, 2001. The red and blue cross marks represent urban peripheral and non-urban stations respectively.

Box plots of LSTs from 17 different less cloudy (> 65% cloud free pixels) dates for two eastern watersheds and their land cover-wise comparison in Figure 2.9 clearly shows urban followed by agriculture as the two highest temperature categories. High and low intensity urban; and communication, transportation, and utility are the five built-up categories which always show higher surface temperatures. High intensity urban, transportation and communication have average surface temperatures higher than 27°C in June 2010 (69% cloud free) which is about 2°C warmer from June of 1991 (67% cloud free). The difference in surface temperature between urban and wetland is found to be > 2°C.

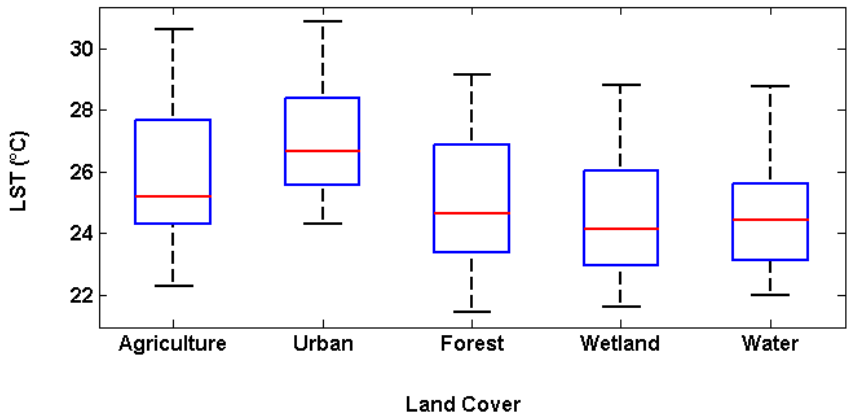

Figure 2.9 Land cover-wise distribution of summer-time land surface temperature derived from Landsat images. The LSTs are the summarized values for five major land cover categories from the zonal means of each category extracted from 17 different less cloudy images.

Figure 2.10 shows a microcosm of the surface heat island in an area near Homestead, Florida. With a change of most of the crop land and forest land (Figure 2.10, a) to urban and built up covers (Figure 2.10, c), a rise of LST of at least 2°C is detected from 1988 to 2010. The heat island is distinct with a steep gradient in the middle of the map where temperature differences of as much as 6 °C are found within a distance of one kilometer. This proper site is the location of a school building. The expansion of built-up covers at and around that location replacing previous cover of parks, ponds and crop lands are reflected in the increase of LST from 22 °C to 30 °C during the period. Very high UHI intensity near the building surrounded by parks and ponds is related with significant differences of energy balance between parks, ponds and buildings, because urban parks and ponds are anomalous sources of moisture in an otherwise dry area (Grimmond and Oke, 1995). The predominant LST distributions are 22–24 °C in wetland, forest, and rangeland; 24-26°C in agricultural areas; and 26-30°C in urban and built-up areas.

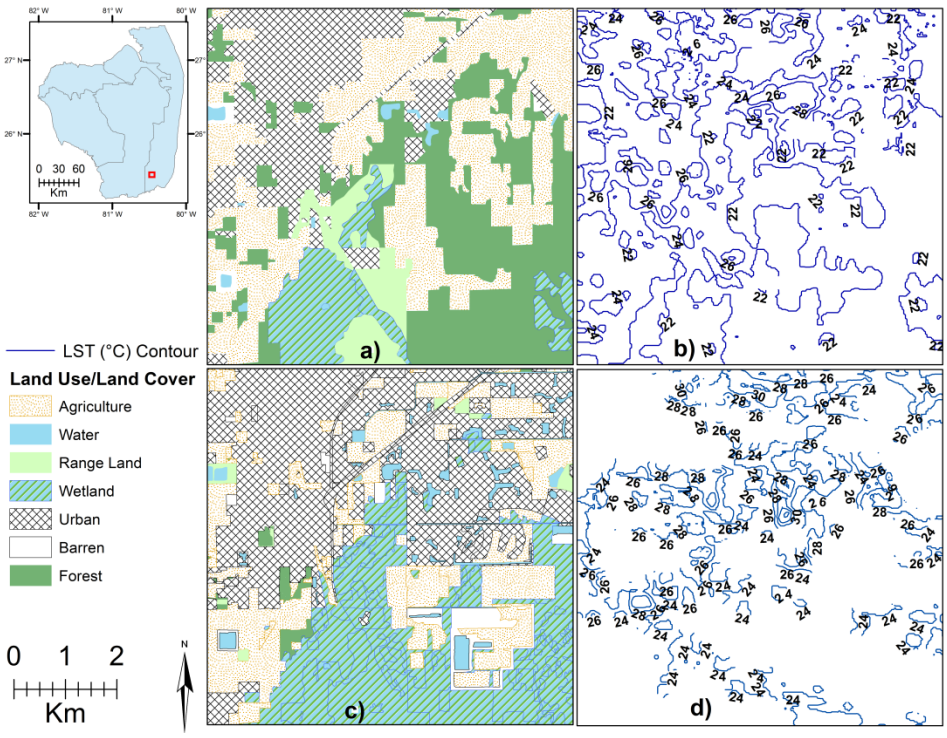

Figure 2.10 Maps showing association of land use land cover and Landsat-derived temperatures and their change with time in an area near Homestead (indicated by a red rectangle on the inset map on the top left). a) and c) are LULC maps of 1988 and 2010; b) and d) a are the contours of estimated land surface temperatures for the corresponding areas for May, 1988 and June 2010.

2.5 Conclusions

This study aimed to examine the immediate effect of land cover change on sensible weather by analyzing meteorologically recorded near surface air temperature, surface layer atmosphere, and remotely sensed land surface temperature in south Florida. A quantitative analysis of the land use/ land cover change in south Florida from 1974 to 2011 revealed an increase of ≈ 10% urban area during this period. Beside the decrease in open water cover, about 22% collective decrease in rangeland, forest, barren land, and crop/ pasture over the period balances the expansion in urban/built-up and wetland. It appears that most of the rangelands were either directly or indirectly (through some

intermediate change, for example, rangelands to crop/pasture, and crop/ pasture to urban) converted to the urban/built-up lands.

Interestingly, variations of land surface and near surface air temperature correspond to changes in land cover. There has been as much as 4°C difference in the summer minimum temperature between urban and natural areas. The land cover change through time is reflected in the form of total temporal rise of summer minimum air temperature by 0.5 °C-1 °C as exemplified by Miami International Airport and La Belle stations. A fairly increasing LCL height except in the years with greater influence of synoptic weather, and continuous fall of DTR from the radiosonde data also conforms to the results of UHI signature explored by weather station minimum temperature records. An increase of nearly 2 °C in LST throughout the period with fairly valid estimations for eastern urbanized areas (LSTs within 1°C of observed temperatures) are found when images with more uniform percentage of cloud free pixels are used in the analysis. The median values of urban LSTs are found to be 2 °C higher than wetland LSTs. The Landsat estimations suffer from limitations, such as lack of continuous data series because of excessive cloud cover, and poor validation statistics in wet and forested areas. Ground surface UHIs are reported to be maximized particularly in calm, clear nocturnal conditions. However, use of Landsat does not permit to analyze the peak UHI because of its late morning overpass time over south Florida. Yet, Landsat surface temperature estimations are proved to be very useful alternative means to investigate the relative change through time and space if a careful attention is given for the distribution of cloud cover over the images. Moreover, estimations of surface skin temperatures in high spatial

resolution supplement the scanty and above–the-ground-only records from meteorological stations.

2.6 Acknowledgments

The authors would like to acknowledge the data sources, mainly, USGS for the surface reflectance product of Landsat, Florida Automatic Weather Network for near surface weather data, Integrated Global Radiosonde Archive for the radiosonde data, NOAA, GH CN for the air temperature data, USGS for historical land use and land cover of 1970s, and NLCD for the land cover data of 1992 and 2011. Also, we would like to acknowledge Dr. Zhe Zhu for his help in making the executable Fmask code available.

2.7 Author Contributions

Hari Kandel was responsible for carrying out the research and the write-up of the manuscript with crucial suggestions, feedbacks and corrections from Assefa Melesse, and Dean Whitman.

2.8 Conflicts of Interest

The authors declare no conflict of interest.

2.9 References

Arya, P. S. *Introduction to micrometeorology*. Academic press: 2001; Vol. 79.

Baik, J.J. Response of a stably stratified atmosphere to low-level heating-An application to the heat island problem. *Journal of Applied Meteorology* **1992,** *31* (3), 291-303.

Baik, J.J.; Kim, Y.H.; Chun, H.Y. Dry and moist convection forced by an urban heat island. *Journal of applied meteorology* **2001,** *40* (8), 1462-1475.

Balling Jr, R. C.; Cerveny, R. S. Long-term associations between wind speeds and the urban heat island of Phoenix, Arizona. *Journal of Climate and Applied Meteorology* **1987,** *26* (6), 712-716.

Balling, R. C., Jr; Brazel, S. W. High-resolution surface temperature patterns in a complex urban terrain. *PHOTOGRAM. ENG. REMOTE SENS.* **1988,** *54* (9), 1289-1293.

Bornstein, R. D. Observations of the urban heat island effect in New York City. *Journal of Applied Meteorology* **1968,** *7* (4), 575-582.

Bornstein, R.; Lin, Q. Urban heat islands and summertime convective thunderstorms in Atlanta: three case studies. *Atmospheric Environment* **2000,** *34* (3), 507-516.

Carlson, T. N.; Ripley, D. A. On the relation between NDVI, fractional vegetation cover, and leaf area index. *Remote sensing of Environment* **1997,** *62* (3), 241-252.

Changnon, S. A. LA PORTE WEATHER ANOMALY-FACT OR FICTION. *Bulletin of the American Meteorological Society* **1968,** *49* (1), 4-&.

Chow, W. T.; Svoma, B. M. Analyses of nocturnal temperature cooling-rate response to historical local-scale urban land-use/land cover change. *Journal of Applied Meteorology and Climatology* **2011,** *50* (9), 1872-1883.

Collier, C. The impact of urban areas on weather. *Quarterly Journal of the Royal Meteorological Society* **2006,** *132* (614), 1-25.

Dabberdt, W. F.; Carroll, M. A.; Baumgardner, D.; Carmichael, G.; Cohen, R.; Dye, T.; Ellis, J.; Grell, G.; Grimmond, S.; Hanna, S. Meteorological Research Needs for Improved Air Quality Forecasting: Report of the 11th Prospectus Development Team of the US Weather Research Program*. *Bulletin of the American Meteorological Society* **2004,** *85* (4), 563-586.

Davies, F.; Collier, C.; Pearson, G.; Bozier, K. Doppler lidar measurements of turbulent structure function over an urban area. *Journal of Atmospheric and Oceanic Technology* **2004,** *21* (5), 753-761.

Dixon, P. G.; Mote, T. L. Patterns and causes of Atlanta's urban heat island-initiated precipitation. *Journal of Applied Meteorology* **2003,** *42* (9), 1273-1284.

Draxler, R. R. Simulated and observed influence of the nocturnal urban heat island on the local wind field. *Journal of climate and applied meteorology* **1986,** *25* (8), 1125-1133.

Duever, M.; Meeder, J.; Meeder, L.; McCollom, J. The climate of south Florida and its role in shaping the Everglades ecosystem. *Everglades: The ecosystem and its restoration* **1994,** *225*.

Gallo, K.; McNab, A.; Karl, T.; Brown, J.; Hood, J.; Tarpley, J. The use of a vegetation index for assessment of the urban heat island effect. *Remote Sensing* **1993,** *14* (11), 2223-2230.

Grimmond, C.; Oke, T. R. Comparison of heat fluxes from summertime observations in the suburbs of four North American cities. *Journal of Applied Meteorology* **1995**, *34*, 873-889.

Hawkins, T. W.; Brazel, A. J.; Stefanov, W. L.; Bigler, W.; Saffell, E. M. The role of rural variability in urban heat island determination for Phoenix, Arizona. *Journal of Applied Meteorology* **2004,** *43* (3), 476-486.

Howard, L. *The climate of London*. W. Phillips, sold also by J. and A. Arch: 1818; Vol. 1.

Huff, F.; Changnon, S., Jr. Climatological assessment of urban effects on precipitation at St. Louis. *Journal of Applied Meteorology* **1972,** *11* (5), 823-842.

Irish, R. R. In *Landsat 7 automatic cloud cover assessment*, AeroSense 2000, International Society for Optics and Photonics: 2000; pp 348-355.

Karl, T. R.; Diaz, H. F.; Kukla, G. Urbanization: Its detection and effect in the United States climate record. *Journal of Climate* **1988,** *1* (11), 1099-1123.

Kato, S.; Yamaguchi, Y. Estimation of storage heat flux in an urban area using ASTER data. *Remote Sensing of Environment* **2007,** *110* (1), 1-17.

Kim, H. H. Urban heat island. *International Journal of Remote Sensing* **1992,** *13* (12), 2319-2336.

Landsberg, H. E. Man-Made Climatic Changes Man's activities have altered the climate of urbanized areas and may affect global climate in the future. *Science* **1970,** *170* (3964), 1265-1274.

Landsberg, H. E. *The urban climate*. Academic press: 1981; Vol. 28.

Li, F.; Jackson, T. J.; Kustas, W. P.; Schmugge, T. J.; French, A. N.; Cosh, M. H.; Bindlish, R. Deriving land surface temperature from Landsat 5 and 7 during SMEX02/SMACEX. *Remote sensing of environment* **2004,** *92* (4), 521-534.

Links, S. High-Resolution Land Use and Land Cover Mapping, in *USGS Fact Sheet*. 1999, USGS.

Lo, C. P.; Quattrochi, D. A.; Luvall, J. C. Application of high-resolution thermal infrared remote sensing and GIS to assess the urban heat island effect. *International Journal of Remote Sensing* **1997,** *18* (2), 287-304.

Marshall, C. H.; Pielke, R. A., Sr; Steyaert, L. T.; Willard, D. A. The impact of anthropogenic land-cover change on the Florida peninsula sea breezes and warm season sensible weather. *Monthly Weather Review* **2004,** *132* (1), 28-52.

Middleton, D. R.; Davies, F. Evaluation of dispersion model parameters by dual Doppler lidars over West London, England. *International journal of environment and pollution* **2005,** *25* (1), 80-94.

Mitchell, A. Winter Weather in Florida. *Science* **1912**, 675-677.

Morris, C.; Simmonds, I.; Plummer, N. Quantification of the influences of wind and cloud on the nocturnal urban heat island of a large city. *Journal of Applied Meteorology* **2001,** *40* (2), 169-182.

Obeysekera, J.; Browder, J.; Hornung, L.; Harwell, M. A. The natural South Florida system I: Climate, geology, and hydrology. *Urban Ecosystems* **1999,** *3* (3-4), 223-244.

Oke, T. R. *Boundary layer climates*. Routledge: 2002.

Oke, T. R. City size and the urban heat island. *Atmospheric Environment (1967)* **1973,** *7* (8), 769-779.

Oke, T. R. *Review of urban climatology, 1973-1976*. Secretariat of the World Meteorological Organization Geneva: 1979.

Oke, T. R. The energetic basis of the urban heat island. *Quarterly Journal of the Royal Meteorological Society* **1982,** *108* (455), 1-24.

Pielke, R. A., Jr. Landsea, C. N. La Nina, El Nino and Atlantic hurricane damages in the United States. *Bulletin of the American Meteorological Society* **1999,** *80* (10), 2027-2033.

Pielke, R. A., Sr; Walko, R.; Steyaert, L.; Vidale, P.; Liston, G.; Lyons, W.; Chase, T. The influence of anthropogenic landscape changes on weather in south Florida. *Monthly Weather Review* **1999,** *127* (7), 1663-1673.

Pielke, R. A.; Pitman, A.; Niyogi, D.; Mahmood, R.; McAlpine, C.; Hossain, F.; Goldewijk, K. K.; Nair, U.; Betts, R.; Fall, S. Land use/land cover changes and climate: modeling analysis and observational evidence. *Wiley interdisciplinary reviews: climate change* **2011,** *2* (6), 828-850.

Price, C. V.; Nakagaki, N.; Hitt, K. J.; Clawges, R. M. *Enhanced historical land-use and land-cover data sets of the US Geological Survey*. US Department of the Interior, US Geological Survey: 2006.

Rabin, R. M.; Stensrud, D. J.; Stadler, S.; Wetzel, P. J.; Gregory, M. Observed effects of landscape variability on convective clouds. *Bulletin of the American Meteorological Society* **1990,** *71* (3), 272-280.

Rao, P. Remote sensing of urban heat islands from an environmental satellite. AMER METEOROLOGICAL SOC 45 BEACON ST, BOSTON, MA 02108-3693: **1972**, *53*, pp 647-&.

Roth, M.; Oke, T.; Emery, W. Satellite-derived urban heat islands from three coastal cities and the utilization of such data in urban climatology. *International Journal of Remote Sensing* **1989,** *10* (11), 1699-1720.

Runnalls, K.; Oke, T. Dynamics and controls of the near-surface heat island of Vancouver, British Columbia. *Physical Geography* **2000,** *21* (4), 283-304.

Schmidt, G.; Jenkerson, C.; Masek, J.; Vermote, E.; Gao, F. *Landsat ecosystem disturbance adaptive processing system (LEDAPS) algorithm description*; 2331-1258; US Geological Survey: 2013.

Schreiber, K.; Stull, R. B.; Zhang, Q., Distributions of surface-layer buoyancy versus lifting condensation level over a heterogeneous land surface. *Journal of the Atmospheric Sciences* **1996**, *53(8)*, 1086-1107.

Shepherd, J. M.; Burian, S. J. Detection of urban-induced rainfall anomalies in a major coastal city. *Earth Interactions* **2003,** *7* (4), 1-17.

Sklar, F. H.; Fitz, H.; Wu, Y.; Van Zee, R.; McVoy, C. South Florida: The Reality of Change and the Prospects for Sustainability: The Design of Ecological Landscape Models for Everglades Restoration. *Ecological Economics* **2001,** *37* (3), 379-401.

Sobrino, J. A.; Jiménez-Muñoz, J. C.; Sòria, G.; Romaguera, M.; Guanter, L.; Moreno, J.; Plaza, A.; Martínez, P. Land surface emissivity retrieval from different VNIR and TIR sensors. *IEEE Transactions on Geoscience and Remote Sensing* **2008,** *46* (2), 316-327.

Sobrino, J.; Raissouni, N. Toward remote sensing methods for land cover dynamic monitoring: application to Morocco. *International Journal of Remote Sensing* **2000,** *21* (2), 353-366.

Stabler, L. B.; Martin, C. A.; Brazel, A. J. Microclimates in a desert city were related to land use and vegetation index. *Urban Forestry & Urban Greening* **2005,** *3* (3), 137-147.

Stewart, I. D.; Oke, T. R. Local climate zones for urban temperature studies. *Bulletin of the American Meteorological Society* **2012,** *93* (12), 1879-1900.

Tarleton, L. F.; Katz, R. W. Statistical explanation for trends in extreme summer temperatures at Phoenix, Arizona. *Journal of Climate* **1995,** *8* (6), 1704-1708.

Vinukollu, R. K.; Wood, E. F.; Ferguson, C. R.; Fisher, J. B. Global estimates of evapotranspiration for climate studies using multi-sensor remote sensing data: Evaluation of three process-based approaches. *Remote Sensing of Environment* **2011,** *115* (3), 801-823.

Vogelmann, J. E.; Howard, S. M.; Yang, L.; Larson, C. R.; Wylie, B. K.; Van Driel, N. Completion of the 1990s National Land Cover Data Set for the conterminous United States from Landsat Thematic Mapper data and ancillary data sources. *Photogrammetric Engineering and Remote Sensing* **2001,** *67* (6).

Voogt, J. A.; Oke, T. R. Thermal remote sensing of urban climates. *Remote sensing of environment* **2003,** *86* (3), 370-384.

Weng, Q.; Lu, D.; Schubring, J. Estimation of land surface temperature–vegetation abundance relationship for urban heat island studies. *Remote sensing of Environment* **2004,** *89* (4), 467-483.

Zhu, Z.; Woodcock, C. E. Object-based cloud and cloud shadow detection in Landsat imagery. *Remote Sensing of Environment* **2012,** *118*, 83-94.

Chapter 3

Land Use/Land Cover Driven Alterations in the Surface Energy Balance in South Florida, USA

Kandel, H., A. M. Melesse, and M. C. Sukop, G. Tachiev (2015) Land Use/Land Cover Driven Alterations in the Surface Energy Balance in South Florida, USA, (Under preparation to submit)

Abstract

Quantitative analysis of land use /land cover change and consequent variation of sources and sinks of heat and moisture in South Florida is of critical value for the local weather, wetland restoration and urban management. Spatial and temporal variation of energy flux components in South Florida were analyzed using Landsat Thematic Mapper (TM) and ground based meteorological data for two different dates, May 7, 1984 and June 16, 2010, in order to assess the impact of land use land cover (LULC) change on surface energy balance. A combination of land cover and Landsat-estimated land surface parameters and meteorological variables employed in empirical and physically-based energy flux models were able to approximate the surface energy balance.

With the increase of urban land cover and decrease of rangelands and forested lands between these two periods, the Bowen's ratio increased in high-intensity developed land cover, a result of the urban encroachment. Highest and lowest Bowen's ratios are found in urban land (3.06) and in forest (0.14), respectively. Sensible heat fluxes are increased from urban and barren lands. In 2010, in the overall study area, an average of 231 Wm^{-2} increase in latent heat (L), 100 Wm^{-2} decrease in sensible heat flux (H) and 112 Wm^{-2} decline in ground heat flux (G) from the 1984 base value are found. The increase in L is related to the increased evapotranspiration from wetland, forest and agricultural lands.

Increase in energy imbalance (-41% of net radiation in 1984 to -48% of net radiation in 2010) from urban areas indicates the rise of anthropogenic energy expulsion and stresses the need to consider anthropogenic flux for more accurate energy balance estimation in urban areas. Substantial storage of energy along with the highest evapotranspiration rates from wetlands, which cover about half of the South Florida, and a profound increase of sensible heat flux from the urban areas, which are expanding, imply that the interplay of moisture and heat energy available from these two sources is highly likely to drive the local hydrology modulating surface- induced convective rainfall.

Key Words: Landsat, Energy Flux, Sensible Heat Flux, Latent Heat Flux, Bowen's Ratio, Evapotranspiration, Apparent Thermal Inertia, Albedo, South Florida

3.1 Introduction

The global trend of urban population growth has been exceeded by South Florida (2%/year) demanding more natural lands to be urbanized. Only between 1973 and 1995, after deducting urban conversion to natural, an excess of 10% of total land area in three eastern counties of South Florida: Palm Beach, Broward and Miami Dade was reported to be converted from natural and agricultural covers to urban cover (Walker, 2001). Natural land covers, such as wetlands, open water, forest and rangelands tend to cool the climate by expending greater amounts of incoming solar radiation as evaporation and transpiration. Developed lands, on the other hand, convert most of the incoming radiation into heat energy thereby warming the local climate. In a spatially heterogeneous land surface, units of different surface cover types have their own combination of radiative, thermal, moisture, and aerodynamic properties such as albedo, soil thermal conductivity,

soil moisture, surface roughness, etc. Each unit distinctly moderates and apportions the available energy and water characterizing it by a unique energy and water budget (Oke, 1978). According to the principle of conservation of energy, the available net radiation (R_n) on the surface is balanced by outgoing energy fluxes to the air by convection of sensible (H) and latent heat (L) and to the subsurface by conduction of ground heat (G). The net radiation on the surface is the excess of incoming solar radiation, which is dominated by short wave radiation, after expending as reflection some of the short-wave radiation and after emission of the long-wave radiation from the surface.

The actual sharing of net radiation by the component fluxes depends on several factors, such as nature of the surface cover, characteristics of the overlying atmosphere, and the thermal properties of the surface and sub-surface medium (Oke, 1982). For instance, the energy budgets of extensive water surfaces (large lakes, seas, and oceans), wet, and forested cover differ from those of agricultural, grass, and urban covers in several different ways. In the former, due to their higher rate of evapotranspiration and large heat capacity, combined L and G balances most of the net radiation leaving only a small share for H (Arya, 2001). Since bare land and surfaces covered by short grass and urban fabrics respond readily to solar heating due to their lower heat capacities (Oke,1978), these surfaces tend to warm the overlying atmosphere faster making H a significant component there. It is reported that lower albedo and low emissivity in urban areas tends to store more heat during the day and emit more during the night as sensible heat flux, resulting in higher daily minimum temperatures (Landsberg, 1970).

One study aimed at investigating the effects of deforestation in South American tropical forest found an increased sensible heat flux in deforested areas (Gedney and Valdes, 2000). They indicated that there was an increased albedo reducing the amount of absorbed radiation and decreasing roughness length lowering the gradient of horizontal temperature. However, they observed that the lower latent heat flux and cloud cover caused by decreased vegetation fraction and leaf area index resulted in increased incident radiation with a consequence of increased sensible heat flux. Generally speaking, when the rural areas are transformed to anthropogenic areas, the albedo, specific heat, and emissivity are all reduced while the thermal conductivity is magnified (Arya, 2001). In addition, there is an added amount of energy from anthropogenic activities, such as the energy ejected mainly from automobiles, industries, and air conditioning units.

South Florida comprises a heterogeneous land cover ranging from freshwater marshes and prairies to pine forest and from tree islands and saw grass plains in the natural categories to crop and pasture land to residential and commercial lands in the anthropogenic. The Everglades, which is a vast and unique wetland system has seen extensive fragmentation after the beginning of the construction of water control structures and settlements since early to mid-20th century. That resulted in the degradation of its ecohydrology and natural habitats (Sklar, 2001). After the realization of these detrimental effects on wetland health, Everglades' restoration plans have been initiated and have passed through many phases. Having a land cover that is dynamic temporally and widely varied spatially, measurements and estimation of energy budgets through time and space in South Florida not only help assess its restoration progress but also warrant an evaluation tool to monitor the effects of anthropogenic alteration.

A number of previous studies noted marked changes in surface energy fluxes associated with land cover change in South Florida. For instance, Marshall *et al.* (2004) have compared modeling results of the warm season sensible weather in South Florida between pre-1900 and post-1980 land cover scenarios. They found two distinct zones of increased sensible heat flux in drained and urbanized areas. Likewise, Shoemaker et al. (2005), while comparing the responses of two natural ecosystem in the Everglades have reported that increased air-water heat exchange was found in open water sites compared to vegetated sites. Melesse *et al*. (2007) carried out a remote sensing study using Moderate Resolution Imaging and Spectroradiometer (MODIS) in the Kissimmee River basin with a result of significant increase of fractional vegetation cover and latent heat flux in the restored areas of the basin. A recent study (Lagomasino *et al*., 2014) comparing two mangrove ecotones in the Everglades found clear signatures of decrease of G and increase of L for post-storm period and after the mangroves recovery. They also found that the scrub mangroves can be distinguished from the tall mangroves by their lower L and higher G values.

All of the above studies have limited their scope either to the sites within the natural Everglades and Kissimmee River Basin or relied on the results of a mesoscale atmospheric modeling. This study is an extension of these findings and aims to estimate all the components of surface energy balance by combining meteorological station records and surface-derived parameters at high spatial resolution for all land cover types that exist in South Florida. The combined approach is advantageous because ground-based meteorological stations provide measurements accurately over a homogenous area, but cannot account for the spatial heterogeneity. The heterogeneity of size, shape,

composition, and arrangement of urban elements make the urban surfaces more complicated for meteorological studies. Remote sensing methods are therefore viable alternative that provide spatial distribution of fluxes at the measurement scale of the satellite sensor resolution. Moreover, Landsat provides a long history of about three decades of records allowing ample opportunity for temporal comparison.

3.2 Study Area and Dataset

Bordered by Lake Okeechobee on the mid-north, the Gulf of Mexico on the west, Florida Bay and the Florida Keys on the south, and the Atlantic Ocean on the east, South Florida encompasses a total land area of about 36000 km^2. South Florida hydrology and land cover have been converted tremendously by drainage activities, such as constructing canals, levees, and water control structures that began in 1906 (Sklar, 2001). These activities continued until the 1960s, partitioning the natural Everglades into Everglades Agricultural Area (EAA), Water Conservation Areas (WCA's) 1, 2a 2b, 3a, and 3b, and disconnecting the northern Everglades from the Everglades National Park (ENP) in the south. After the need for conservation of the natural areas was realized, South Florida currently hosts the world's costliest wetland restoration project, called the Comprehensive Everglades Restoration Plan (CERP) that began in 2001.

3.2.1 Study Area

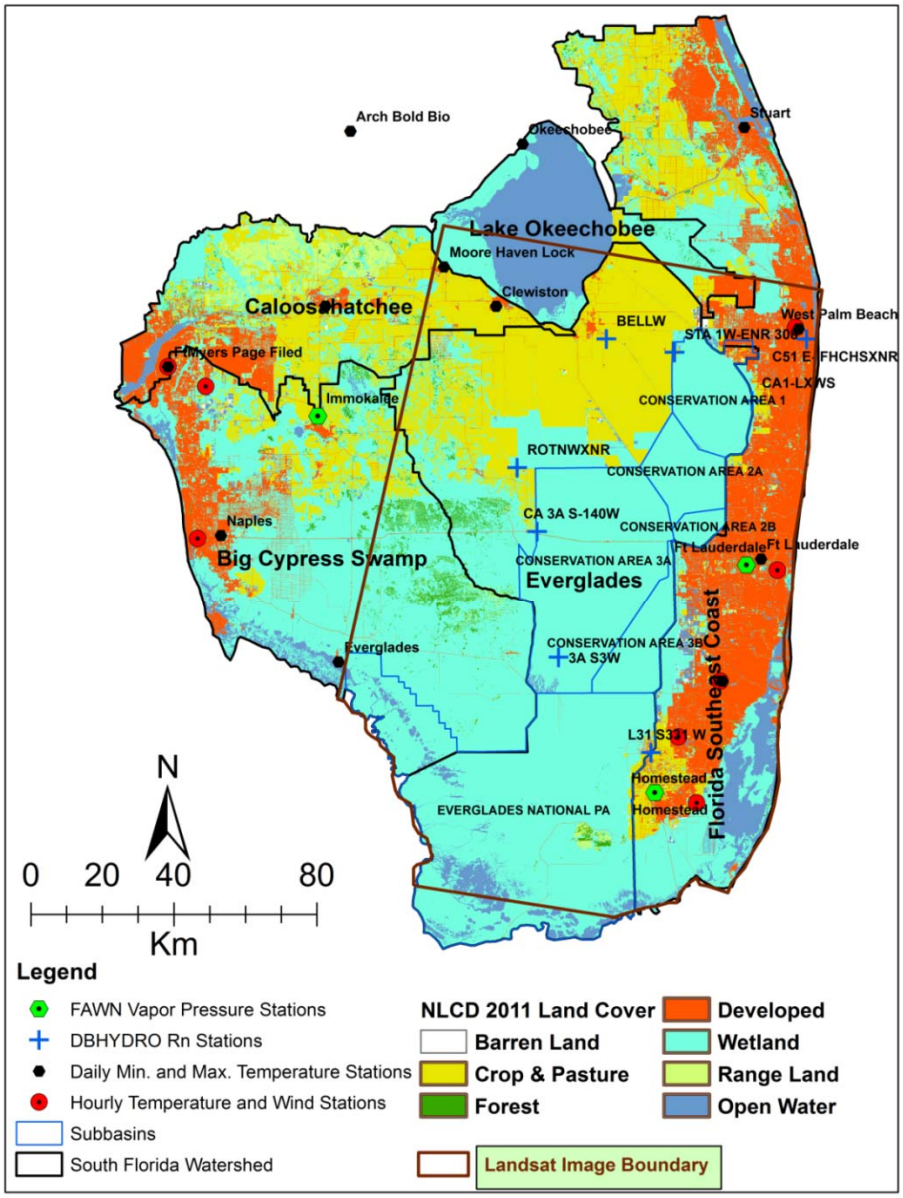

Figure 3.1 Study area showing locations of various meteorological stations, important hydrologic sub-basins, land cover map of 2011 and outline of Landsat image boundary.

Reconnection of the fragmented wetlands and restoration of some of the pre-drainage flow are the priorities of this project. Even with the restoration projects in place,

conversion of original undeveloped land into agricultural lands and agricultural and natural land to urban land are ongoing transformations and represent two major types of land use change practices over this period. As a result, the urban and built-up land cover in South Florida which was about 5.12% of the total land area in 1974, has grown to 15.59% in 2011 (Kandel et al., 2015, unpublished). In the same manner, during the period, 14.65% of rangelands have been shrunk to 2.29%. More than five and half million people live in urban clusters of the eastern three counties (Miami Dade, Broward, and Palm Beach) of South Florida with a rate of increase of nearly one million per decade (US Census Bureau, 2013).

Characterized by subtropical warm and humid climate, South Florida's rainfall is highly seasonal with three to four time greater rainfalls in the wet period (May- October) than in the dry months. Wet season precipitation is produced primarily by localized thunderstorms (Duever et al., 1994). Average daily maximum temperatures exceed 27°C from April through October and average annual precipitation ranges from 119 -157 cm, falling more than 60% between June and September (NOAA). 70 -90% of the rainfall is reported to be lost via evapotranspiration, which is greatest in summer wet season months (Duever et al., 1994).

3.2.2 Dataset

Remotely-sensed Landsat 5 TM, land-based meteorological stations, and observations from eddy covariance tower are utilized in this study.

3.2.2.1 Meteorological Station Records

Weather records from ground-based meteorological stations, such as surface and near-

surface temperature, wind velocity, relative humidity, and vapor pressure were obtained mostly from the National Climatic Database global hourly surface data. The records measured by the Florida Automatic Weather Network, whose 5 stations fall in our study area, have also been utilized. A few station's records of net radiation available from the DBHYDRO database of the South Florida Water Management District (Figure 3.1) were obtained for the purpose of validation. Sensible and latent heat fluxes for pine upland, dwarf cypress, and wet prairie sites were obtained from Barclay Shoemaker of the USGS (personal communication) and for Shark River Slough (SRS) and Taylor Slough (TS) sites from Ameriflux websites.

3.2.2.2 Landsat-5 TM

Surface reflectance data of Landsat 5 TM are used in this study. Landsat Climate Data Record's (CDR) Land Surface Reflectance products processed using Landsat Ecosystem Disturbance Adaptive System (LEDAPS) are the archived scenes from 1982 to present in the USGS Earth Explorer website: http://earthexplorer.usgs.gov/. In the global notation system, the World Reference System (WRS-2), the study area corresponds to the path 15 and row 42. This scene covers part of the Everglades sub-basin and the Florida Southeast Coast sub-basin (Figure 3.1). The principal use of these data was to derive shortwave albedo, land surface emissivity, and land surface temperature. Images of two dates, May 7, 1984 and June 16, 2010 are used in this study considering their equivalent percentage of cloud free pixels.

3.3 Analysis Methods

Details regarding specification and processing of input data, and the algorithms used for

the calculation of different energy flux components are outlined here. The station records for ground- based meteorological variables were interpolated using the ordinary kriging method of the geostatistical wizard in ArcGIS.

3.3.1 Net Radiation Calculation

A balance between different components of energy is the surface energy balance as given in (1).

$$R_n = H + L + G \quad (1)$$

$$R_n = R_S(1-\alpha) + L_w - \varepsilon\sigma T_s^4 \quad (2)$$

where R_n is net radiation, R_S is insolation, α is surface albedo, L_w is downward long-wave radiation (W m^{-2}), ε is the surface emissivity, σ is the Stefan-Boltzman constant (5.6703×10^{-8} W m^{-2} K^{-4}), and T_s is the land surface temperature (K). R_S, the portion of the extraterrestrial radiation that penetrates the atmosphere to reach to the Earth's surface, is a function of the solar constant (S_0 = 1368 W m^{-2}), atmospheric transmittance (V), solar declination angle (δ), the angle of latitude (φ), and the phase angle of the diurnal solar cycle (Ωt) as formulated in equation (3) (Price, 1977):

$$R_s = S_0 V\ (\text{Sin}\,\delta\ \text{Sin}\,\varphi + \text{Cos}\,\delta\ \text{Cos}\,\varphi\ Cos\ \Omega t) \quad (3)$$

The commonly used values of the solar constant (S_0 = 1368 Wm^{-2}) and atmospheric transmittance (V = 0.75) (Price, 1977) were used in Eq. 3 to calculate down-welling shortwave radiation. The solar declination angle (δ) for a given calendar day, which is the

angular distance of the sun (in our case north of the Earth's equator) was calculated from Equation (4).

$$\delta = 23.45 \times Sin\left(\frac{360}{365}\frac{\pi}{180}(284 + day)\right), \quad (4)$$

where day represents the day number such that day =1 on the 1st of January. The down-welling long wave radiance is the portion of the solar radiation absorbed by the atmosphere and later exuded as long wave towards the surface and can be calculated using (5).

$$L_w = \varepsilon_a \sigma {T_a}^4 \quad (5)$$

where $\boldsymbol{\varepsilon_a}$, the emissivity of atmosphere was obtained using $\varepsilon_a = 1.24(e_0 / T_a)^{1/7}$) (Brutsaert, 1975) where e_0 and T_a are vapor pressure (mb) and air temperature (K), respectively.

The phase angle (Ωt) in Equation (3) is actually an hour angle (24-hour equivalent to 360°) of the diurnal solar cycle that starts at local noon with an angle of 0°. The angle was determined using the 15°/hour relation and the local time of Landsat overpass that was read from image metadata. In this way, the phase angles for the overpass time before noon, in our case, were obtained negatives. Also, the central latitude of the scene was obtained from image metadata to use in (3).

The rest of the terms, land surface albedo (α), emissivity (ε) and the temperature (T_s) were derived from Landsat data as described in the following section.

3.3.2 Landsat Derivatives

3.3.2.1 Cloud Masking and Selection of Landsat Scenes

Surrounded by major water bodies in all sides, the sky cover over the land of South Florida is widely known for its extensive cloud cover. Since clouds and their shadows introduce errors in the estimated values of land surface temperatures (Irish, 2000), identifying cloud and cloud shadows in a scene and masking them out is very important. An automated cloud mask algorithm called function of mask (Fmask) was used for the purpose of detecting clouds and cloud shadows in the scenes. The details of input data, working procedure, and output grids of Fmask are given in Zhu and Woodcock (2012). The percentage of cloud free pixels was a criterion to choose image dates for comparison to make sure that the results compared are from equivalent land surface areas. The Fmask grid, with no data for all cloudy pixels, was later combined with other input layers for calculating albedo, emissivity and temperature in a GIS model in such a way that only the cloud free pixels are used in the calculation.

3.3.2.2 Derivation of Albedo

The total shortwave albedo was estimated using an algorithm developed by Duguay and Ledrew (1992). Their model is a linear formula based on the reflectance of band 2, band 4 and band 7 of Landsat TM as shown in (6):

$$\alpha_{short} = 0.562\,\alpha_2 + 0.314\,\alpha_4 + 0.112\,\alpha_{7.} \qquad (6)$$

The results of this model are reported as well fitted with the albedos of all land cover types derived from narrow band to broad band conversion (Liang, 2001). The input data, calculation steps, and the outputs are shown in an ArcGIS model in Figure 3.2.

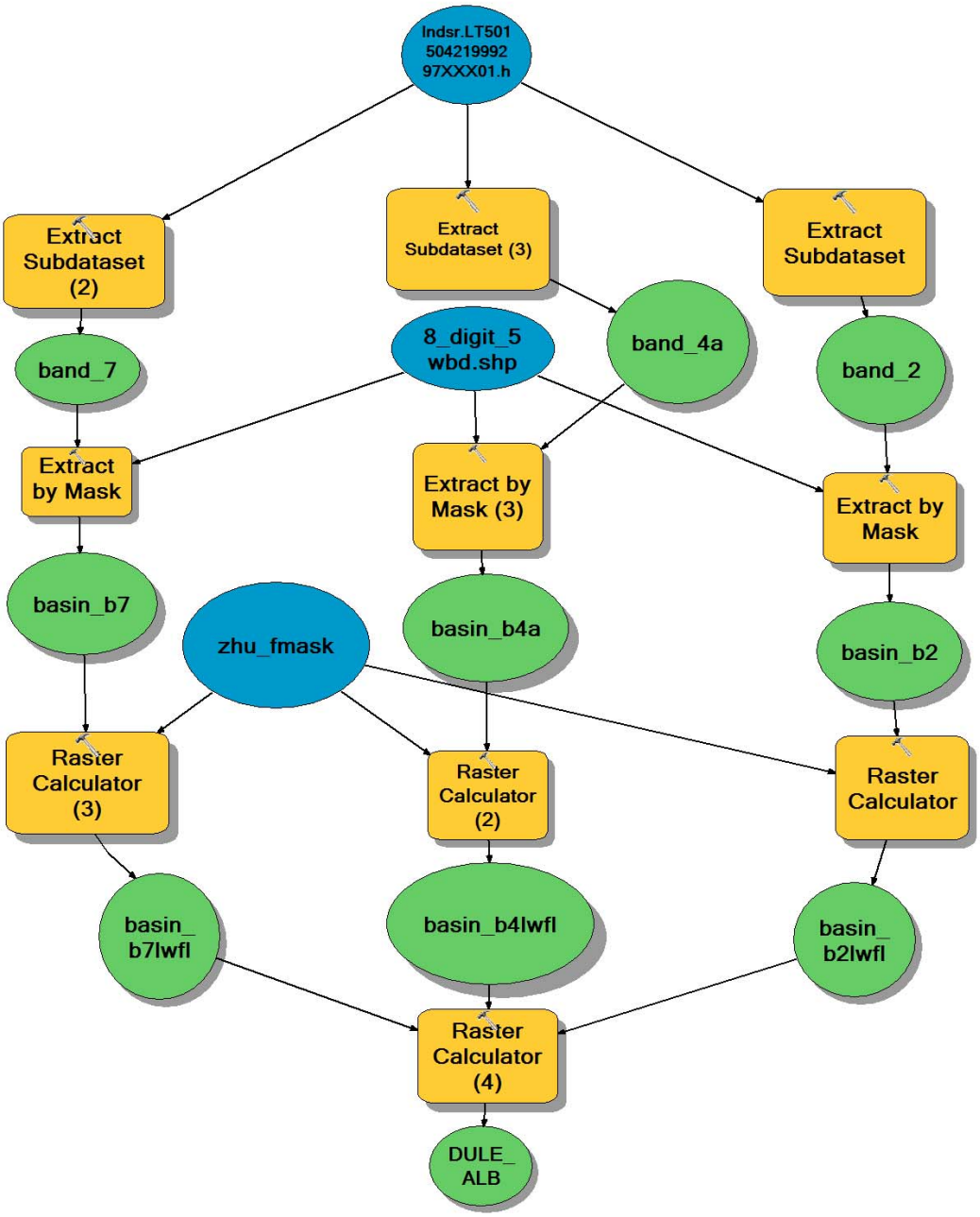

Figure 3.2 A GIS model to calculate land surface albedo from Landsat data. The blue ovals represent the input data (bands of Landsat and a cloud mask grid), orange rectangles represent the tools of ArcGIS and the green ovals represent the intermediate and end prod products of the model. The raster calculators 1, 2 and 3 perform the conditional analysis with cloud-mask grid to extract non-cloudy pixel values and to change the values to floating point, whereas the raster calculator 4 computes equation (6).

3.3.2.3 Derivation of Surface Emissivity

A normalized difference vegetation index (NDVI) threshold method proposed by Sobrino and Raissouni (2000) and Sobrino *et al.* (2008) was used to compute land surface emissivity (LSE). The lower (0.2) and upper (0.5) threshold NDVIs were suggested to distinguish mixed pixels from bare pixels in the lower end and from fully vegetated pixels in the upper end in this method. The following set of algorithms (7) compute composite emissivity from a Landsat image:

$$LSE = \begin{cases} a + b\rho_{red}, & NDVI < 0.2 \\ \varepsilon_v P_v + \varepsilon_s (1 - P_v) + C, & 0.2 \leq NDVI \leq 0.5 \\ \varepsilon_v + C, & NDVI > 0.5 \end{cases}, \quad (7)$$

where a and b are spectral statistical fit coefficients (a = 0.980, and b = -0.042) as used in Advanced Very High Resolution Radiometer(AVHRR) channel 4 (Sobrino and Raissouni, 2000), ρ_{red} is the reflectivity of the red band of Landsat (equivalent to channel 1 of AVHRR, ε_s, and ε_v are the emissivity values for non-vegetated pixels (0.97) and vegetated pixels (0.985), respectively. *C* is a term that accounts for the cavity effect due to surface inhomogeneity. Avoiding too exhausting method of determining *C* using satellite images (Muñoz *et al*., 2005), it was obtained as an average of the value used by Sobrino and Raissouni (2000) from channel 4 and channel 5 of AVHRR. This value was found to be equal to $0.016 - 0.01P_v$. P_V is the proportion of vegetation and was computed as in (8) (Carlson and Ripley, 1997).

$$Pv = \left(\frac{NDVI - NDVIs}{NDVIv - NDVIs} \right)^2, \quad (8)$$

where $NDVI_v$ and $NDVI_s$ are the NDVI values for non-vegetated and vegetated pixels, respectively. The results of calculating P_V using (8) were considered only for the pixels whose NDVI falls between 0.2 and 0.5. The values beyond these lower and upper thresholds were assigned 0 and 1, respectively. Finally, the layer of composite emissivity was calculated using conditional function in raster calculator of ArcGIS.

3.3.2.5 Derivation of Surface Temperature

The brightness temperature data from band 6 of CDR images were corrected for scale factor. An emissivity correction was then applied to convert brightness temperature into land surface temperature using the method suggested by Weng and Schubring (2004). Only brightness temperatures for cloud free pixels were used to calculate LST, and no-data was entered for masked pixels. The entire process of LST calculation was carried out by running a model built in ArcGIS.

3.3.3 Ground Heat Flux Estimation

Ground heat flux is the flow of heat energy to the soil column underneath the surface per unit area per unit time towards or away from the surface as dictated by the temperature gradient in a soil column. An analytical solution of heat transfer in a one-dimensional soil layer for unbounded condition directed by a diffusion equation (9) was used in this study. The governing equation is:

$$\frac{\partial T}{\partial t} = \frac{\kappa}{\rho c}\frac{\partial^2 T}{\partial Z^2}, \qquad Z \leq 0 \tag{9}$$

where T is soil temperature (K), κ is soil thermal conductivity (W m^{-1} K^{-1}), ρ is bulk density (kg m^{-3}), c is specific heat (J kg^{-1} K^{-1}) and Z is the vertical coordinate with the

origin set at the ground surface. From the above equation, ground heat flux at the surface $Z = 0$ at time t, $G(t)$, can be deduced at any location as a function of the time history of T on the surface through a widely known half-order time derivative (e.g., Miller and Ross, 1993) as given in (10):

$$G(t) = \sqrt{\frac{\rho c \kappa}{\pi}} \int_{-\infty}^{t} \frac{dT\,(0,s)}{\sqrt{t-s}} \tag{10}$$

where $T(0, t)$ is the skin temperature (time series), and s is a dummy integration variable. The soil constants outside the integration in (10) can be replaced by a single variable called soil thermal inertia I as given in (11):

$$I \equiv \sqrt{\rho c \kappa} \quad . \tag{11}$$

Equation (10) is a very simplified ground heat flux equation for many reasons. First, it does not need a vertical profile of soil temperature; second, it allows a time-averaged estimation of ground heat flux; third, it reduces three soil parameters to a single variable, thermal inertia, that helps reduce the sensitivity factors of the estimated flux; and fourth, as shown in equation (12) below, any arbitrary sampling interval of soil temperature can be used without compromising the effectiveness of the estimated flux (Bennett *et al*., 2008).

A removal of singularity (at $t^{-1/2}$) from equation (10) and the integration with respect to the time intervals (S_i, S_{i+1}) solves the integral part of the equation and eventually a solution (12) emerges combining equations (10) and (11) for the approximation of ground heat flux (Bennett *et al*., 2008):

$$G(t) = \frac{I}{\sqrt{\pi}} \times 2 \sum_{i=0}^{n-1} \frac{T^{i+1} - T^{i}}{s_{i+1} - s_i} \left(\sqrt{t - s_i} - \sqrt{t - s_{i+1}} \right) \qquad (12)$$

where T^i = T(0, s_i) and t is the total period of temperature records (Appendix 6).

Because the model uses surface-level temperature but the stations report the temperatures at elevation ranging from 1.5 m to 9.44 m, a logarithmic relationship of the vertical profile of temperature (Campbell and Norman, 2000) was used to extrapolate the air temperature values to surface level. For this purpose, regression coefficients were derived from the Florida Automatic Weather Network stations which report the temperatures from three different levels (0.6 m, 2 m and 10 m) and the same coefficients were used in the extrapolation for those and other nearby stations.

In this study, to get the benefit from both the meteorological station records and the remote sensing data, a frequently used parameter, apparent thermal inertia (ATI), was used to replace thermal inertia. Since ATI was easily obtained from satellite data, it enhanced the applicability of the term thermal inertia. Apparent thermal inertia is written as in (13) (Price, 1985):

$$ATI = \frac{2S_0 V}{\sqrt{\omega}} \frac{(1 - A)C_1}{T_{max} - T_{min}} \quad , \qquad (13)$$

where T_{max} and T_{min} are the daily maximum and minimum temperatures obtained from meteorological stations, A is spectral albedo obtained from equation (6), S_0 and V are as defined in equation (3), C_1 is the coefficient related to earth-sun distance obtained from the first term of Fourier solution as given in Price (1985), and ω, the angular frequency

(2π/T) is calculated for a daily cycle. The values of C_1 were found to be 0.51 for 1984 and 0.52 for 2010. The product of the terms S_0V in Eq. (13) results 997 Wm^{-2} for May 7, 1984 and 1021 Wm^{-2} for June 16, 2010. Since albedo was calculated from the Landsat data and the overpass time of Landsat is usually at or around 1100 local standard time, the ground heat flux estimated in this study corresponds with this time. The hourly temperature series in second part of equation (12) begins at 0700 local standard time and ends at corresponding Landsat overpass hour. Starting point of time for positive gradient of hourly temperature makes 0700 as the beginning hour.

3.3.4 Sensible Heat Flux Estimation

The sensible heat flux is the convective flow of heat along the temperature gradient between the surface and the near-surface atmosphere. The sensible heat flux can be expressed as:

$$H = \rho C_p (T_s - T_a) / r_a , \quad (14)$$

where ρ, the density, and $C_{p,}$ specific heat of air at constant pressure are both constants equal to 1.225 kg/m^3 and 1004 J/kg.K, respectively. T_s is the surface temperature (K) from Landsat-derived LST and T_a is the air temperature (K) obtained as interpolated maps from station-observed temperatures for the stations shown in Figure 3.1. The term r_a is the stability-corrected aerodynamic resistance, which for unstable and stable surface layers is given as in (15i) and (15ii), respectively (Moran *et al.*, 1989):

$$r_a = \{\ln[(z - d + z_0)/z_0]/k\}^2 \times \left\{1 - \frac{15R_i}{\left[1 + C(-R_i)^{1/2}\right]}\right\}^{-1} \Big/ U \qquad (15i)$$

$$r_a = \{\ln[(z - d + z_0)/z_0]/k\}^2 \times (1 + 15R_i)(1 + 5R_i)^{1/2} \Big/ U, \qquad (15ii)$$

where R_i, the Richardson number, a parameter that accounts for atmospheric stability, was calculated with (16) (Monteith, 1973):

$$R_i = g(T_a - T_s)\frac{z - d}{T_a U^2}\ , \qquad (16)$$

where g is acceleration because of gravity (9.8 ms^{-2}), and z is the height at which wind and air temperatures are measured. The elevation (z) ranges from 1.5 m to 9.44 m for different stations. A maximum elevation of 9.44 was used for the purpose of uniformity. The aerodynamic properties, zero-plane displacement height (d), and the roughness length (z_0), are estimated using a height-based approach (Grimmond and Oke, 1999). According to this approach, $d = f_d \overline{z_H}$ and $z_0 = f_0 \overline{z_H}$, where, $\overline{z_H}$ is the average height of the surface elements that cause resistance. The values of f_d and f_0 are suggested as: 0.63 and 0.13 for field crops and grass canopies; 0.8 and 0.06 for forests; and 0.5 and 0.1 for urban areas, respectively. U is wind speed (m/s), and k is Von Karman's constant (0.4). The height of the surface elements: trees, shrubs, grass, crop and urban buildings, which are presented in Table 3-1, were obtained from land cover metadata of 1974 and 2011 to use for 1984 and 2010, respectively. The non-vegetated wetlands, natural as well

as artificial water bodies, roads, urban open spaces, and barren lands were assigned with zero roughness length.

Table 3-1 Height of various surface elements used for the calculation of zero-plane displacement height and roughness length.

Land Cover Category	Z_h (m)
Urban-High Intensity	22
Urban- Medium Intensity	13
Urban- Low Intensity	10
Crop and Pasture	3
Scrub/Shrub, Herbaceous	2
Forest	8
Vegetated and Non-forested Wetland	2
Wet Forested Mixed	5

Since the objective of the research here is to examine the variation of energy fluxes introduced by land cover change, variations of the parameters that are directly extracted from the land cover (*d, z_0, and T_s*) are considered explicitly. Temporal change in surface cover was taken into account by changing these surface-derived parameters from 1984 to 2010.

3.3.5 Latent Heat Flux Estimation

Latent heat in this study was obtained as the residual term of the energy balance equation (1). Instantaneous rate of evapotranspiration was obtained dividing the latent heat flux by a conversion factor (28.94) to convert Wm^{-2} to mm/day. The daily average ET was calculated as one-third of instantaneous ET (Kustas et al., 1990).

3.4 Results and Discussion

This section presents the outcomes from each model for the parameters and component fluxes of the surface energy balance. The zonal averages of net radiation, sensible,

ground, and latent heat fluxes by land cover zones are discussed in terms of their variation.

3.4.1 Net Radiation

As balanced by incoming and outgoing short- and long-wave radiation, variations in surface albedo, land surface temperatures, vapor pressure, and air temperatures interact to produce the variation of net radiation. The highest zonal average net radiation is found for water (1984: 870 (±48) Wm^{-2}, 2010: 935 (±29) Wm^{-2}) followed by wetlands, and forests, with lowest values in urban areas (1984: 728 (±50) Wm^{-2}, 2010: 772 (±46) Wm^{-2}) (Figure 3.3). Because spatial variation of incoming shortwave radiation was not taken into account, albedo is the only variable to cause fluctuation in net shortwave radiation. The incoming shortwave radiation value for the entire study area indicated a slight increase (997 Wm^{-2} for 1984 and 1021 Wm^{-2} for 2010) (Appendix 4). Being surrounded by wetland and water bodies, relative urban albedo in South Florida is higher than natural surroundings (Table 3-2) as opposed to usual reduction of albedo by urban materials. The apparent increase in incoming shortwave radiation may have been caused by use of May data for 1984 and June data for 2010.

Average albedo showed a slight increase in the high intensity urban areas and deciduous forest, and a profound increase in barren land. Smaller increase of net radiation from 1984 to 2010 on barren lands (1.4%), high intensity urban lands (4.02%) and deciduous forests (5.2%) compared to an average of ~8% increase in other categories implies that albedo may be the primary driver of net radiation. Higher albedos in agricultural lands in comparison to wet and forested lands are consistent with the previous findings that

albedos are increased with tropical deforestation (Shukla *et al*.,1990; Gash and Shuttleworth, 1991; Gedney, and Valdes, 2000).

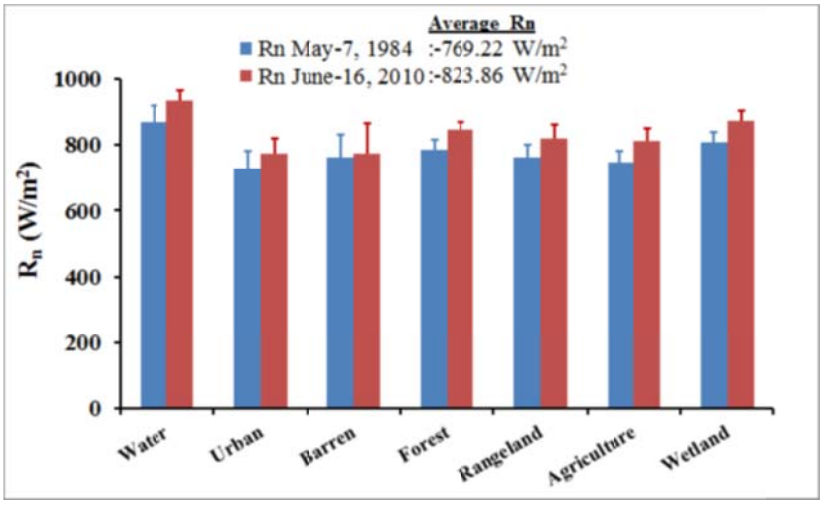

Figure 3.3 Comparisons of zonal averages of net radiation for two study dates. The zones are the land covers taken from NLCD 2011. The error bars represent plus one standard deviation.

Table 3-2 Variation of albedo in South Florida by land cover and time.

Land Cover	1984 Mean Albedo	2010 Mean Albedo
Water	0.06	0.05
Developed Open Space	0.17	0.17
Developed Low Intensity	0.19	0.18
Developed Medium Intensity	0.2	0.2
Developed High Intensity	0.2	0.21
Barren	0.17	0.24
Deciduous Forest	0.15	0.16
Evergreen Forest	0.14	0.12
Mixed Forest	0.14	0.12
Scrub/Shrub	0.14	0.13
Herbaceous	0.17	0.16
Hay/Pasture	0.17	0.15
Cultivated Crops	0.16	0.16
Woody Wetland	0.13	0.11
Emergent Herbaceous Wetland	0.12	0.09

The other factor that may have contributed to this land cover-driven variation in net radiation is land surface temperature. Urban areas with ~2° K higher land surface temperatures than the surrounding natural areas would lose more radiation in the form of outgoing longwave, making the overall net radiation lower. A barely higher values of summer-time daily average down-welling long-wave radiation for urban stations obtained from long-term analysis (Fort Lauderdale: 414.55 Wm^{-2}, Homestead: 410.44 Wm^{-2}, and Immokalee: 407.76 Wm^{-2}) may have been surpassed by higher outgoing longwave radiation from urban surfaces.

3.4.2 Ground Heat Flux

Relative values of thermal inertia indicate that highest ATIs were found for water followed by urban and wetlands in both the years. Large heat capacity and heat conductivity render higher thermal inertia to water and wetlands. Likewise, high heat conductivity and density of urban fabrics contributes to its higher thermal inertia. Given similar thermal properties of wet soils and urban materials, comparable heat fluxes towards the sub-surface is observed in wetland, and urban areas. Higher average ratio of ground heat flux to net radiation is resulted in 1984 (0.56) than in 2010 (0.38), which are higher than commonly reported values of 0.35 (Norman *et al.,* 1995). A slight reduction was observed in average diurnal temperature range (-0.46°C) from 984 to 2010. Also, temperature gradient term, Gt in equation (12) except the term I, was found decreased from 0.05 $Ks^{-1/2}$ in 1984 to 0.03 $Ks^{-1/2}$ in 2010. Both these reductions contributed for a decrease in ground heat flux from 1984 to 2010 predominantly in urban and barren lands (Figure 3.4). Substantial decrease of G from 1984 to 2010 (-227 Wm^{-2}) in urban cover

owes to an increase of DTR (~3°K) which was resulted by a larger increase in daily maximum temperatures compared to daily minimum temperatures.

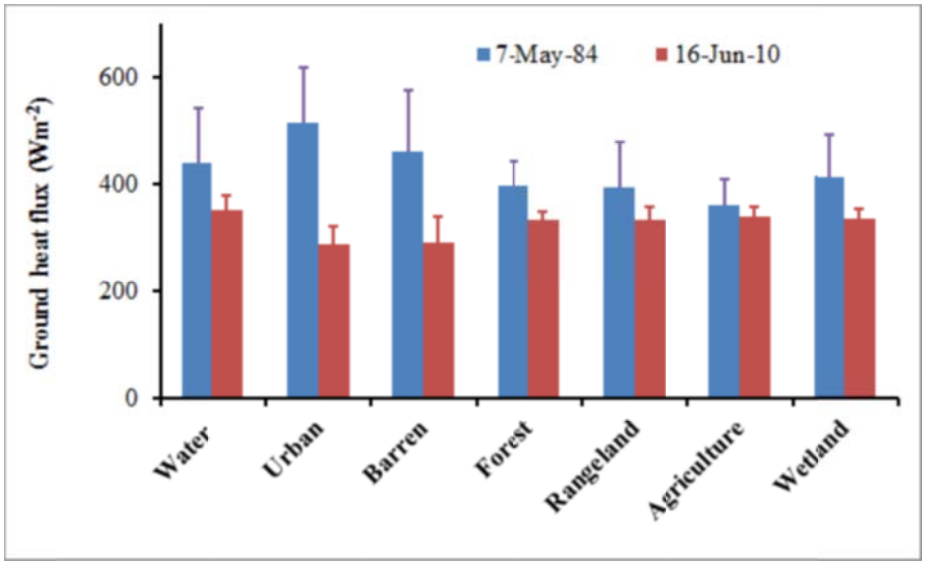

Figure 3.4 Comparison of zonal average ground heat flux for the study dates. The zones are the land covers taken from NLCD 2011. The error bars represent plus one standard deviation.

Ground heat flux is found lowest in agricultural areas 360 (±50) Wm^{-2} in 1984 and in urban areas 288 (± 34) Wm^{-2} in 2010 owing to the relatively higher sensible heat fluxes from those covers.

3.4.3 Sensible Heat Flux

The average sensible heat fluxes are: 200.83 (±279.27) Wm^{-2} for 1984, and 307.76 (± 376.05) Wm^{-2} for 2010 with highest values for high intensity urban (775 Wm^{-2} in 1984 and 1057 Wm^{-2} in 2010) and lowest for deciduous forest (50 Wm^{-2} in 1984 and -7 Wm^{-2} in 2010) (Appendix 5). The average percentage of sensible heat flux of the average net radiation increased from 37% in 1984 to 39% in 2010. Figure 3.5 depicts area-weighted zonal averages of fifteen subcategories summarized into eight major categories for 1984

and 2010. Sensible heat flux is found to have increased for water, urban and barren lands, remained unchanged in herbaceous and wetlands, and decreased in forest, scrub/shrub, and agricultural lands. The standard deviations are very high with the highest in urban area in 1984 and second highest in 2010, when barren land showed extreme variation within the category.

The average air temperature and wind speed for 1984 were obtained as 300.49 K and 3.28 ms^{-1}, respectively and the same values were used for 2010 as well. The average values of stability- adjusted aerodynamic resistance, $r_{a,}$ for the entire area was found to be 38.86 sm^{-1} in 1984 and 21.60 sm^{-1} for 2010 with the standard deviations of 23.14 sm^{-1} and 12.68 sm^{-1}, respectively. The small difference in the average surface temperatures between 1984 and 2010, but a profound decrease in aerodynamic resistance indicates that land surface parameters are vital to the increase or decrease of sensible heat fluxes. Table 3-3 shows the parameters derived to calculate the sensible heat flux from the surface.

The zonal average roughness length for vegetated only areas, where sensible heat flux decreased from 1984 to 2010, ranges from 0.27 m to 0.36 m with an average of 0.32 m for 1984, and from 0.20 m to 0.37 m with an average of 0.28 m in 2010. Cultivated crop has the average roughness length of 0.36 m in 1984 and 0.37 m in 2010.

The difference in canopy height, fractional vegetation cover, and leaf area index (LAI) of the plants probably is a reason for the decrease of sensible heat flux in forested areas. The aerodynamic resistance for these vegetated areas ranged from 21 sm^{-1} (deciduous forest and cultivated crops) to 24 sm^{-1} (evergreen forest) with an average of 22.54 sm^{-1} in 1984 and ranged from 22 sm^{-1} (herbaceous) to 28 sm^{-1} (deciduous forest) with an average of 26.32 sm^{-1} in 2010.

Table 3-3 Descriptive statistics of various parameters used to calculate sensible heat flux.

Parameters	Average	
	1984	2010
d (m)	1.54 (±1.72)	1.76 (±2.53)
Z_0 (m)	0.22 (±0.24)	0.30 (±0.46)
$T_{s\,(K)}$	300.41 (±2.84)	299.15 (±2.05)
Ta (K)	297.84 (±0.33)	300.49 (±0.75)
R_i	-0.06 (±0.07)	-0.03 (±0.04)
U (m/s)	3.32 (±0.33)	
R_a (sm^{-1})	38.86 (±23.14)	21.60 (±12.68)

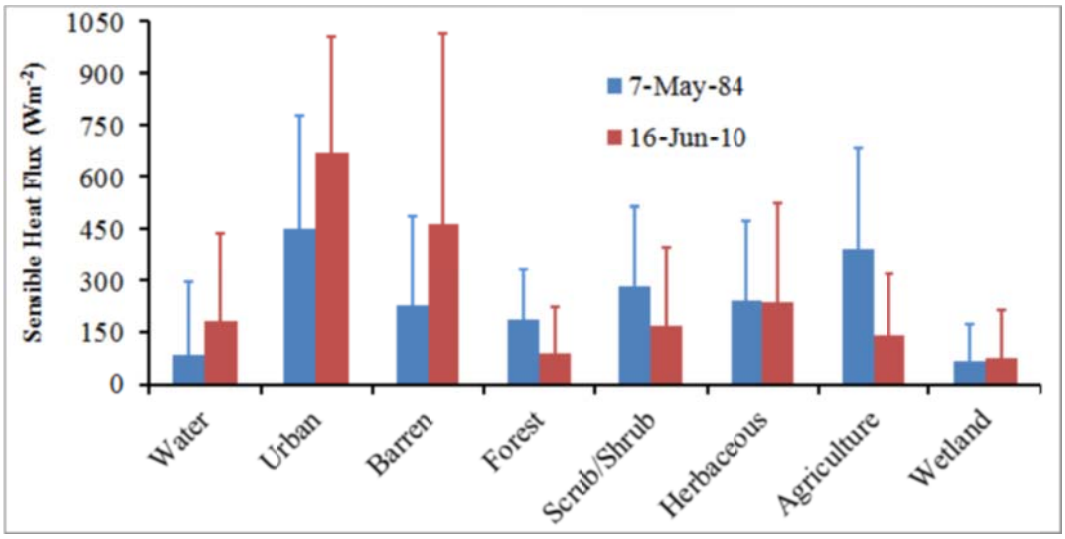

Figure 3.5 Comparison of zonal average sensible heat flux for the study dates. The zones are the land covers taken from NLCD 2011. The error bars represent plus one standard deviation.

Studies on surface resistance to vapor transport (R_c) and consequent changes of Bowen's ratio (β) during the summer at multiple FLUXNET sites revealed the lowest values of R_c and β from agricultural and deciduous forest sites and relatively larger R_c and β from

coniferous forest (Wilson et al., 2002). Also, they noticed a negative correlation between R_c and seasonal maximum leaf area index (LAI) suggesting a decrease in sensible heat flux with an increase in LAI. The lower stomatal resistance and greater photosynthetic capacity of agricultural species was attributed to the decrease in sensible heat flux, i.e., lower β, from agricultural sites (Kelliher et al., 1995; Körner et al., 1979; Wullschelger, 1993). The decrease in sensible heat fluxes from the vegetated areas in this study may also be attributed to the decreased roughness length resulting in increased aerodynamic resistance. Increased LAI and decreased stomatal resistance of vegetated cover in 2010 compared to 1984 may also have played a role. Since the zones are defined from the 2011 land cover data for both 1984 and 2010, sparsely vegetated or less intensely cultivated areas in 1984 perhaps have been intensified with increased LAI in 2011.

The increase in the proportion of pixels included in the analysis from 1984 to 2010 for all the vegetation categories, with the highest increase in agriculture may also have contributed for the decrease in sensible flux in those categories. The percentage change of pixels included from each category in the two periods probably contributes to the change in flux depending on whether it is urban, plant covered, or wet and water. For instance, an increase in sensible heat flux from urban areas is associated with the increased percentage of pixels from 1984 to 2010. Urban pixels (low, medium and high intensity) cover 13% of the total in 1984 which is found increased to 27% in 2010. Similarly, water and wet pixels are found decreased from 58.92% in 1984 to 13.75% in 2010. From this pixel percent observation, it can be deduced that sensible heat flux increases either with an increase in urban pixels or with a decrease in water and wet pixels and decreases with an increase of vegetated pixels.

3.4.5 Latent Heat Flux

The latent heat flux from vegetated areas increased significantly between 1984 and 2010. The highest latent heat flux was found in deciduous forest (405 Wm^{-2} in 1984 and 508 Wm^{-2} in 2010) followed by water (336 Wm^{-2}) in 1984, and by herbaceous wetland (477 Wm^{-2}) in 2010. Cultivated crops show profound increase of latent heat flux between 1984 and 2010 (Appendix 5). The increase in latent heat flux from cultivated crops are probably linked with the series of best management practices adopted in the Everglades Agricultural Area that include construction of storm water treatment areas, leveling the field, use of cover crops, slowing down of the drainage etc. The daily average ET was found to have increased from the value of 2.29 mm/day in 1984 (maximum in water) to 3.56 mm/day in 2010 (maximum in wetland) (Figure 3.6).

3.4.6 Energy Balance

Three urban categories: low, medium and high intensity developed show energy deficit in both years. Average energy deficit in 1984 was estimated to be 250 Wm^{-2} which increased to 418 Wm^{-2} in 2010. Additional deficit was also observed in barren land in 2010 (Figure 3.7). The appreciable increase of Bowen's ratio is found in urban and barren lands. Increases in Bowen's ratios were observed from emergent wetland, herbaceous, water, and developed open space categories.

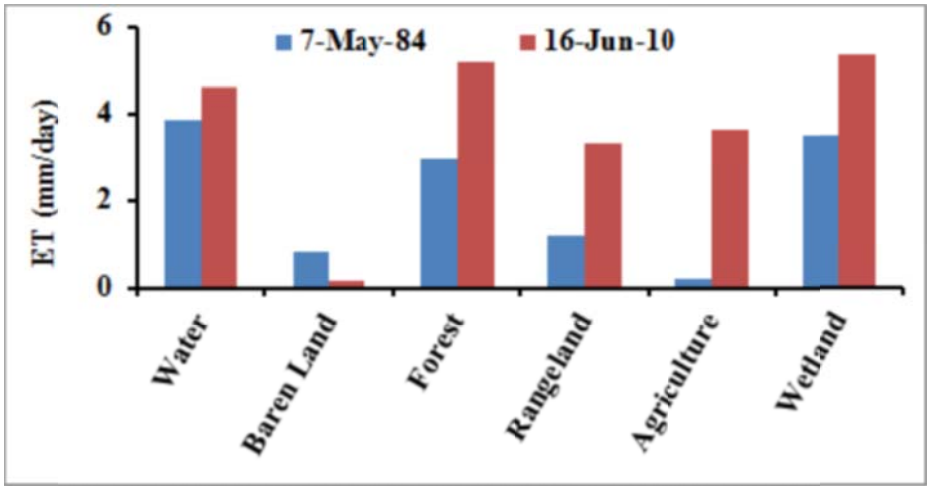

Figure 3.6 Comparison of daily average evapotranspiration rates over different land cover classess in South Florida for 1984 and 2010.

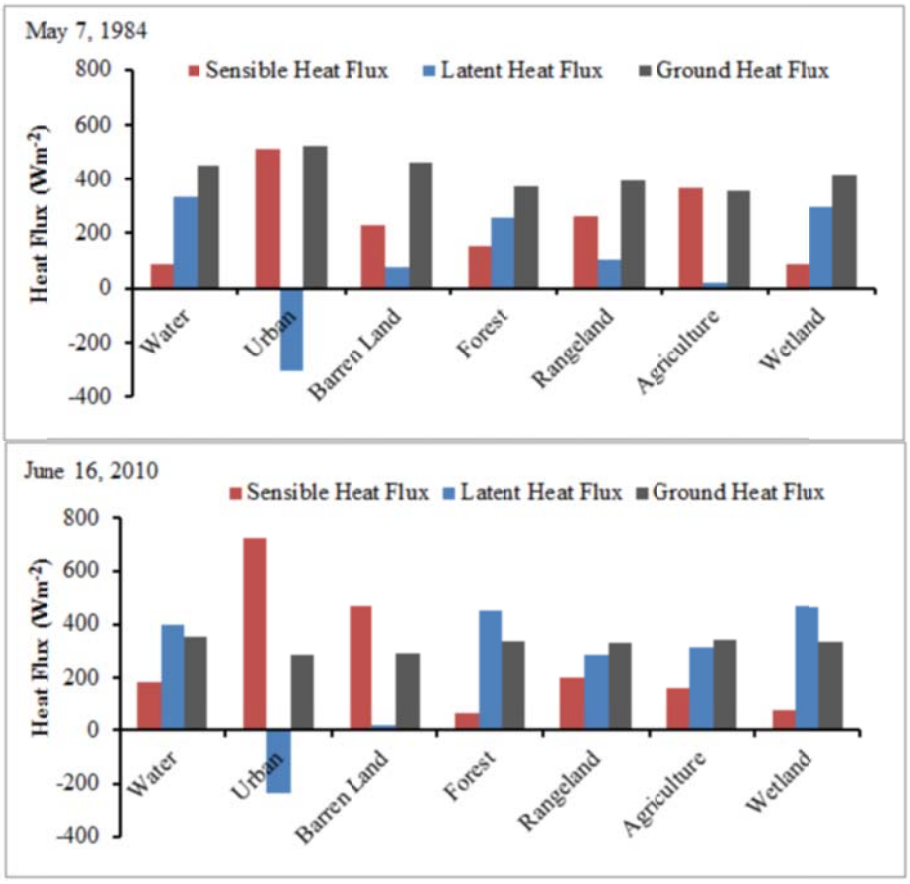

Figure 3.7 Comparison of zonal averages of surface energy balance components in different land covers for 1984 and 2010.

3.5 Validation

The predicted versus observed net radiations from seven different stations located in South Florida are illustrated in Figure 3.8. It shows that the majority of the predicted values are overestimated. Stations located in northern agricultural and rangelands adjacent to WCA 1, such as BELLW, LXWS, and ENR-308 have better estimated results than in southern water conservation areas and Levee L 31S331 (Figure 3.1). Total RMSE is 60.84 Wm^{-2}, which, after decomposition into systematic ($RMSE_s$) and unsystematic ($RMSE_u$) parts, produced 63.52 Wm^{-2} and 35.80 Wm^{-2}, respectively. The ratio of $RMSEs^2/RMSE^2$, an indication of where the errors stem from, is 109% suggesting that the source of error is systematic and agreement between observed and estimated is poor. The discrepancy of height of measurements and use of replacement of cloudy pixels by neighboring pixels for Landsat estimations may have contributed to this error. For the reason, a model $Rn_{mod} = 0.625Rn_{est} + 229.62$ (R^2 =1 and error = 0.005%) is proposed by calibrating the coefficients of the linear equation with observed net radiation of June 16, 2010.

For the dates studied, there are no multiple stations in South Florida that measure sensible and latent heat fluxes. Moreover, the study was carried out to see how different land covers in space and time modulate energy partitioning by keeping wind speed and air temperature constant and changing only the land surface parameters for the two dates. Therefore, the value measured by the Ameriflux tower at Shark River Slough -6, which is a mangrove forest site on the date June 16, 2010 at 1130, and from Tylor Slough, which is a sawgrass marsh site were compared only to see site-wise variation.

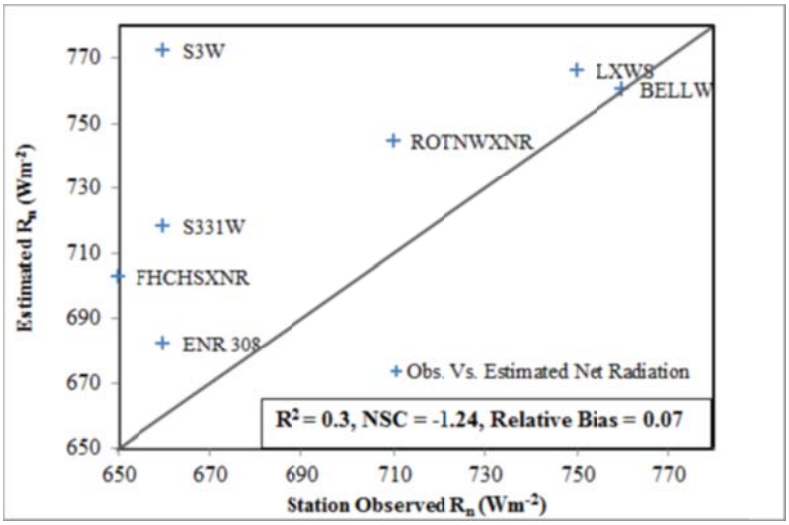

Figure 3.8 Plot of observed versus estimated net radiations for the stations shown in Figure 1. The observed values are obtained from the SFMD-DBHYDRO database for the time 11:00 to 11:45 am LST. The diagonal line from bottom left to top right is a 1:1 line.

The sensible (140.6 W/m^2) and latent heat fluxes (230.8 W/m^2) reported from SRS are 20% and 33% of the net radiation, respectively. Similarly, values reported from TS short hydro-period sites are 150.54 Wm^{-2} for sensible heat flux and 226.79 Wm^{-2} for latent heat flux, which are 30% and 45% of the net radiation. It shows that the saw grass marsh exhibits significantly higher convective fluxes compared to mangrove forests, which probably stores the energy in its biomass. Bowen's ratio measured on June 16 2010 averaged for 1000, 1030 and 1100 local standard time from Florida Everglades Tylor Slough for short hydro-period is 0.59, and for long hydro-period is 0.20. Likewise, long hydro-period Bowen's ratio is 0.19 in Everglades Shark River Slough. Our estimated wetland average Bowen's ratio, 0.16, closely resembles the long hydro-period ratios. Our results for sensible heat flux for evergreen forest resembling mangrove forest sites are slightly higher than in emergent herbaceous wetland, whereas the latent heat fluxes are slightly lower. The results are consistent with Shoemaker et al. (2015) in which they

reported higher sensible and lower latent heat flux for pine upland and dwarf cypress sites than for Wet Prairie and Cypress Swamp.

June average ETs reported by Shoemaker from various sites within the Everglades are: 3.49 mm/day for a wet prairie site (2008-2010), 4.01 mm/day for a cypress swamp site (2007-2009), 3.35 mm/day for dwarf cypress site (2007-2009), 2.8 mm/day for marsh site (2007-2009), and 3.04 mm/day from pine upland site (2007-2009). Our estimated overall ETs for 2010 (3.56 mm/day) fall in the agreeable range with above mentioned sites as well as with the reported values of 3.6 mm/day (Abtew, 2004) from a constructed wetland in South Florida.

3.6 Conclusion

In this study, a combined approach taking benefits from both remotely-sensed and ground-based meteorological data has been used to relate surface energy flux to land surface parameters. The approach is derived from a simple hypothesis that anthropogenic conversion of land modulates the energy partitioning increasing sensible heat flux in those areas. Local surface cover changes not only influence climate of the immediate vicinity, but large-scale land cover changes may influence global circulation affecting the water and energy budgets in areas not affected by land cover change.

A common presumption that urban albedos are lower compared to undeveloped counterparts is invalidated. The sensible heat flux from high intensity urban cover was >100% of net radiation in both the years 1984 and 2010 justifies that net radiation in urban area is not just a mere balance of incoming and outgoing short and long-wave radiation; a significant portion of it comes from anthropogenic expulsion. Sensible heat fluxes averaged from all the urban subcategories increased from 70% of net radiation in

1984 to 93% in 2010. Water and wet vegetated covers tend to enhance heat flow towards the sub-surface, whereas the agricultural covers in 1984 and urban covers in 2010 have the least ground heat flux. Substantial increase of sensible heat flux from urban and barren lands and a subsequent decrease in ground heat flux is indicating that the surface fabrics in those covers tend to vigorously transfer heat upwards to the atmosphere rather than conducting it downwards. Agricultural lands are found to have intensely increased latent heat flux in the later period. The daily average ET rates are decreased overall, and are in the agreeable range when compared to previous studies. A substantial increase of ET rates in agricultural vegetation from the least ET in 1984 to closer to ET values of forest may suggest an increased availability of water on or close to the surface.

3.7 References

Abtew, W. (2004) Evapotranspiration in the Everglades comparison of Bowen ratio measurements and model estimations, *Technical paper EMA 417*, South Florida Water Management District, West Palm Beach Florida.

Ameriflux Site and Data Exploration System, http://ameriflux.ornl.gov/ Accessed on October 20, 2014.

Arya, S.P. (2001) *Introduction to Micrometeorology*, i*nternational geophysical series, v*ol.36, edited by R. Dmowska, J. R. Holton, and H. T. Rossby, Academic Press, New York.

Bennett W.B., J. Wang, and R.L. Bras (2008) Estimation of ground heat flux, *Journal of Hydrometeorology,* 9: 744-759.

Betts, R.A. (2001) Biogeophysical impacts of land use on present-day climate: near-surface temperature change and radiative forcing, *Atmospheric Science Letters* 1, doi:10.1006/asle.2001.0023.

Brutsaert, W. H. (1975) On a derivable formula for long-wave radiation from clear skies, *Water Resour. Res.,* 11,742 744.

Campbell, G.S. and J.M. Norman (2000) An introduction to environmental biophysics, 2nd ed. 286 pp Springer-Verlag, New York.

Chen, Z., S. Li, J. Ren, P. Gong, M. Zhang, L. Wang, S. Xiao and D. Jiang (2008) Monitoring and management of agriculture with remote sensing, in *Advances in Land Remote Sensing* (S. Liang ed.), 397-421.

DBHYDRO Hydrological and Physical Data, South Florida Water Management District, Accessed on October 17, 2015.

Duever, M.J., J.F. Meeder, L.C. Meeder, J.M. McCollom (1994) The climate of South Florida and its role in shaping the Everglades ecosystem, In *Everglades the ecosystem and its restoration* edited by Steve Davis, John C. Ogden, CRC Press, 860 pp.

Duguay, C.R. and E.F. Ledrew (1992) Estimating surface reflectance and albedo from Landsat 5 thematic mapper over rugged terrain, *Photogrammetric Engineering and Remote Sensing*, 58,551-558.

Flux measurements from the SRS-6 Tower, Shark River Slough, Everglades National Park (FCE), South Florida from October 2006 to Present, Florida Coastal Everglades, LTER Program, Accessed on 25 October, 2014.

Gash, J.H.C; and W. J. Shuttleworth (1991) Tropical deforestation: albedo and the surface energy balance, *Climatic Change* **19**: 123-133.

Gedney, N. and P.J. Valdes (2000) The effect of Amazonian deforestation on the northern hemisphere circulation and climate, *Geophysical Research Letters*, 27(19): 30530-3056.

Grimmond, C.S.B., and T.R. Oke (1999) Aerodynamic properties of urban areas derived from analysis of surface form, *Journal of Applied Meteorology*, 38 (9): 1262-1292.

Global Surface Hourly Observations, National Climatic Data Center, National Oceanic and Atmospheric Administration, Accessed on October 22, 2014.

Irish, R. R. (2000) In Landsat 7 automatic cloud cover assessment, *AeroSense*, International Society for Optics and Photonics, 348-355.

Jiménez-Muñoz, J. C., J. A. Sobrino, L. Guanter, J. Moreno, A. Plaza and P. Matínez (2005) Fractional vegetation cover estimation from proba/chris data: methods, analysis of angular effects and application to the land surface emissivity retrieval, Proc. of the 3rd ESA CHRIS/Proba Workshop, 21–23 March, ESRIN, Frascati, Italy.

Kelliher, F. M., R. Leuning, M. R. Raupach, and E.D. Schulze (1995) Maximum conductance for evaporation from global vegetation types, *Agric. For. Meteorol.,* 73, 1 – 16.

Körner, C., J. A. Scheel, and H. Bauer (1979) Maximum leaf diffusive conductance in vascular plants, *Photosynthetica*, 13, 45 – 82.

Liang, S. (2001) Narrowband to broadband conversions of land surface albedo I: Algorithms, *Remote Sensing of Environment*, 76(2), 213-238.

Lagomasino, D., R. M. Price, D. Whitman, A. Melesse, S. F. Oberbauer (2014) Spatial and temporal variability in spectral-based surface energy evapotranspiration measured from Landsat 5TM across two mangrove ecotones, *Agricultural and Forest Meteorology,* doi:10.1016/j.agrformet.2014.11.017

Landsberg, H. E. (1970) Man-Made climatic changes Man's activities have altered the climate of urbanized areas and may affect global climate in the future, *Science*, 170 (3964), 1265-1274.

Marshall, C.H., R.A. Pielke Sr., L.T. Steyeart, D.A. Willard (2004) The Impact of Anthropogenic Land-Cover Change on the Florida Peninsula Sea Breezes and Warm Season Sensible Weather, *Monthly Weather Review*, 132 (1), 28-52.

Melesse, A.M., V. Nangia, X, Wang, and M. McClain (2007) Wetland restoration response analysis using MODIS and groundwater data, *Sensors,* 7(9),1916-1933.

Miller, K. S., and B. Ross (1993) An Introduction to the Fractional Calculus and Fractional Differential Equations. Wiley,366 pp.

Monteith, J. L. (1973) Principles of Environmental Physics, Arnold, London, 241 pp.

Moran, M. S., R. D., Jackson, L. H., Raymond, L. W., Gay and P. N. Slater (1989) Mapping surface energy balance components by combining Landsat Thematic Mapper and ground-based meteorological data, *Remote Sensing of Environment*, *30*(1), 77-87.

Norman, J.M., W.P. Kustas, K.S. Humes (1995) Source approach for estimating soil and vegetation energy fluxes in observations of directional radiometric surface temperatures, *Agricultural and Forest Meteorology*, 77, 263-293.

Price, J.C. (1977) Thermal inertia mapping: a new view of the earth, *Journal of Geophysical Research*, 82(18), 2582-2589

Oke, T.R. (1982) The energetic basis of the urban heat island. *Quart. J. Met. Soc*., 108, pp. 1-24.

Oke, T.R. (1978) *Boundary Layer Climates*, 372 pp, Methuen and Co Ltd, New York.

Shoemaker, W. B., D. M. Sumner, and A. Castillo (2005), Estimating changes in heat energy stored within a column of wetland surface water and factors controlling their importance in the surface energy budget, *Water Resour. Res.*, 41, W10411, doi:10.1029/2005WR004037

Shoemaker, W.B., F. Anderson, J.G. Barr, S.L. Graham and D.B. Botkin (2015) Carbon exchange between the atmosphere and subtropical forested cypress and pine wetlands, *Biogeosciences*, 12, 2285-2300.

Shukla, J., C. Nobre, and P. Sellers (1990) Amazonian deforestation and climate change, *Science*, 247: 1322-1325.

Sklar, F. H., H. Fitz, Y. Wu, R. Van Zee, C. McVoy (2001) South Florida: The Reality of Change and the Prospects for Sustainability: The Design of Ecological Landscape Models for Everglades Restoration. *Ecological Economics*, 37 (3), 379-401.

Sobrino, J., N. Raissouni (2000) Toward remote sensing methods for land cover dynamic monitoring: application to Morocco, *International Journal of Remote Sensing* , 21 (2), 353-366.

Sobrino, J. A., J. C ., Jiménez-Muñoz, G. Sòria, M. Romaguera, L. Guanter, J. Moreno, A. Plaza, P. Martínez (2008) Land surface emissivity retrieval from different VNIR and TIR sensors, *IEEE Transactions on Geoscience and Remote Sensing*, 46 (2), 316-327.

U.S. Bureau of the Census, Population Estimates Program (PEP), Population 2013 estimate, http://quickfacts.census.gov/qfd/states/12/12086.html Accessed on June 26, 2014.

USGS, Landsat Surface Reflectance Climate Data Records, http://earthexplorer.usgs.gov/ Accessed on May 29, 2014.

Walker, R. (2001) Urban Sprawl and natural areas encroachment:linking land cover change and economic development in the Florida Everglades, Ecological Economics, 37, 357-369.

Weng, Q., D., Lu, J., Schubring (2004) Estimation of land surface temperature–vegetation abundance relationship for urban heat island studies, *Remote sensing of Environment*, 89 (4), 467-483

Wilson, K. B., et al., (2002) Energy partitioning between latent and sensible heat flux during the warm season at FLUXNET sites, *Water Resour. Res.,* 38(12), 30-1-30-11, doi:10.1029/2001WR000989.

Wullschleger, S. D. (1993) Biochemical limitations to carbon assimilation in C3 plants—A retrospective analysis of the A/Ci curves from 109 species, *J. Exp. Bot*., 44, 907 – 920.

Zhu, Z.; C. E., Woodcock (2012) Object-based cloud and cloud shadow detection in Landsat imagery, *Remote Sensing of Environment*, 118, 83-94.

Chapter 4

Radar Reflectivity Based Convective Rainfall Change in South Florida: An Implied Effect of Land Use/Land Cover Change

Kandel, H., A.M. Melesse, P. Zhu (2015) Radar Reflectivity Based Convective Rainfall Change in South Florida: An Implied Effect of Land Use/Land Cover Change, *Hydrological Processes,* (under review)

Abstract

The most plausible micrometeorological effects of drainage and development in South Florida are discernible in the increase of sensible heat flux and development of urban heat island above the urban centers. These effects alter timing, rate, and spatial axis of sea breeze convergence, thereby modifying the amount and location of surface induced convective precipitation. The present study is the first in South Florida showing a relation between land use land cover and radar based warm season convective rainfall for duration of 18 years. Base radar reflectivity from lowest elevation angle of the Weather Surveillance Radar (WSR-88D) is used to estimate the density and intensity of convective rainfall. Spatial density, intensity, and variability of ≥40 dBZ radar reflectivity obtained from the radar station in Miami (KAMX) for eighteen years (1995-2012) of synoptically benign three-hour summer afternoon are analyzed. Rain rate is calculated using a standard Z-R relationship. Analysis of land use land cover change is carried out in entire South Florida and eastern urbanized South Florida separately for the temporal range equivalent to radar data. The spatiotemporal comparison of radar reflectivity and derived rain rate indicates that both cell densities and rates of change of thunderstorm intensity are higher (mean density difference = 5.9/1000 Sq. km, difference in increase of rain rate = 0.24 mm/hr/summer) in urbanized South Florida compared to the entire South

Florida. Daily maximum rain rate is also found increasing at the rate of 6.43 mm/hr and 6.67 mm/hr per summer for entire and urbanized South Florida, respectively.

Key Words: Radar reflectivity; convective rainfall; urbanization; land cover change; South Florida; WSR-88D

4.1 Introduction

Land use land cover (LULC) in South Florida, here defined as the land area south of Lake Okeechobee, has been modified extensively since the early 20th century by anthropogenic activities such as wetland drainage, water management structures, deforestation, agricultural and pasture land expansion, and rapid development of settlements (McVoy *et al.,* 2011). Changes in surface cover directly affect various physical parameters e.g., albedo, specific heat, and thermal conductivity that control absorption and disposition of incoming radiation at the Earth's surface (Feddema *et al*., 2005). Variations in surface albedo, specific heat, and soil moisture content determine the rate and magnitude of heat and moisture fluxes (Pielke, 2001). For instance, albedo, the reflective property of the Earth's surface, modifies the absorption rate of solar radiation and hence modulates the forms of energy available at the Earth's surface (Betts, 2001). Built-up areas store more heat than their rural surroundings, leading to the temperature gradient across urban-rural boundary and creating their own mesoscale convergence (Niyogi *et al*., 2011). Physical properties of the underlying land surface have direct impact on the timing and magnitude of the land-water temperature gradient; thereby altering the structure and diurnal evolution of sea breezes and cumulus clouds (Schrieber *et al*., 1996, Rabin *et al.,* 1990). Also, changes in spatial distribution of land cover types

can force local circulations, which can interact with sea breezes and cause convergence and convection (Pielke *et al.,* 1991).

Generally, precipitation can be classified into convective and stratiform (Houze, 1993) types. Strong vertical velocity, small areal coverage and high rainfall intensity characterize convective regime; conversely, relatively weak vertical velocity, larger horizontal homogeneity, and lower rainfall intensity characterize stratiform regime. Convective systems are associated with an unstable or conditionally unstable atmospheric boundary layer (Baik *et al*., 2007).

There are several studies on the mechanisms that create urban-induced convective precipitation. Enhanced convergence resulting, either from urban surface roughness or Urban Heat Island (UHI)-sea breeze-coastal interactions, and destabilization of the boundary layer resulting from UHI-thermal perturbation generating downstream circulation of convective clouds, are the possible suggested mechanisms for urban-induced rainfall (Shepherd *et al*., 2002). Urban heat island is the positive temperature gradient in urban areas with the surrounding rural areas, which creates a pressure field, setting a concentric breeze into motion (Landsberg, 1970). Dixon and Mote (2003), from their study of UHI initiated precipitation in Atlanta during 1996-2000, suggested that weak synoptic flow, slightly unstable atmosphere, high moisture content, and anomalous heat of UHI are conducive for the development of convective layers. Weak synoptic flows are favorable because strong advection tends to eliminate the local effect of UHI. Slight instability also favors convective cloud generation over the urban surface because intense convective mixing in highly unstable boundary layers also erases the local effect of UHI.

Shepherd *et al.* (2010) carried out a study of urban impact on coastal precipitation from the Houston area and noted a connection between the enhanced rain clouds and the convergence zones along the low-pressure urban fringe. They found that the interaction of UHI-sea breeze front not only amplifies the convective forcing but also induces secondary interaction precipitation which is an important contributor to urban rainfall budgets. Even though UHI in the city is more apparent after sunset (Oke, 1987), UHI induced circulation is more evident during the afternoon hours because of the urban-rural pressure gradient and vertical mixing in those hours (Shepherd and Burian, 2003). Carter *el al.* (2011) realized a large impact of urban environment on the evolution of sea-breeze mesoscale boundary from a modeling study of sea-breeze urban interactions in Houston. They observed decreased dwell-time of sea-breezes over urban area and increased strength of vertical velocity anomaly as sea-breezes accelerate and strengthen after coming into contact with the Houston urban area. They also noted that most of the interactions began between mid and late afternoon.

Diem and Brown (2003) recognized that augmented input of surface to atmosphere water vapor from the irrigated areas, greater convergence from the rough urban surfaces, and enlarged cloud condensation nuclei of urban pollution as the possible causative factors for human-enhanced precipitation in urban Arizona. They further used a 108-year rain gauge record and showed statistically significant results of increased summer rainfall by 11-14% during post-urban period in Lower Verde basin, Arizona. Similar other studies indicate that warm season rainfall increases by 9% to 17% in major cities. An extensive study of mesoscale and convective rainfall modification by major US cities, Metropolitan

Meteorological Experiment (METROMEX), showed increased precipitation in the summer months within 50-75 km downwind of the cities (Changnon *et al.,* 1977).

A summer time (May-August) radar image analysis during both day and night hours from 2000 to 2009 in the Indianapolis urban area concluded that positive buoyancy within the urban environment during the day causes more changes in storm composition than during the night (Niyogi *et al.*, 2011). Ashley *et al.* (2012) used high resolution radar-based climatology for warm season convection in Southeastern U.S. cities and demonstrated significant details of urban effects on thunderstorm frequency and intensity. A large impact of the urban area on the timing and intensity of sea-breeze front (Kusaka, 2000; Ohasi and Kida, 2004 and Martilli, 2003) have been noted in several other cities of the world.

Since surface driven convective thunderstorm is one of the primary processes responsible for the wet season rainfall in South Florida (Pielke, 1974), questing an association between the land cover change and convective rainfall is believed to be valuable for a better understanding of the spatiotemporal pattern of South Florida rainfall. Marshall *et al.* (2004) employed pre-1900 and 1997 land covers in an atmospheric numerical model and concluded that anthropogenic land cover change in the Kissimmee River Basin of Florida increased surface temperatures and decreased rainfall in the region.

Several of the studies rely on results produced by coupled land surface -atmosphere numerical models simulating the specific events. There are many complications in using numerical models for the simulation of the atmospheric convection which cannot be overlooked. Parameterization representing the ground surface reality in models is always stacked with errors. These errors are propagated throughout the boundary layer during the

integration in various mathematical formulations. Furthermore, requirements of intensive data, and considerable time as well as the need of super capacity computing resources for the simulation make modeling a daunting task.

To gain a preliminary insight on spatiotemporal rainfall pattern in South Florida, monthly rainfall summary from cooperative weather stations in South Florida were obtained from NCDC. Station total annual rainfall interpolated for two eastern sub-basins of South Florida showed a higher rainfall in the eastern coastal ridge, which is dominantly an urbanized area. Time series analysis of total annual rainfall for 1982-2010 revealed a very slight decrease throughout the period, beside noticeable year-to-year variability. Sole effect of LULC change on convective rainfall, however, needs to consider two important aspects (Lowry, 1998): 1) an analysis of the events only when the surface driven convection is active, which is during the afternoon hours in summer, and 2) exclusion of the synoptically influenced weather events from analysis.

The present study with the motivation from the findings of previous radar based study carried out in Southeastern US cities by Ashley *et al.* (2012), employs radar reflectivity data for the analysis of the thunderstorms in South Florida. As opposed to a single event simulation or short time analysis, this eighteen-year study in South Florida is the first to analyze the nature of warm season thunderstorms for long period using base radar reflectivity. It covers three afternoon hours (12:00 – 3:00 PM LST) of the three summer months (June, July, and August) for the period of 1995 to 2012. The study separates the synoptic weather disturbances from the analysis in order to conform to the objective that the thunderstorms are the effects only of local surface thermodynamics. Using observational radar data, this work also aims to review the model based results of Pielke

et al. (2007), which concluded that changes on surface fluxes of moisture, sensible heat, and latent heat lead to the changes on warm season rainfall in a region of deep cumulus convection. The specific objectives of this study are to (1) analyze the spatial and temporal changes in radar reflectivity that characterize thunderstorms for South Florida, (2) identify and exclude synoptically active days from the study period, (3) Analyze spatial variation of LULC and quantify the LULC changes by major categories in South Florida and (4) compute the rain rate using reflectivity-rain rate (Z-R) relationship and relate that with LULC change.

4.2 Study Area

The spatial coverage of this study includes entire South Florida bordered by Lake Okeechobee, Florida Bay, Atlantic Ocean and Gulf of Mexico towards north, south, east and west respectively. Hydrologically, the area is comprised of six different sub-basins namely: Lake Okeechobee, Everglades, Big Cypress Swamp, Caloosahatchee, Florida Southeast Coast and Florida Bay-Florida Keys with the total area of 35,552 km^2 (Figure 4.1). Prominent land cover units such as Everglades Agricultural Area (EAA) towards north, three Water Conservation Areas WCAs- 1, 2, and 3 in the middle and conserved wetland, the Everglades National Park (ENP) in the south constitute the biggest watershed, the Everglades. Big Cypress Swamp is a partly forested and partly grassy swamp, consisting of slough and marshes, and intersected by canals in places.

Florida Southeast Coast sub-basin is the mostly urbanized basin in the eastern part of the three counties: Palm Beach, Broward, and Miami Dade. This is the main urban region in South Florida housing Miami, Fort Lauderdale and Pompano Beach Metropolitan Statistical Areas (MSAs) and hosting major cities, such as, Boca Raton, Boynton,

Deerfield, Delray, Ft Lauderdale, Homestead, Kendall, Miami, Pompano Beach, and West Palm Beach. Two old cities: Naples and Everglades lie in the Big Cypress watershed in the west. Fort Myers, another old city in South Florida, lies in the western part of the Caloosahatchee basin. Lake Okeechobee and its shoreline constitute the northernmost watershed. For the purpose of spatial comparison, two overlapping spatial units, entire South Florida (ESF: -80.08W to -81.76 W longitude and 24.98 N to 26.93 N latitude) and Eastern Urbanized South Florida (EUSF: -80.08 W to -80.63 W longitude and 25.15 N to 26.93 N latitude) are selected (Figure 4.1). The southern strip of the Florida Bay and the Florida Keys are excluded from the analysis accounting their insignificant land areas to influence on the land-atmosphere dynamics of South Florida. Above all, the big water bodies and the vast wetland as the sources of moisture, and a narrow strip of urban land as a source of buoyant energy make South Florida a unique experimental site for this study.

4.3 Methodology

The type, source, and characteristics of the data and the methods of their analysis are presented in this section.

4.3.1 Land use/Land Cover Change

In general, the three natural classes of land use land cover: wetlands, water bodies and forests are the dominant surface cover types in the entire South Florida, which in the eastern part are replaced by urban built-up and agricultural covers. Various agencies

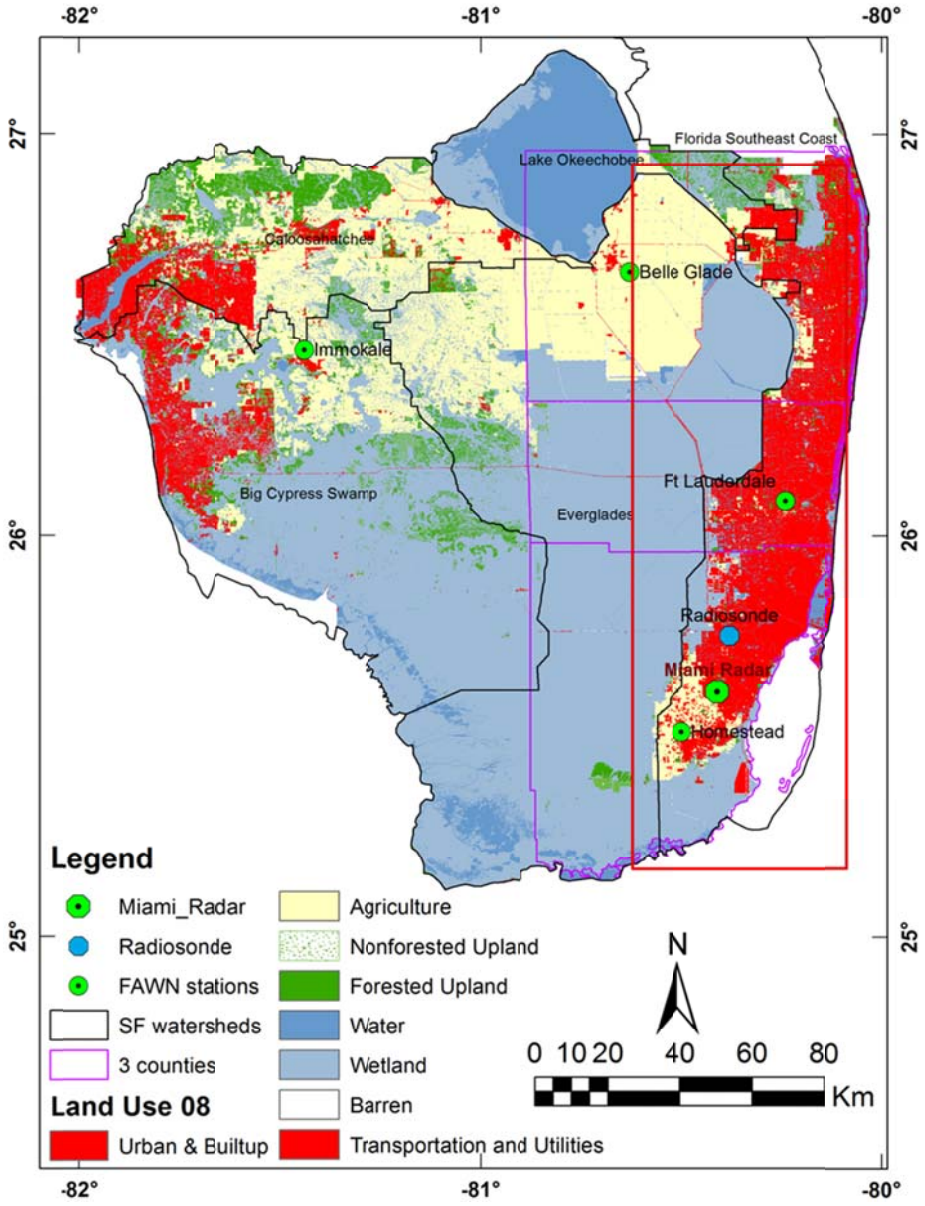

Figure 4.1 Study area basin map overlaid with SFWMD land use map of 2008 and different weather stations locations. The red rectangle in east is the selected portion (EUSF) for radar analysis that represents dominant urban and agricultural use.

archive statewide and nationwide land use land cover data in vector and raster format.

South Florida Water Management District (SFWMD) produced a 1995 land use land cover map by the photointerpretation of 1:40,000 USGS 1994/1995 National Aerial Photography Program's (NAPP) color infrared photography. These data use Florida Land

Use Land Cover Classification System (FLUCCS). The Florida Natural Area Inventory (FNAI) has developed an improved statewide land cover map called Cooperative Land Cover (CLC) in 2010 derived from local, regional, and site-specific sources. This latest available data is a compilation partly from the aerial photo review and partly from the land use land cover data developed by the Florida Department of Environmental Protection (FDEP) and water management districts in Florida. The data also use the codes as derived by FLUCCS. Since both of these datasets, from 1995 and from 2010, contain standardized field names and were developed using similar sources with compatible scales, they were used in this comparative study. Land use land cover change was reported in terms of percentage change of the major category from 1995 to 2010 in both the entire South Florida and the eastern urbanized South Florida. Also, LULC data of 1996 and 2006 were accessed from Coastal Change Analysis Program (CCAP) for loss and gain analysis of the major land cover types in the three eastern counties.

4.3.2 Historical Daily Weather

The National Oceanic and Atmospheric Administration, National Weather Service (NOAA, NWS) archives the historical daily weather maps prepared by the Weather Prediction Center of National Centers for Environmental Prediction. Daily surface weather maps show isobars, locations of pressure highs and lows, wind speeds and directions, frontal boundaries, hurricanes, and tropical depressions, storms, waves. These maps show the analysis results based on the ground based station and upper atmospheric conditions of six, twelve or twenty-four hours before 7:00 AM Eastern Standard Time (EST).

Historical daily weather maps were read to identify the synoptic scale weather phenomena, such as: low pressures; cold and stationary fronts; tropical depressions, waves and storms; and hurricanes at the surface; and low pressures at the mid-tropospheric level. Synoptic scale atmospheric motions range in size from 100 to 2000 km horizontally, and can persist from days to weeks (Orlanski, 1975). A region approximately 500 km around the centroid of the study area was considered as an area of influence for synoptic systems while reading the daily weather map. The days with notable signatures of these events within 20° to 30° latitude and -75° to -85° longitude were identified, listed and later excluded from the analysis of radar metrics. Being larger in horizontal scale and longer in time scale, these flows identified on daily weather maps at 7 AM LST are interpreted as the weather disturbances for the corresponding afternoon.

4.3.3 Radar Reflectivity

Weather Surveillance Radar -1988 Doppler (WSR-88D), also called NEXt Generation Radar (NEXRAD), is an S band (10 cm wavelength) radar. Level II base reflectivity of the WSR-88D is the backscattered power of the returning signal after the emitted microwave energy from the radar strikes the hydrometeor target. The instrument collects echo at different elevation angles. The one used in this study is the echo from the lowest tilt angle of 0.5° with respect to horizontal. There are two resolution eras in the history of WSR-88D: the legacy era prior to 2008, and the super-resolution era after 2008. The data have a range resolution of 1 km (250 m) and azimuthal resolution of 1° (0.5°) for legacy (super resolution) era. The instrument averages all the scans for each five-minute and records them in eight bit digital format. A predefined control for pulse repetition

frequency and antenna rotation speed, called Volume Coverage Pattern (VCP), of the analyzed data is 21 and 12, as these are the designed VCPs to detect shallow and deep convective precipitations, respectively. Measured in logarithmic scale of decibels of reflectivity (dBZ), the reflectivity factor, Z, corresponds to the sixth power of drop diameter (ΣD^6). Hence, the higher the reflectivity value, the larger is the size of the drop. The base reflectivity in precipitation mode has the dynamic range of 5 to75 dBZ, estimated standard deviation of 1 dB, range coverage of 0 to 460 km, range increment of 1 to 460 km, and data resolution of 0.3 dB (WSR 88D functional overview, 2005). Radar reflectivity files of each five-minute intervals from the three afternoon hours between 1600 and 1900 UTC for Miami station (KAMX) were downloaded from the National Oceanic and Atmospheric Administration -National Climatic Data Center – called Hydromet Decision Support System (NOAA-NCDC-HDSS). The three afternoon hours is the time period in which a major development of convection in both coasts occurs, along with the enhanced convergence and the stronger convective elements inland (Blanchard and Lopez, 1985). Extracted data were imported into NOAA weather and climate toolkit. With the help of this toolkit, reflectivity as the moment, 0.5° as the elevation angle, point shape file as the format, ESF and EUSF as the geographic boundaries, and 40 dBZ as the minimum reflectivity were extracted. Macro code in Microsoft Excel was used to merge the individual files.

The results of radar reflectivity were prepared in five different forms: vertical profile, point (cell) density, maximum reflectivity, reflectivity variance, and daily maximum rain rate. Convective boundary layer is taller vertically, but narrower horizontally. Therefore, a vertical cross section of radar reflectivity is diagnostic in distinguishing stratiform and

convective types of precipitation. Stratiform precipitation, having been fairly homogenous in horizontally, gives rise to layered structure in the vertical cross sections. On the other hand, convective precipitation appears on a radar as a tall column of high reflectivity (Houze, 1997). Reflectivities from all elevation angles were extracted from a selected area around Miami International Airport (MIA) for two time periods 16:02 UTC and 18:16 UTC for August 17,1995. The time stamps correspond with no thunderstorm and thunderstorm events, respectively, as observed in the hourly historical weather records of MIA obtained from wunderground website. The vertical profiles of reflectivities and corresponding radar echo maps for those two events were compared. Number of high echo cells (≥40 dBZ) were counted and divided by the areas of the respective study sections in order to get the average cell density. The density calculation facilitates the comparison of thunderstorm distribution between ESF and EUSF. The cell density analysis was limited until 2007 because the super resolution counts cannot be compared directly to the legacy counts.

In order to make the maximum reflectivity and variance results of the legacy era comparable with the super resolution era, a simple linear relative difference algorithm was formulated and applied as an up-scaling factor. The super resolution data is four-times finer in range, and two times finer in azimuth than the legacy data. Therefore, focal statistics was calculated taking eight cells as neighborhood (four cells along height and two cells along width) using the focal statistics tool in ArcGIS. Separate relative difference (RD) factors for maximum reflectivity and variance were derived using the following simple linear method:

$$RD = \frac{\text{Super Resolution Max.(Var.)}}{\text{Focal Max.(Var.)}} - 1 \quad (1)$$

The idea is that the focal maximum (Focal Max.) and the focal variance (Focal Var.) derived from eight adjacent cells up-scale the super resolution to legacy resolution at their best approximation. The RD was found to be 0.04 for maximum reflectivity, and 0.44 for reflectivity variance.

The maximum reflectivity and variances were computed for each five-minute intervals. Average maximum reflectivity and variance of a day represent spatial maxima and spatial variances from each five –minutes, which were averaged for three hours (thirty six sweeps). Two arbitrarily divided time phases, 1995 to 2003 as the early phase and 2004 to 2012 as the late phase, were used for temporal comparison. Statistical significance was tested using paired sample t-test that compares two periodic means of the data drawn from similar population.

Finally, the rain rate from each daily maximum reflectivity was calculated for both units, ESF and EUSF. The following standard Z-R relationship was used in order to calculate the rain rate:

$$Z = AR^b \quad (2)$$

where R is the rain rate (mm/hr), and Z is the equivalent reflectivity. The reflectivity factor (dBZ) and the equivalent reflectivity Z (mm^6m^{-3}) has the relationship of dBZ = 10logZ, such that, for Z = 1 mm^6m^{-3}, the reflectivity factor is 0 dBZ; likewise, for Z = 10^5 mm^6m^{-3}, the reflectivity factor is 50 dBZ. The fitting coefficients used in Z-R relationship are A = 300 and b =1.4, which were developed for convective events (Fulton *et al*.,

1998). A time series decomposition of daily rain rate was carried out in order to obtain monthly components.

4.3.4 Wind, Temperature, and Moisture

Being that South Florida is bordered by major water bodies in all four directions, sea and lake breeze circulations play a crucial role in its weather, particularly in warm season precipitation. As study results suggest, for example, 10-40% of the continental precipitation is contributed by local water vapor (Burbaker, 1993), a better insight on convective precipitation can be gained by analysing wind divergence, moisture status and surface based convective available potential energy (CAPE) of the region. Lower level (2 m and 10 m elevation) wind, temperature and relative humidity data obtained from the Florida Automatic Weather Network (FAWN) were used in this section. Summer afternoon wind speeds and directions from two representative stations (Immokalee for natural cover, and Ft Lauderdale for urbanized cover) at 10 m elevation were used to calculate the wind component vectors u and v. The u and v were averaged for a summer from each stations and a trend was obtained from the available South Florida stations. The trend was removed and the deviations were employed to derive the divergence as given in (3):

$$\text{Div} = \frac{\partial u}{\partial x} + \frac{\partial v}{\partial y} \tag{3}$$

where the first and second terms on the right are the horizontal gradients of zonal (u) and meridional (v) components of wind, respectively from Fort Lauderdale to Immokalee stations. Unavailability of longer time series data at other stations limit this analysis only for these two locations.

Specific humidity from three stations (Ft Lauderdale, Homestead, and Immokalee) was computed using (4) with summer time daily average temperatures and relative humidities at 2 m level as two input variables obtained from FAWN.

$$\mathrm{RH} = \frac{q}{q_s} \tag{4}$$

where q (kg/kg) is specific humidity; q_s (kg/kg) is saturated humidity (= $e.e_s/P$, e = 0.622, e_s, the saturated vapor pressure = $e_0 \times \exp[(L/R_v)\times(T-T_0)/T\times T_0)]$, e_0 = 0.611 kPa, T_0 = 273.15° K, T = temperature in Kelvins), P is the atmospheric pressure and is assigned as 100 kPa, Rv is the gas constant for water vapor which is equal to 461 $JK^{-1}kg^{-1}$, and L (latent heat of vaporisation) is equal to 2.5×10^6 $J.kg^{-1}$.

Convective Available Potential Energy (CAPE) is the sum of the positive buoyant energy (in joules per kilogram) a rising parcel would possess as it travels from the Level of Free Convection (LFC) to the Equilibrium Level (EL) as defined in equation (5):

$$\int_{LFC}^{EL} \frac{T_{par} - T_e}{T_e} g dz \tag{5}$$

where T_{par} is the temperature of the parcel in different elevation levels, T_e is the equivalent level ambient air temperatures, g is acceleartion due to gravity (9.8 ms^{-2}) and dz (m) is the change in elevation between two calculation levels. The LFC and EL are the lower and higher elevation points where ambient and parcel temperatures intersect. Environmental air temperatures are used from the upper air sounding data of Miami radiosonde. The following lapse rates were used in order to assign temperatures to the ascending air parcel in different atmospheric levels: 9.8 °C/km below lifting

condensation level; 4 °C/km between LCL and 2 km; and 5 °C/km, 6 °C/km, 7 °C/km, 8 °C/km for each elevations levels between 2 to 5 km, 5 to 6 km, 6 to 7 km, and 7 to 8 km respectively. The lowest level lapse rate (9.8 °C/km) was repeated for the levels above 8 km. First, the observed temperature and relative humidity were averaged at each elevation levels from all summer evenings and those averages were used to calculate one representative CAPE value for a summer (Appendix 8).

4.4 Results

This section presents the results of the analysis of population status and land use land cover; synoptic weather; radar reflectivity; wind divergence, air temperature, humidity; and CAPE in both illustrative and statistical terms.

4.4.1 Population and Land Use/ Land Cover

Population change is a direct measure of the changes in land use land cover for any geographic unit. More than 5.5 million people live in urban clusters of the eastern three counties of South Florida: Miami Dade, Broward, and Palm Beach with a rate of increase of nearly one million (> 20%) per decade (Figure 4.2). Expansion of developed areas in the period between 1995 and 2010, i.e., low intensity (+0.49%), medium intensity (+0.78%) and high intensity (+0.51%) appeared to replace the scrub/shrub (-0.39%), pasture/ hay (-0.51%), and cultivated crop land (-1.02%) in these counties (Figures 4.3 and 4.4).

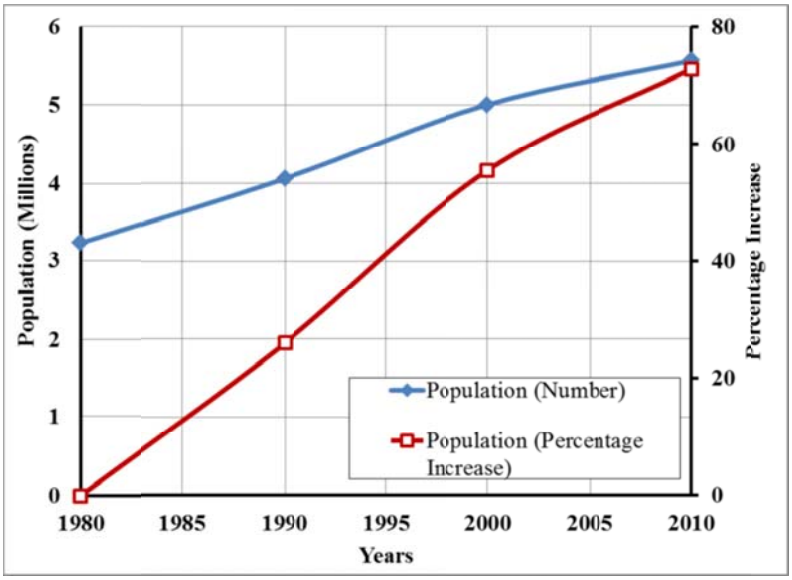

Figure 4.2 Increase of population between 1980 and 2010 in urban South Florida (Miami- Ft Lauderdale- Pompano Beach MSA) (US Census Bureau, 2010).

4.4.2 Synoptic Scale Signatures

The total numbers of days contaminated with synoptic disturbances are found to be 243 out of the total 1656 days (Appendix 7). The highest and the lowest disturbance years are 2005 with twenty two disturbed days and 1999 with two disturbed days, respectively. Tropical low pressures, cold fronts, tropical storms, and hurricanes are the dominant synoptic weather systems that caused heavy rain or thunderstorms predominantly in the months of July and August (Table 4-1). The total of 1208 afternoons are found benign after deducting data days that are either disturbed or have none to very few data files. It is noticed during the filtering of the reflectivity data that very high reflectivity days were associated with two tropical weather phenomena: tropical storms, and hurricanes.

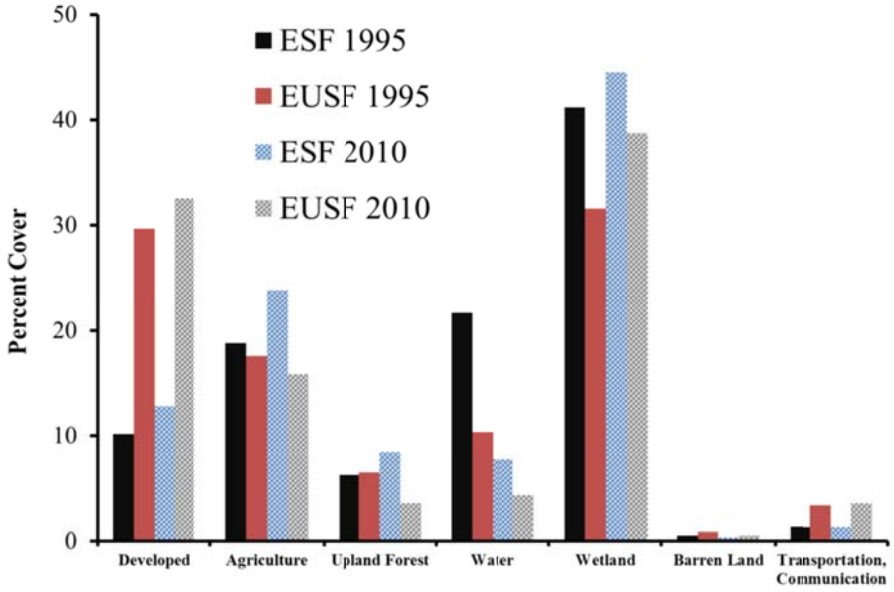

Figure 4.3 Land use/ land cover change within ESF and EUSF from 1995 to 2010 (from SFWMD and FNAI).

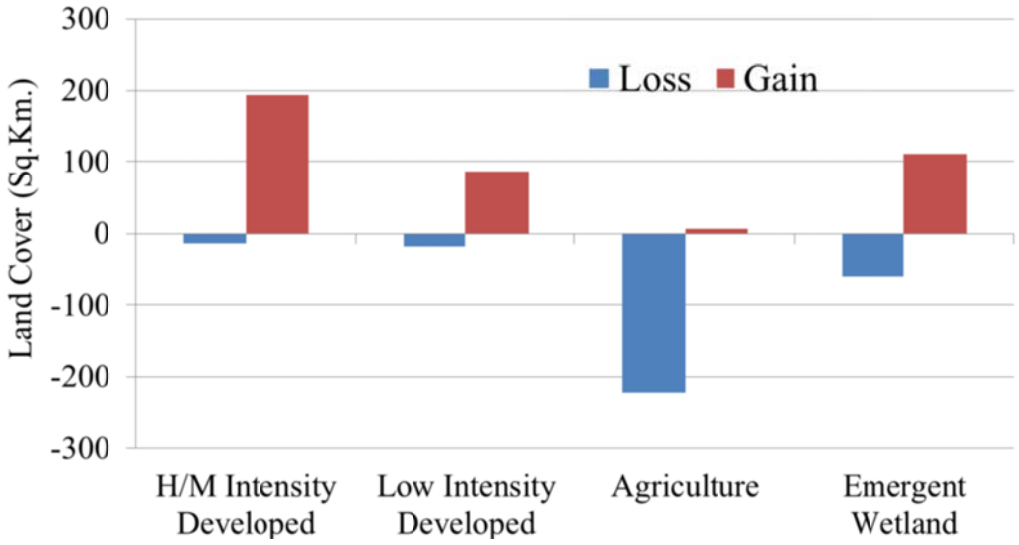

Figure 4.4 Land use/ land cover change in eastern three counties (Palm Beach, Broward, and Miami-Dade) of South Florida during 1996- 2006.

4.4.3 Radar Reflectivity

4.4.3.1 Thunderstorm Detection

The profiles in Figure 4.5, which show vertical cross sections of radar reflectivities from the selected area around MIA, clearly dintinguish thunderstorm event. Thunderstorms are apparent from the cluster of near surface ≥ 40 dBZ reflectivities with the profile height of above eight kilometers (Figure 4.5- 2:16 PM). On the other hand, the non-thunderstorm profile has the reflectivities restricted below 20 dBZ, and the profile height below three kilometers (Figure 4.5 -12:02 PM).

4.4.3.2 Point Density

Both mean and median values of point density demonstrate spatially denser thunderstorm distributions in EUSF (Table 4-2, Figure 4.6). Gently negative slopes of the linear regression manifest declining rates of number of thunderstorm cells in both ESF and EUSF, with slightly lower declining rate in the later. However, the null hypothesis that the cell densities do not change through time could not be rejected. Monthly averages of point density are in decreasing order from June through August, among which, June stands with prominently greater density (+ 25% of August) compared to July (+1% of August) and August. It sheds light on the fact that June over the three summer months tends to favor the formation of much more thunderstorm cells. The higher standard errors for EUSF compared to ESF account for greater point density difference between June, July and August.

Table 4-1 Synoptic weather events within the influencing zone of 500 km around South Florida for the period: 1995-2012.

Synoptic Events	1995	1996	1997	1998	1999	2000	2001	2002	2003	2004	2005	2006	2007	2008	2009	2010	2011	2012
Low Trough	June:21-25, 30, Aug: 23,29,30, 31	June27	Aug: 11,12,23	Aug:13	Aug:5	July: 29, Aug: 30,	June: 27, July: 6	June: 11-13, 20-22, July: 1-3, 10, 24, Aug: 3, 30								Aug: 8,9	June: 11-12, July: 2,7-8, Aug: 2, 15,17	June: 2, 14, 20, 27, July:13, 15, Aug: 4
Surface/Mid-Tropospheric Low	July:18,19 Aug:22, 24	June: 29	June: 11,	June:26, July:12-14, Aug:2	June: 16	June: 10,11, July:19, Aug:9, 29			July: 25, 27,28, Aug: 14, 22,26	July: 29-31, Aug: 1, 8, 10	June: 20,22, 24-25, July: 29,31, Aug: 23,25	June: 25,26, July: 20-22, Aug: 15,16	June: 13,22, July:23, Aug: 24,31	July: 16, Aug: 19-23, 31		Aug: 10,11, 23	July: 17-18, Aug: 7,	
Cold Front	June:13,		Aug: 6,7,22, 23	June:7		June: 7, July:2, 8	June: 17,24, July: 14, Aug: 22	June: 15,17	June: 23	July: 20, Aug 6-7		June: 4,6, July: 7, 9	July: 22, Aug: 1-2	June: 18-19, July: 112,16, Aug: 9,10	June: 23, July: 20, Aug:23-25	June: 8	Aug: 29	June: 2, 14
Occluded Front		June:30, Aug: 15	Aug:24														Aug: 16,17	June: 7-9
Stationary Front			Aug: 8,9,26, 27	June:8, Aug: 2-5,21		July: 3,25,26	July: 15-17, Aug: 1, 15,	June: 16	June: 24		June: 19	July: 8, Aug: 14	July: 4			July: 2-5		
Tropical Storm							Aug: 3-6	Aug: 7	June: 30, July: 13-14, Aug: 15	Aug: 2	June: 10-11, July: 5,6, 22	June: 12-13, July: 20, Aug: 29	June: 2	Aug: 4, 20,23		July: 24	July: 19	June: 24-25
Tropical Wave							June: 28, Aug: 2				July 24 *TC						Aug: 31	July: 11, 12, 17
Tropical Depression									July: 16		June: 12, Aug: 24	June: 14		July: 19		Aug: 11	Aug: 7	June:27
Hurricane	June: 4,5								July: 15	Aug: 13, 14, 15	July: 9,10, Aug:25-29	Aug: 30,31		July: 23, Aug: 20-23, 31		Aug: 31	July: 18, Aug: 25, 26	June: 26, Aug: 26-28

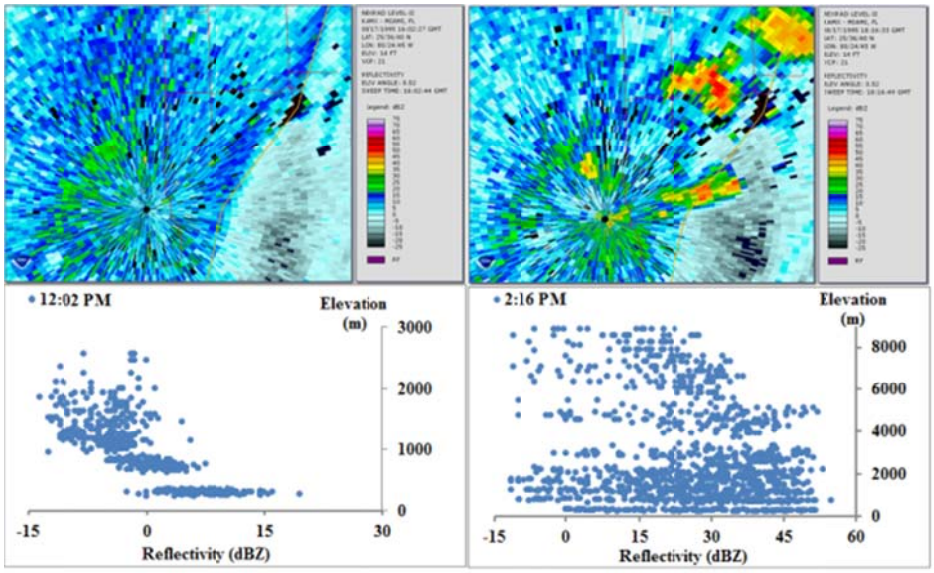

Figure 4.5 Vertical profiles of convective (2:16 PM) versus non-convective (12:02 PM) boundary layer. Each profile follows corresponding display of radar reflectivity showing high reflectivity values towards northeastern corner of the display.

Table 4-2 Comparison of point density for thunderstorm type reflectivities.

Coverage\ Statistics	Mean (/1000 Sq Km.)	Standard Error	Median	Range	b_1	p
Entire	8.74	0.033	5.4	62.16	-0.001	0.39
Urban	14.64	0.74	6.73	182.38	-0.001	0.73

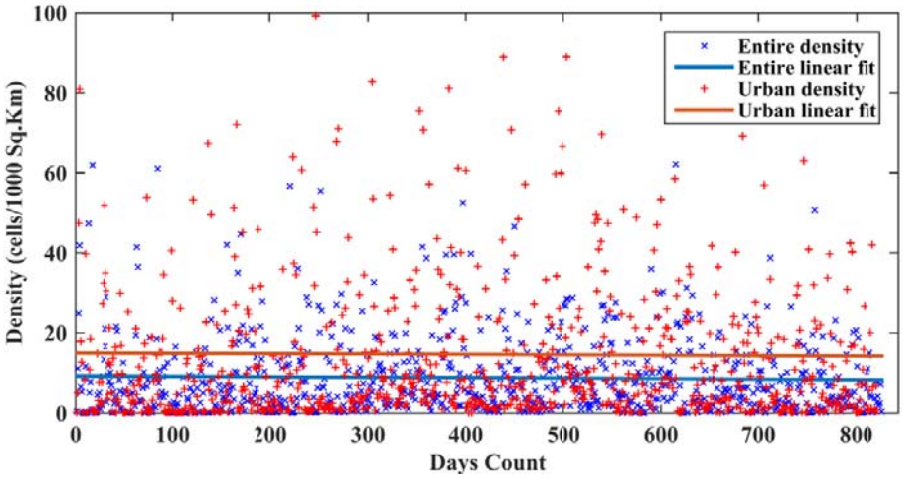

Figure 4.6 Point (thunderstorm cell) density comparison between ESF and EUSF from 1995 through 2007.

4.4.3.3 Maximum Reflectivity and Variance

Reflectivity maxima averaged by day are found to have increased from early (1995-2003) to late (2004-2012) phase, which are slightly decreasing over the summer months (Figure 4.7). The rise is more pronounced with the total increase of ~ 3 dBZ in EUSF compared to ~ 2 dBZ in ESF. Albeit with different level ($\alpha << 0.01$ for ESF, and $\alpha < 0.05$ for EUSF),

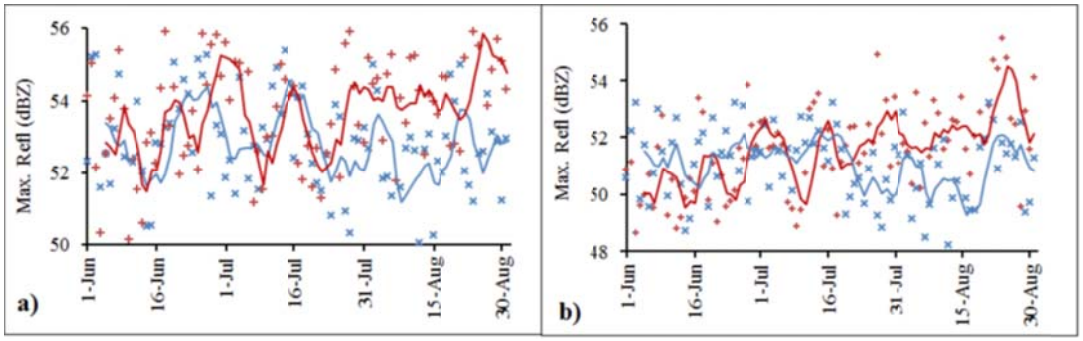

Figure 4.7 Maximum reflectivity averaged by day (blue: 1995-2003 average and red: 2004-2012 average). Crosses represent the data points and lines represent 5-point moving average for a) entire South Florida, and b) eastern urbanized South Florida.

Table 4-3 Pair sample statistics for mean rain rate comparison derived from maximum reflectivity.

Pair No	Pairs	Coverage	Mean (mm/hr)	Std. Deviation
1	Maximum RainRate 1995 to 2003	Entire	100.59	22.93
	Maximum Rain Rate 2004 to 2012	Entire	116.51	28.00
2	Maximum Rain Rate 1995 to 2003	Eastern Urban	73.05	17.15
	Maximum Rain Rate 2004 to 2012	Eastern Urban	83.03	21.58

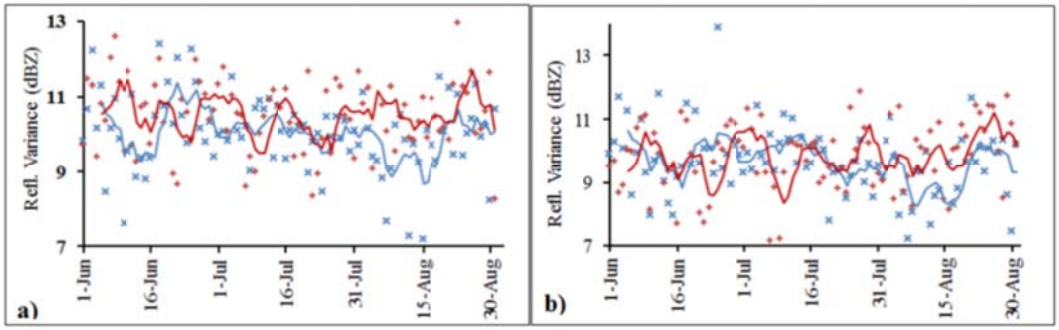

Figure 4.8 Reflectivity variance averaged by day for (blue: 1995-2003 average) and (red: 2004-2012 average). Crosses represent the data points and lines represent 5-point moving average for a) entire South Florida, and b) eastern urbanized South Florida.

The variance of ≥40 dBZ reflectivity of each five-minute scan depicts the spatial variation of surface forced convection. If land cover were the singlemost influential variable to alter convective intensity, reflectivity variance would reveal land cover variation of the study area. It is also a way to verify that strong convection has higher reflectivity variance in the horizontal dimension. The maximum reflectivity is found significantly higher for the latter phase in both spatial units (Table 4-4). Like maximum reflectivity, variance is also significantly higher ($\alpha << 0.001$) (Figure 4.8, Table 4-4) for the latter half of the analysis for ESF ascertaining the increasing strength of convection. However, the difference in variance between early and late phase in EUSF is not significant ($\alpha > 0.1$). No increase in variance is found during the course of summer; rather, it is constant and/ or negligiblly decreased for the early phase in both spatial units.

4.4.3.4 Rain Rate

The statistics (not presented) of the monthly average of the maximum rain rate reveals that August has the biggest change in rain rate (35% in ESF and 31.5% in EUSF) from the early to late phase.

Table 4-4 Statistical results of comparison of maximum reflectivities and reflectivity variance using paired sample t-test for early and late phase.

		Paired Differences						
					95% confidence interval of the Difference			
Pairs	Coverage	μ	σ	Std Error Mean	Lower	Upper	t	Sig. 2-tailed
Max 04 to 12– Max 95 to 03	Urban	0.55	2.06	.21	.13	0.98	2.58	.011
Max 04 to 12– Max 95 to 03	Entire SF	0.87	2.10	.21	0.43	1.30	3.95	.000
Var 04 to 12- Var 95 to 03	Urban	0.19	1.48	.15	-.11	.50	1.25	.21
Var 04 to 12- Var 95 to 03	Entire SF	0.49	1.36	.14	0.21	0.77	3.46	.000

Likewise, July has as a moderate change (8.9% in ESF and 10.3% in EUSF) and June, has the smallest change (4% in ESF and -8.8% in EUSF). The negative change of rain rate from early to late phase in June is similar to negative change in reflectivity variance, but this is contradictory with the point density which is increased in June.

Comparison of the daily maximum rain rate for ESF and EUSF are shown in Figure 4.9 and phase-wise statistics are presented in Table 4-3. Visual inspection of the graph shows that daily maximum rainfall intensity for ESF is slightly higher compared to EUSF. Years seven, ten, and eighteen corresponding to 2001, 2004, and 2012, and years six, nine, and fourteen corresponding to 2000, 2003, and 2008 show above average peaks of rain rate for ESF and EUSF, respectively. Similarly, rain rates in years one to three and eleven to

thirteen are below average for both spatial units. Rain rate in year fourteen is above average for EUSF, whereas for ESF the rain rate in year fourteen is below average. The trends of daily maximum rain rate and the subsequent regression statistics, resulting a rain rate increase of 6.43 mm/hr and 6.67 mm/hr per summer ($\alpha < 0.005$) for ESF and EUSF, respectively, elucidates the significant enhancement of overall rain rate with slightly higher rate for EUSF (Figure 4.9). Decomposition of the monthly rain rate time series of EUSF produced largest factor for August (5.51 mm/hr) followed by July (0.47 mm/hr) and June (-5.98 mm/hr).

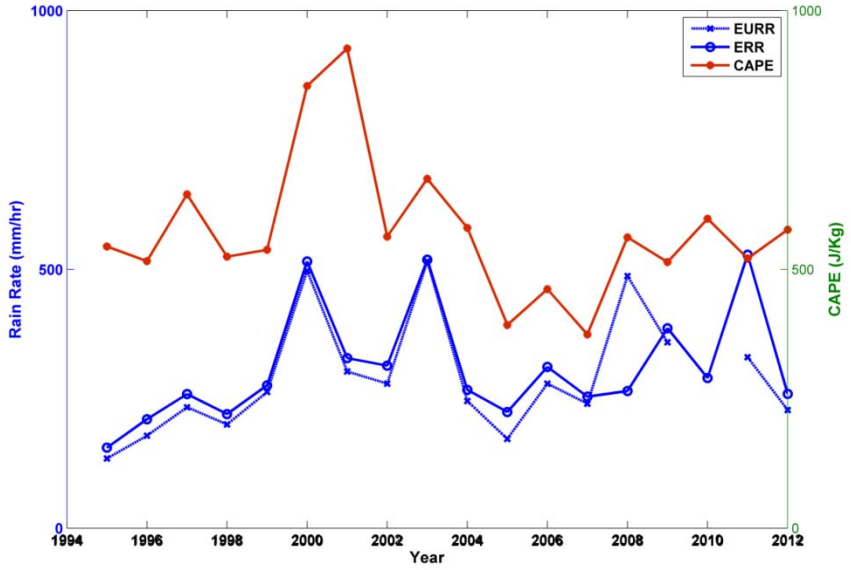

Figure 4.9 Time series daily maximum rain rate averaged by each summer (blues) for ESF (ERR) and EUSF (EURR) derived from radar and summer-average surface based CAPE (red) derived from Miami radiosonde.

4.4.4 Atmospheric conditions

The trend removed divergence does not take the prevalent wind direction into account. Hence the results (Figure 4.10) obtained for diveregence are the values of local

perturbation. The negative divergence implies convergence. The increasing temporal trend of convergence implies that convergence of moist air from western natural areas towards Fort Lauderdale has become stronger with time. The relative and specific humidity profiles for three different locations, Immokalee, Homestead and Ft. Lauderdale, compared in Figure 4.11 illustrate consistently lower relative humidity, but higher specific humidity at Ft Lauderdale, which is relatively warmer area. The higher temperature in Ft Lauderdale seems to increase the saturation vapor pressure resulting in lower relative humidity, even though the specific humidity in Ft Lauderdale is higher.

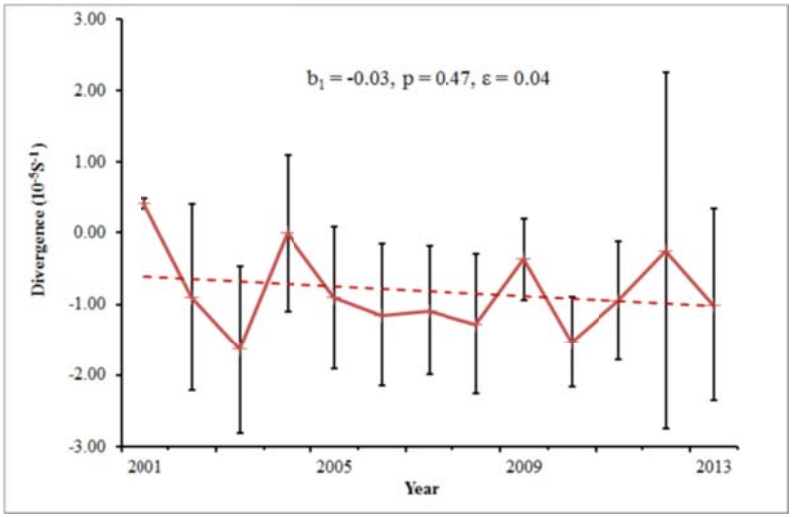

Figure 4.10 Summer average wind divergence calculated from Fort Lauderdale to Immokalee for 10 m level from the surface. The numbers on the figure signifies the statistics of the trend line (b1 = slope, p = level of significance, ε = standard error). Vertical error bars represent the standard deviations for corresponding summer.

Figure 4.9 also shows the time series summer-average CAPE from 1995 to 2012. Both the correlations between CAPE and rain rates of ESF ($r_{err–CAPE} = 0.42$) and EUSF ($r_{eurr–CAPE} = 0.46$) are found to be moderately positive with a higher coefficients for EUSF. Time series CAPE shows a slight decrease.

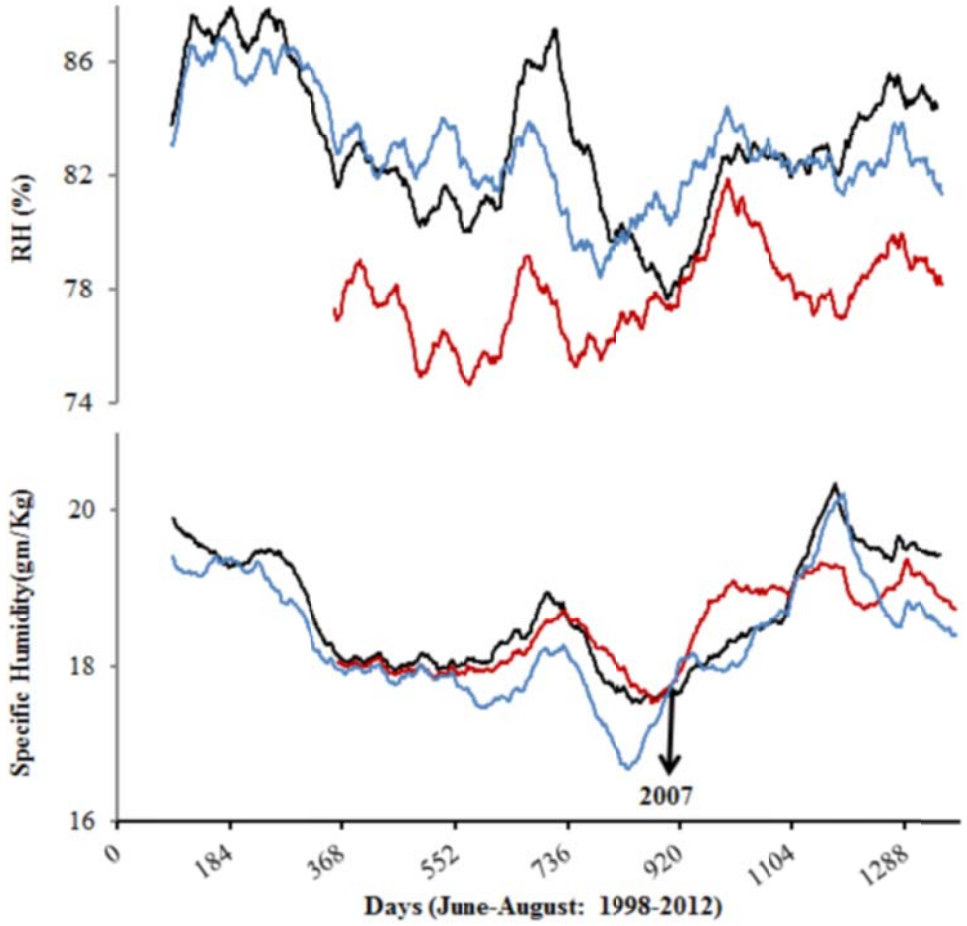

Figure 4.11 Daily averages of relative humidity (upper panel) and specific humidity (lower panel) for three summer months plotted for Homestead (1998-2012), Ft Lauderdale (2001-2012), and Immokalee (1998-2012) stations at the height of 2 m from the surface. The lines represent 92 points (one summer) moving averages; black for Homestead, red for Ft Lauderdale, and blue for Immokalee.

4.5 Discussion

Convection over South Florida is a very complex phenomenon resulting from the interactions of flows of several types and scales. Major scales, as summarized by Blanchard and Lopez (1985) are: regional (Atlantic high pressure circulation), synoptic (waves and fronts), peninsular (sea and lake breezes), local (surface feature variations) and cloud scale (cloud merger, outflow boundaries etc.). The present study has removed

the synoptic scale disturbances to focus its aim on examining the changes on nature of the thunderstorms that are induced by local scale surface feature variation interacting with the peninsular scale breezes. The study assumes the effects of the flows, such as Atlantic Multidecadal Oscillation (AMO) and El-niño Southern Oscillation (ENSO), are either erased from the long term trend or canceled out by their own opposing phases. Variations in landscape are capable of generating strong local circulations when the wavelength of surface heating is about the Rossby radius, which is closely equal to 90 km (Pielke, 2001). The increased roughness length (rural: 0.001 to urban: 1.5), and reduced albedo (rural: 0.23 to urban: 0.15), along with the lower specific heat, lower emissivity, and higher thermal conductivity of urban surface fabrics, result in the increased Bowen's ratio (urban: 4-5 from rural: 2) (Brutsaert, 198, Oke,1978). Acknowledging the above changes as the norm, the convergence towards Fort Lauderdale (Figure 4.10), which exhibits a warmer day time temperature, can be interpreted as the effects of the surface cover. The evidence of convergence at only one location is hardly sufficient for drawing any definite conclusion as to the entire urbanized area. However, on the basis of a few years' analysis results showing divergence from Ft Lauderdale to Homestead and to Belle Glade, it is reasonable to assume that the axis of convergence lies a little west of urban fringe. The apparent shift of the axis of convergence slightly towards the west of the urban fringe is not completely understood; nevertheless, it may be attributed to the pushing effect of relatively stronger easterlies. Still, it confirms the indications of the previous studies that the sea breezes from the east and west converge and collide in the Florida east coast, invigorating the thunderstorms there.

The monthly average temperatures for Florida revealed that July and August, which have very close average temperatures, are warmer by about 1°C than June. Therefore, urban convergence and subsequent convection can be expected to be relatively more vigorous in July and August than in June allowing the thunderstorm cells to be larger in general. The peak rain rates in August, followed by July suggested by monthly factors of the time series rain rate in the EUSF are consistent with the temperature variations, indicating high temperature areas and seasons to be more conducive for larger rainfall intensity.

Bearing the evidences that the heavily urbanized cities wider than 10 km can clearly interact with mesoscale circulations (Yoshikado, 1994), it is quite possible that the thunderstorms classified as benign are the results of interaction of UHI with sea breezes. It is likely that each cluster of built-up areas, separated by urban parks, ponds and lakes, may have acted as individual convergence zones and developed convective cells resulting in the higher thuderstorm density in the EUSF. It could also be possible that the anthropogenic activities in urban centers increase concentrations of pollution-derived cloud condensation nuclei, which typically produce more and smaller droplets than natural clouds do (Alkezweeny *et al.,*1993).

Despite the slightly declining trend of CAPE, the established correlation between rain rate and surface based CAPE suggests that the surface thermodynamics can explain the change in the rain rates. As reported by Pielke (2001), change in dew point temperature, which is the function of moisture, produces a greater effect on CAPE in warmer atmosphere. Hence, decrease in CAPE can be attributed to the decrease in moisture on the surface. Increase in specific humidity (0.11 g/kg year^{-1}, $p = 0.005$) at Fort Lauderdale would certainly increase CAPE thereby increasing the convective rainfall. On the other

hand, a very negligible increase in specific humidity at Homestead and a decrease in Immokalee imply less effective convective strengths at those locations.

The uncorrelated portion of the rain rate with the surface based CAPE perhaps links the convective rainfall with the mechanisms other than surface induced convection. One of such mechanisms could be the sea-breeze front outflow convergence that directly affect mid-trophospheric moisture, as pointed out by Shepherd *et al*. (2001).

The warmer and moister surface in South Florida in the late summer may have increased the CAPE resulting in an increase of thunderstorm intensity, which agrees with what Pielke (2010) has found. Patchy convergences resulting in focussed CAPE as opposed to widespread convection are attributed to the higher density and lower intensity thunderstorms during early summer. In addition, the absence of mergers in the upper level, because of more cleaner convections that are less influenced by the remnants of synoptic systems, can result into numerous, but weaker thunderstorms in June.

Both maximum reflectivity and rain rates indicate the occurrence of most of the intense thunderstorms in urbanized portions. Because ESF covers the eastern urbanized portion, plus the western vast wet, grass, and forested land, the slightly higher rain rate in ESF compared to EUSF is not only insubstantial, but also disproportionate with the land area it covers. Lower mean differences of variance between early and late phases, but higher standard deviations in EUSF than in ESF, suggest that year to year variations of convective response of the land cover are less than the variation with underlying land surface. Despite the smaller spatial coverage of EUSF, the closer statistics of five-minute maximum reflectivity and daily maximum rain rate of EUSF with that of ESF is a clear

indication that urban portions account for a considerable amount of changes observed in these variables.

As noted by Shepherd *et al*.(2010), a moistened lower troposphere along with a source of lift are necessary conditions for the development of convective rainfall. Concentration of higher intensity thunderstorms in eastern areas than in western areas is consistent with the Pan *et al.* (1996) observation that that local rainfall is enhanced with the increase in soil moisture only when the lower atmosphere was thermodynamically unstable and relatively dry. They also noted that it is decreased when the atmosphere was humid and lacked sufficient thermal forcing to initiate convection.

It is difficult to determine exactly how the slight decrease in thunderstorm density and increase in intensity would eventually impact the total rainfall in South Florida. Therefore, rather than making a comparative statement between the results from this study and the conclusion of Pielke *et al.* (1999) modeling, which states that the spatially averaged grid total rainfall decreases in response to conversion of landscape from natural to anthropogenic, this study agrees with their findings that some locations along the coast show a modest increase in rainfall.

4.6 Conclusions and Recommendations

South Florida represents a unique study site comprised of a mosaics of land cover. The land cover ranges from wet, water, forested, and scrub/shrub type natural covers in the west and middle to crop/pasture and urban covers towards notrtheast and east with a clear signature of UHI. Moreover, provenance of sea and lake breezes in the surroundings make South Florida a real experimental laboratory for the study of locally induced convective rainfall. Replacement of natural areas by anthropogenic cover is the general

mode of land use land cover change noticed particularly in South Florida during the 15 year period of 1995-2010. With the rapid increase of population, land use land cover in the eastern coastal counties gained medium and high intensity developed type of residential land use losing crop, pasture and scrub/shrub between 1995 and 2006.

The present study used radar data from Miami station (KAMX) and statistically differentiated the multi-year average of radar reflectivity from three-hour summer afternoons (12:00–15:00 LST). Three simple measures were obtained: maximum reflectivity, reflectivity variance, and maximum rain rate. The total duration of the study of 1995 and 2012 was arbitrarily divided into two phases of multiple years, 1995-2003 and 2004-2012, representing the early and the late phase temporally. It also divided the spatial coverage into two land units: entire South Florida and eastern urbanized South Florida. Point density, the fourth measure, that represents cell density of thunderstorms, is analysed as a long term trend of 5-minute counts and the average counts by day.

Thoroughout the study period, the results are a slight decrease in thunderstorm density, but a significant increase in the intensity of reflectivity, and the rain rates. The reflectivity variance is significantly higher for the later phase in the entire South Florida. The vertical profiles of reflectivity, and the echo display maps, which were verified with the observed records of hourly weather confirmed that above 40 dBZ reflectivity is the effective measure for thunderstorm identification.

The spatial and monthly variation and the increasing temporal trend of the intensity of summer afternoon convective rainfall, supported by the moderately positive correlation between surface based CAPE and the rain rate corroborates the statement, at least in certain degree, that the surface thermal properties interacting with converging sea breezes

induce convective rainfall in South Florida. A weaker rain rate enhancement and lower cell density in ESF than in EUSF also warrants the role of urban landscape on thunderstorm intensity. Since biases of radar-estimated rainfall have been reported, further work is recommended to derive site-specific parameters in Z-R relationship, and to validate with the observed storm rainfall in order to treasure the results for operational use.

4.7 Acknowledgement

We would like to acknowledge the data sources, such as NOAA- NCDC for radar and rainfall data; SFWMD, FNAI, and CCAP for land use land cover data; and FAWN for wind, humidity and temperature data. We also thank anonymous reviewers for their valuable comments and feedbacks, which helped us a lot in the journey of this manuscript to its current form.

4.8 References

Ashley WS, Bentley ML, Stallins JA. 2012. Urban induced thunderstorm modification in the Southeast United States. *Climatic Change* **113**: 481-498. DOI: 10.1007/s10584-011-0324-1.

Baik JJ, Kim YH, Kim JJ, Han JY. 2007. Effects of boundary layer stability on urban heat island-induced circulation. *Theoretical and applied climatology* **89** (1-2):73-81.

Betts RA. 2001. Biogeophysical impacts of land use on present-day climate: near surface temperature change and radiative forcing. *Atmospheric Science Letters* **1**:1-13. doi:10.1006/asle.2001.0023

Blanchard DO and Lopez RE. 1985. Spatial patterns of convection in South Florida. *Monthly Weather Review* **113**: 1282-1299.

Brutsaert W. 1982. *Evaporation into the atmosphere-theory, history and applications*. D. Reidel Publishing Company, p.299.

Burbaker KL, Entekhabi D, and Eagleson PS. 1993. Estimation of continental precipitation recycling. *Jornal of Climatology* **6**: 1077-1089.

Carter M, Shepherd JM, Burian S, and Jeyachandran I. 2012. Integration of Lidar data into a coupled mesoscale-land surface model: a theoretical assessment of sensitivity of urban-coastal mesoscale circulations to urban canopy parameters. *Journal of Atmospheric and Oceanic Technology* **29**:328-346.

Changnon SA, Huff F A, Schickedanz PT, and Vogel JL. 1977. Summary of METROMEX, Vol. I: Weather Anomalies and Impacts. *Illinois State Water Survey, Bulletin* **62**, Champaign, IL, 260 pp.

Coastal Change Analysis Program (CCAP): High Resolution Land Cover. Regional Change for Florida Counties 1996-2006, http://csc.noaa.gov/ccapftp/ Accessed on June 15, 2013

Diem JE, and Brown DP. 2003. Anthropogenic impacts on summer precipitation in central Arizona, U.S.A. *Professional Geographer* **55**: 343– 355.

Dixon PG, and Mote TL. 2003 Pattern's and causes of urban heat island-initiated precipitation. *Journal of Applied Meteorology* **42:** 1273-1284.

Feddema JJ, Oleson KW, Bonan GB, Mearns LO, Buja LE, Meehl GA, Washington WM. 2005. The Importance of land-cover change in simulating future climates. *Science* **310:** 1674-1678.

WSR-88D Functional Overview. 2005. *Federal Meteorological Handbook No 11, Doppler Radar meteorological Observations*, http://www.ofcm.gov/fmh11/fmh11B.htm , FMH-11-PART-B. 4-1 to 4-13.

Florida Department of Transportation, Surveying and Mapping Office.1999. *Florida land use, cover and forms classification system handbook.* Tallahasse, FL, USA.

Fulton RA, Breidenbach JP, Seo DJ, Miller DA, and O'Bannon T. 1998. The WSR-88D rainfall algorithm. *Weather Forecasting* **13:** 377-395.

Gedney N, and Valdes PJ. 2000. The effect of Amazonian deforestation on the northern hemisphere circulation and climate. *Geophysical Research Letters* **27** (19): 3053-3056.

Houze RA Jr. 1993. *Cloud Dynamics*. Academic Press. 573pp.

Houze, RA. 1997. Stratiform precipitation in regions of convection: a meteorological paradox? *Bulletin of American Meteorological Society* **78** (10): 2179-2196.

Jackson, RB, Jobb´agy EG, Avissar R, Baidya Roy S, Barrett DJ, and co-authors. 2005. Trading water for carbon with biological carbon sequestration. *Science* **310**: 1944–1947.

Kusaka H.2002. Formation mechanism of urban heat island, numerical study on flow and heat budget. *PhD Dissertation.* University of Tsukuba. Japan, 153 pp.

Landsberg HE. 1970. Man-made climatic changes. *Science* **170**: 1265-1274.

Lowry WP. 1998. Urban effects on precipitation amount. *Progress in Physical Geography* **22** (4): 477-520.

Marshall CH, Pielke RA, Steyaert LT, Willard DA. 2004. The impact of anthropogenic Land-cover change on the Florida Peninsula sea breezes and warm season sensible weather. *Monthly Weather Review* **132**: 28-52.

Martilli A. 2003. A two-dimensional numerical study of the impact of a city on atmospheric circulation and pollutant dispersion in a coastal environment. *Boundary-Layer Meteoology* **108**: 91–119.

McVoy CW, Said WP, Obeysekera, J, VanArman JA, and Dreschel TW. 2011. Phases of Everglades drainage, 1880s to early 1950s. In the book *Landscapes and Hydrology of Predrainage Everglades*. University Press of Florida, Gainesville, Fla.

National Climatic Data Center (NCDC), HDSS Access System NEXRAD level II, Asheville, NC. http://has.ncdc.noaa.gov/pls/plhas/HAS.FileAppSelect?datasetname=6500, Accessed in summer 2013.

National Oceanic and Atmospheric Administration (NOAA).,National Weather Service. Daily Weather Maps, prepared by National Centers for Environmental Prediction, Hydrometeorological Prediction Center. http://www.wpc.ncep.noaa.gov/dailywxmap/index_20030608.html Accessed in August, 2013.

Niyogi D, Pyle P, Lei M, Arya SP, Kishtawal CM, Shephard M, Chen F, and Wolfe B. 2011. Urban modifications of thunderstorms: An observational storm climatology and model case study for the Indianapolis Urban Region. *Journal of Applied Meteorology and Climatology* **50**: 1129-1144.

NOAA, Atlantic Oceanographic and Meteorologic Laboratory (NOAA, AOML).

Ohashi Y, Kida, H. 2004. Local circulations developed in the vicinity of both coastal and inland urban areas. Part II: Effects of urban and mountain areas on moisture transport. *Journal of Applied Meteorology* **43**: 119–133.

Oke TR. 1987. Boundary Layer Climates. 2nd ed. Routledge, 435 pp.

Orlanski I.1975. A rational subdivision of scales for atmospheric processes. *Bulletin of American Meteorological Society* **56**: 529-530.

Pan Z, Takle E, Segal M, and Turner R. 1996. Influences of model parameterization scheme on the response of rainfall to soil moisture in the central United States, *Monthly Weather Review* **124**: 1786-1802.

Pielke RA, Adegoke JA, Hiemstra CA, Lin J, Nair US, Niyogi D, and Nobis TE. 2007. An overview of regional land use land-cover impacts on rainfall. *Tellus* **59**B: 587-601.

Pielke RA, Dalu G, Snook JS, Lee TJ, and Kittel TGF. 1991. Nonlinear influence of mesoscale land use on weather and climate. *Jounal of Climatology* **4**: 1053-1069.

Pielke RA, Walko RL, Steyaert LT, Vidale PL, Liston GE, Lyons WA, and Chase TN. 1999. The influence of anthropogenic landscape change on weather in South Florida. *Monthly Weather Review* **127** (7): 1663-1673.

Pielke RA. 1974. A three-dimensional numerical model of the sea breezes over south Florida. *Monthly Weather Review* **102**, 115–139.

Pielke RA. 2001. Influence of the spatial distribution of vegetation and soils on the prediction of cumulus convective rainfall. *Reviews of Geophysics* **39** (2): 151-177.

Price CV, Nakagaki N, Hitt KJ, Clawges RC. 2006. Enhanced Historical Land-Use and Land-Cover Data Sets of the U.S. Geological Survey. *U.S. Geological Survey Digital Data Series* 240

Rabin RM, Stadler S, Wetjel PJ, Stensrud DJ, and Gregory M. 1990. Observed effects of landscape variability on convective clouds. *Bulletin of American Meteorological Society* **71**: 272-280.

Schrieber K, Stull R, and Zhang Q.1996. Distributions of surface layer buoyancy versus lifting condensation level over a heterogeneous land surface. *Journal of Atmospheric Science* **53**: 1086-1107.

Shepherd JM, Ferrier BS, and Ray PS. 2001. Rainfall morphology in Florida convergence zones: a numerical study. *Mon. Wea. Rev.* **129**: 177–197.

Shepherd JM, Burian SJ. 2003. Detection of urban induced rainfall anomalies in a major coastal city. *Earth Interactions* **7**(4): 1-17.

Shepherd JM, Carter M, Manyin M, Messen D. and Burian S. 2010. The impact of urbanization on current and future coastal precipitation: a case study for Houston. *Environment and Planning B: Planning and Design* **37**: 284-304.

Shepherd JM, Pierce H, and Negri AJ. 2002. Rainfall modification by major urban areas: Observations from spaceborne rain radar on the TRMM satellite. *Journal of Applied Meteorology* **41**: 689–701.

South Florida Water Management District (SFMD) 1995 LCLU Map. Accessed on October 27, 2013.

-2004-2011 LCLU Map, Accessed on November, 18, 2013

System Status Report. 2010. Greater Everglades Wetland Modules, Restoration Coordination and Verification (RECOVER). Comprehensive Everglades Restoration Plan (CERP), 148pp.

U.S. Department of Commerce, United States Census Bureau, States and County Quick Facts, Population.2010. http://quickfacts.census.gov/qfd/states/12000.html. Accessed on July 25, 2013.

Yoshikado H. 1994. Interactions of the sea breeze with urban heat islands of different sizes and locations. *Journal of the Meteorological Society of Japan* **72**: 139-142.

Chapter 5

Conclusions and Recommendations

The present study examines three critical effects of the land use/ land cover change in South Florida. First, it examines the effect land cover change has on land surface and surface layer atmospheric temperature as well as the urban heat island. Second, it investigates the variation of the distribution of radiant energy and surface energy balance by land cover type. The analysis of energy partitioning quantifies the turbulent transfer of heat and water to the atmosphere, and the conductive transfer towards the sub-surface. Finally, it analyzes the density and intensity of synoptically-benign convective rainfall, as a result of energy and moisture contrasts on the surface.

To address the research questions, data for the land surface and near-surface-atmosphere were utilized from remote sensing products (Landsat, radiosonde, and radar) and ground-located meteorological stations. The extent of urbanization in South Florida was quantified using land use land cover maps of 1974, 1992, 1995, 2006, and 2011 for spatial coverage of all of South Florida, coverage equivalent to land area of Landsat image (Path 15, Row 42), and for the eastern urbanized South Florida. Day and night-time surface and near-surface heat island in the urban area was delineated using Landsat-derived surface temperatures and summer-time daily minimum temperatures, respectively. In addition, changes in diurnal temperature range, and lifting condensation level, a function of surface level temperature and relative humidity, from Miami radiosonde data in summer months, was analyzed. Surface cover parameters (roughness length and zero plane displacement height) derived from land cover maps, air

temperature, wind speed and vapor pressure from weather stations in South Florida, and land surface temperatures from Landsat estimations were employed in empirical and physically-based models of energy balance. And finally, radar reflectivity ≥ 40 dBZ for summer afternoons were analyzed to estimate the density and intensity of thunderstorms for South Florida and the eastern urbanized part of South Florida separating the effects of synoptic weather.

Growth of 10% in urban area is found with a resultant major loss in range lands (12%) between 1974 and 2011. The results of associated changes in radiative, thermophysical, and aerodynamic properties along with their derivative energy fluxes and surface-induced convective rainfall support the following conclusions.

Distinct manifestation of the urban heat island is displayed by variety of measures. A difference in minimum temperature between urban and natural areas (≈ 4°C) with a rise of 0.5 °C - 1°C over 40 years, heightening lifting condensation level in the atmospheric surface layer (>20 m), and declining diurnal temperature range (DTR = -1°C, p = 0.005) from station-based and radiosonde results are observed. These findings on the signatures of UHI are further corroborated by higher Landsat-based land surface temperatures ($\overline{LST}_{u\text{-}r}$ = 2.8 °C) in urban areas. With the expansion and intensification of urban land, average emissivity decreased by 0.015 coupled with no surfaces for latent heat loss in high intensity developed cover attests the fact that additional storage of incoming radiation during the day and its release during the night is the most plausible explanation for the rise of nocturnal temperature. Significant UHI intensity in South Florida increases the awareness that even with the neutralization effect of breezes, a subtropical coastal city can also build its own microclimate. Also, urban open spaces behaving very closely to

natural lands as noted from Landsat-based temperatures is an implication that alternate patches of buildings and pavements, and parks and ponds help alleviate UHI stress for urban dwellers.

Anthropogenic conversion of land cover in South Florida is found to modulate the energy partitioning. In contrast with other rural-urban comparisons, the albedos are highest for high-intensity developed land and lowest for water and herbaceous wetlands, uniqueness rooted in the geographic setting of South Florida. The greatest net radiation is observed in water and wetlands, possible reflections of their lower surface temperatures and lower albedos. Bowen's ratios are increased in urban areas (considering the energy closure) from 1.67 in 1984 to 3.06 in 2010, and are decreased in natural lands (water, wetland, rangeland and forested land) from the average value of 0.92 in 1984 to 0.36 in 2010. Considerable increase of daily ET rates from agricultural areas (0.21 mm/day in 1984 to 3.60 mm/day in 2010) is perhaps linked with improved BMPs in EAA that allow agricultural surfaces to remain moister than before. Owing to a profound increase in sensible heat flux and a slight decrease of emissivity, urban areas showed a reduced heat transfer towards ground in 2010 from their 1984 value. The energy deficit in urban areas suggests a significant contribution of energy expelled by human activities in cities. More efficient moisture transfer from vegetated wetlands than from open water could be a crucial piece of information from the water conservation perspective. Likewise, different rates of evapotranspiration and ground conductance of heat from different types of forest, such as the expectation of least subsurface flux as estimated in 1984 and negative sensible heat flux as estimated in 2010 from deciduous forest are valuable information for urban forestry.

The present study presents an analysis of eighteen year-long radar reflectivity-based summer afternoon convective rainfall for the first time. A slight decrease in the density but progressive increase in the intensity of summer-afternoon thunderstorms obtained from the radar reflectivity suggests an ongoing enhancement of surface- induced convection in South Florida. A moderate correlation (0.42) between synoptically-benign daily maximum intensity of convective rainfall and surface-based CAPE verify our hypothesis, to a certain level, that changes in surface thermal properties can stimulate sea breeze convergence to alter local updraft and the intensity and pattern of thunderstorms. Higher rain rate (+0.24 mm/hr per summer), and a larger correlation coefficient of rain rate with CAPE (+0.04) from urban areas is suggestive of stronger convective enhancements there.

Consistency of the data remains a major constraint in this analysis. Cloud cover in the summer-time Landsat images, availability of only one radiosonde station for the upper air observations, nonexistence of eddy covariance towers for the validation of urban energy balance, and absence of locally-regressed coefficients for radar rain rate estimations were some noteworthy challenges. Appraising these limitations, this study strongly recommends further studies aimed at the development of a more robust cloud masking algorithm for improved Landsat-based estimations, acquisition of ground heat flux data for energy balance validation, inclusion of anthropogenic energy in the energy balance, and the development of a local fit coefficient for radar-rain rate estimation.

To sum up, this study is a first of its kind in South Florida that interlinks the surface and climatic response of land cover change to changes in sensible weather. This study has implications in a broad array of disciplines that range from urban health, wetland

ecology, urban microclimatology and hydrology, particularly the extreme events, such as drought and floods. The results may also be valuable in the aspects of land, water, and agricultural managements as the study is suggesting the possible causes of higher water loss from vegetation and heat stress in urban areas.

APPENDICES

Appendix 1 Percentage changes in land cover within 10 km radius of selected stations

Land Cover	Wet, Water, Forest and Range		Urban and Barren		Crop and Pasture	
Stations/Year	1974	2011	1974	2011	1974	2011
Naples	51.84	41.66	40.76	57.5	8.14	0.83
Miami	17.14	11.39	75.52	88.3	7.34	0.32
La Belle	44.37	34.6	4.17	16.6	51.65	48.81
Big Cypress	69.86	60.4	8.59	1.6	21.54	37.86

Appendix 2 ArcGIS raster calculator methods of computing NDVI and emissivity

NDVI

1. Band 3 and band 4 exported using extract sub-dataset

2. Raster Calculator algorithms:

(Float (band4)/10000-Float(band3)/10000)/ (Float (band4)/10000+Float(band3)/10000)
% 10000 is scale factor

3. Landwater NDVI = SetNull("zhu_fmask" >= 2,"ndvi ") in raster calculator
4. Basin_lwndvi = extract by mask

EMISSIVITY

1. Basin_lwb3 = Float("band3")/10000
2. Raster calculator algorithms:

PvPrepNDVI = SetNull("basin_lwndvi" < 0.2,SetNull("basin_lwndvi" >
0.5,"basin_lwndvi")) % sets real ndvi values for 0.2≤ndvi≤0.5, otherwise null

Composite_Pv = Con("basin_lwndvi" < 0.2,0,Con("basin_lwndvi" <
0.5,Square(("PvPrepNDVI" - 0.2) / 0.3),1))

emissivity = Con("basin_lwndvi" < 0.2,0.980 - 0.042 *
"basin_lwb3",Con("basin_lwndvi" < 0.5,0.986 + 0.003 * "composite_Pv",0.985 + 0.005))

Appendix 3 Percentage cloud free versus Landsat-estimated urban surface temperatures

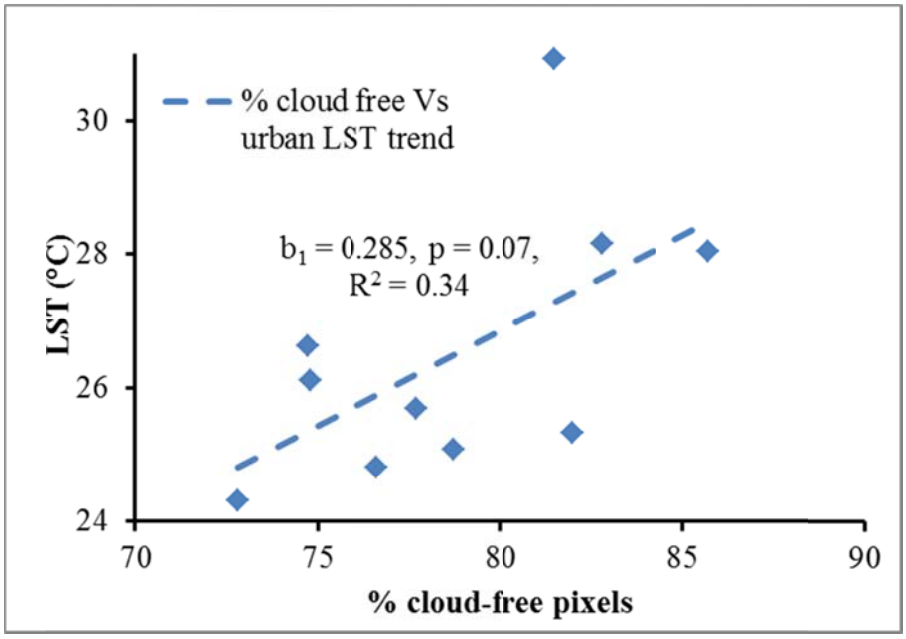
% cloud free Vs
urban LST trend
$b_1 = 0.285$, $p = 0.07$,
$R^2 = 0.34$
LST (°C)
30
28
26
24
70
75
80
85
90
% cloud-free pixels

Appendix 4 Intermediate results obtained in the process of energy flux estimations

Variable	Date	Average (standard deviation)
Solar Influx	7-May-84	996.98 Wm^{-2}
	16-Jun-10	1021.68 Wm^{-2}
Downwelling Long Wave	7-May-84	390.63 (±2.12) Wm^{-2}
	16-Jun-10	411.19 (±0.2) Wm^{-2}
Surface Emissivity	7-May-84	0.986 (±0.004)
	16-Jun-10	0.987 (±0.004)
Upwelling Long Wave	7-May-84	455.90 (±18.28) Wm^{-2}
	16-Jun-10	448.48 (±12.89) Wm^{-2}

Appendix 5 The difference maps (2010-1984) of sensible (H) and latent (L) heat fluxes in South Florida. μ is average and σ is standard deviation from the whole analysis area

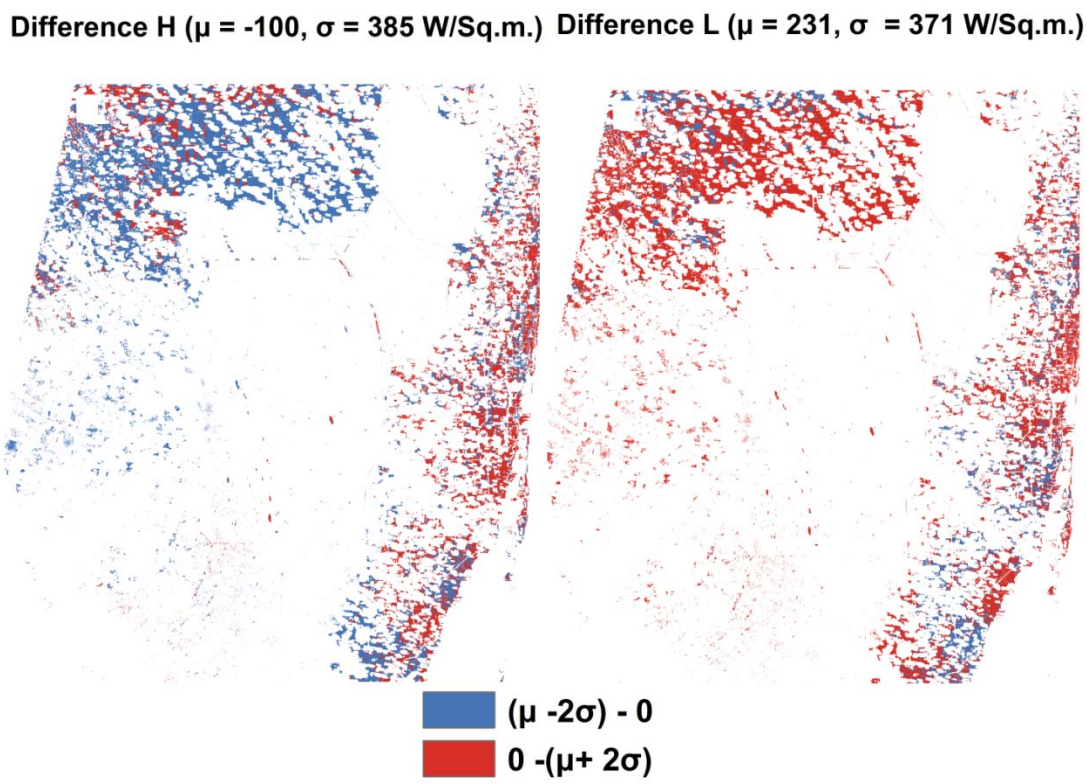
Difference H (μ = -100, σ = 385 W/Sq.m.)
Difference L (μ = 231, σ = 371 W/Sq.m.)
(μ -2σ) - 0
0 -(μ+ 2σ)

Appendix 6 An example of ground heat flux (equation (12)) calculation except the term I using hourly air temperatures.

Year	Month	Day	Time	T (k)	T_Surf (K)	s (Hr)	s(Sec)	$\frac{T^{i+1}-T^{i}}{s_{i+1}-s_{i}}\left(\sqrt{t-s_{i}}-\sqrt{t-s_{i+1}}\right)$	Sum(preceeding column)	$\frac{2}{\sqrt{\pi}}$ pr.cell
1984	5	7	700	298.15	299.09				0.0314	0.0354
1984	5	7	800	298.15	299.09					
1984	5	7	900	298.15	299.09					
1984	5	7	1000	298.15	299.09					
1984	5	7	1100	297.55	298.49	0	0	0.0047		
1984	5	7	1200	298.75	299.69	1	3600	0.0049		
1984	5	7	1300	299.85	300.79	2	7200	0.0058		
1984	5	7	1400	300.95	301.89	3	10800	0.0076		
1984	5	7	1500	302.05	302.99	4	14400	0.0083		
1984	5	7	1600	302.55	303.49	5	18000			

Appendix 7 Frequency distribution of synoptic events during the study period analyzed by reading historical daily weather maps

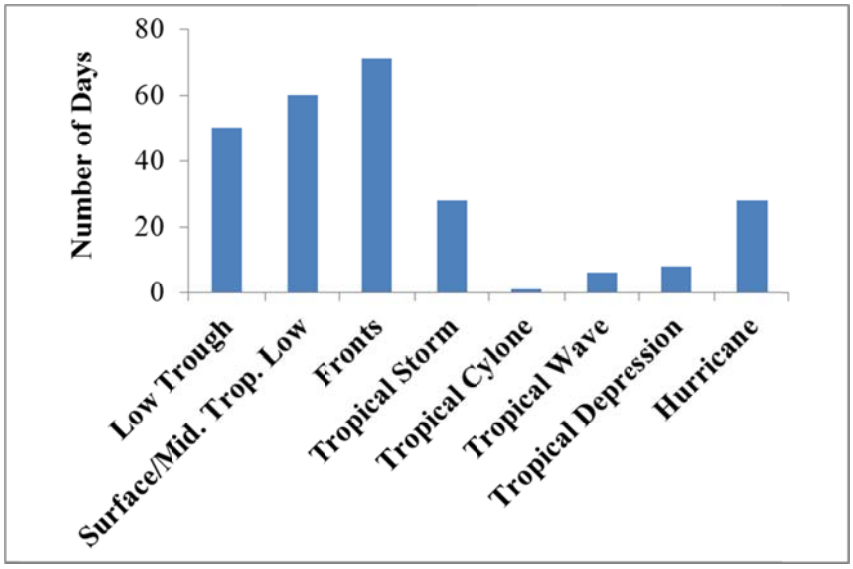
Number of Days
80
60
40
20
0
Low Trough
Surface/Mid. Trop. Low
Fronts
Tropical Storm
Tropical Cylone
Tropical Wave
Tropical Depression
Hurricane

Appendix 8 A sample Matlab code used for CAPE calculation

```
s_1996= xlsread('1996Summer.xlsx','Sheet6');%read data from excel file
et = s_1996(:,2)/10;z=s_1996(:,1);rh = s_1996(:,3)/10;% defining variables
% et = environmental temperature in K, z = observed height, rh = relative
% humidity in %
td = 273.15+(et-273.15)-(100-rh)/5;%dew point calculation according to
%Mark G Laurence paper
%which states the formula uses surface level temperature in degree
%centigrade
z_lcl = 125*(et(1)-td(1));% calculation of lifting condensation level
% computation of parcel temperature
t_par(1) = et(1);% parcel temperature at the surface is equivalent to
%environmental temperature
for k=1:length(z)-1
  if z(k)<=z_lcl
      t_par(k+1)=t_par(k)-0.0098*(z(k+1)-z(k));
  elseif z(k) > z_lcl & z(k) <= 2000
      t_par(k+1)=t_par(k)-0.004*(z(k+1)-z(k));
  elseif z(k) >2000 & z(k) <= 5000
      t_par(k+1)=t_par(k)-0.005*(z(k+1)-z(k));
  elseif z(k) >5000 & z(k) <= 6000
      t_par(k+1)=t_par(k)-0.006*(z(k+1)-z(k));
  elseif z(k) >6000 & z(k) <= 7000
      t_par(k+1)=t_par(k)-0.007*(z(k+1)-z(k));
  elseif z(k) >7000 & z(k) <= 8000
      t_par(k+1)=t_par(k)-0.008*(z(k+1)-z(k));
  else
      t_par(k+1)=t_par(k)-0.0098*(z(k+1)-z(k));
  end

end
t_par = reshape(t_par,2770,1);
% computation of equillibrium level
p1 = polyfit(et,z,2);% using secord order polynomial
p2 = polyfit(t_par,z,2);
x_intersect = fzero(@(et)polyval(p1-p2,et),7);% the starting value 7 has
%been found working number for this iteration. can start with 1 and if does
%not work change it to the value that works just by testing.
y_intersect = polyval(p1,x_intersect);
z_el = y_intersect;
% now calculate CAPE.
cape_sum =0;
g = 9.8;
for k = 1:length(z)-1
if z(k) > z_lcl & t_par(k)>et(k)& z(k) < z_el
cape_sum = cape_sum + (z(k+1)-z(k))*g*((t_par(k)-et(k))/et(k));
end
end
```

VITA

HARI P. KANDEL

1999-2003	B.Sc.- Major Geology Tribhuvan University, Kathmandu, Nepal
2005 - 2007	M.Sc. Geology- Natural Resources Studies Tribhuvan University, Kathmandu, Nepal
2008-2010	M.S. in Geology and Geospatial Science Bowling Green State University, Bowling Green, Ohio, USA
	Teaching and Research Assistant, Department of Geology, Bowling Green State University

PUBLICATIONS AND PRESENTATIONS

Cristobal C., Melesse, A., Price, R., Dessu, S., and Kandel, H. (2015) Operational Actual Wetland Evapotranspiration Estimation for South Florida Using MODIS Imagery, *Remote Sensing*, 7: 3613-3632.

Kandel, H; Melesse A; and Zhu P (2015) Radar Reflectivity Based Convective Rainfall Change in South Florida: An Implied Effect of Land Use Land Cover Change, *Hydrological Processes* (In review)

Kandel, H.; Melesse, A., and Whitman D. (2015) Delineation of Urban Heat Island in South Florida Using Land-Based Stations, Radiosonde Profiles and Landsat Imageries (Submitted in *International Journal of Remote Sensing*)

Kandel, H. and Melesse, A. (2014) Alteration of surface energy balance in South Florida driven by land use land cover change, American Water Resource Association, Annual Water Resources Conference, November 3-6, 2014, Session-54, Tysons Corner, Virginia, USA.

Kandel, H. and Melesse, A. (2013) Human induced changes on land surface temperature and convective rainfall in South Florida, American Water Resource Association, Annual Water Resources Conference, November, 4-7, 2013, Portland, Oregon, USA.

Kandel, H. and Melesse, A. (2013) Effect of land use /land cover change on radar reflectivity based convective precipitation in South Florida, Geological Society of America, 125th Anniversary Annual Meeting and Expo, October 27-30, Denver, Colorado, USA.

Kandel, H. and Melesse, A. (2012) Change in minimum temperature as a response to land cover change in South Florida, American Geophysical Union, Fall Meeting, December 3-7, 2012, San Francisco, California, USA.

Kandel, H. and Gomezdelcampo, E. (2010) Spatial Variability of Sediment Delivery in the Sandusky Watershed, Ohio, 53rd Annual Conferences on Great Lake Research, International Association for Great Lake Research, May 17-21, 2010, Toronto, Ontario, Canada.

Kandel, H. and Melesse, A. (2012) Pre- and post-drainage South Florida: land cover change and temperature response, Rookery Bay National Estuarine Research Reserve, GIS Symposium 2012: Discovering Technology-Based Solutions, October 17, 2012, Naples, Florida.

Kandel, H. and Melesse, A. (2013) Land cover change and its hydro-climatic impact in South Florida, American Water Resource Association, 22nd Annual Southwest Florida Water Resource Conference, January, 25, 2013. Fort Myers, Florida.